Device Shot Noise and Saturation Effects on Oscillator Phase Noise

Scott E. Brock

Thesis submitted to the Faculty of the
Virginia Polytechnic Institute and State University
in partial fulfillment of the requirements for the degree of

Master of Science
in
Electrical Engineering

Dr. William A. Davis, Chair
Dr. Charles W. Bostian
Dr. Steven W. Ellingson

September 8, 2006
Blacksburg, Virginia

Keywords: Oscillator, Shot Noise, Phase Noise

Device Shot Noise and Saturation Effects on Oscillator Phase Noise

Scott E. Brock

(ABSTRACT)

Oscillator phase noise is an important factor in designing radio frequency (RF) communications hardware. Phase noise directly contributes to adjacent-channel interference and an increase in bit error rate (BER).

Understanding the operation of an oscillator can help with the oscillator design process. Also, the understanding of the noise processes within an oscillator can add insight to the design process, allowing an intelligent low-noise design. It will be shown that although simulation software can be helpful, the understanding of the oscillator operation is a valuable tool in the design process.

Oscillator design will be discussed, and then the noise processes of the oscillator will be investigated. A new method of decomposing shot noise into in-phase and quadrature components will be discussed. The noise processes discussed for a non-saturating bipolar junction transistor (BJT) Colpitts oscillator will be extended to the case of a saturating BJT Colpitts oscillator. This new method gives insight into the design of low-noise oscillators, and provides guidelines for design of low-noise oscillators. Example oscillators will support the theory and low-noise design guidelines. It will be seen that although designing an oscillator to saturate can provide a stable output level over a wide bandwidth, the added noise production may degrade the performance of the oscillator through both a lower effective Q and restricted signal level compared to the noise.

Acknowledgments

There are many people I would like to thank that have helped me both professionally and personally through this journy. First, I would like to thank my advisor, Dr. Davis, for helping me through this process. His patience with me has helped me learn more about oscillators and RF circuits than I ever thought I would want to know. His patience with my writing skills has helped me considerably too. In the three years I have been here, I feel that my writing ability has progressed greatly with the help of Dr. Davis. Also, after hour or more discussions about topics in this thesis, getting sidetracked and talking about other things, like amateur radio, was a welcome distraction. I would also like to thank the other members of my comittee, Dr. Bostian and Dr. Ellingson, whose knowledge I did not utilize as much as I probably should have. I would also like to thank the people at DRS who sponsered this research.

Everyone at CWT, thank you for your support and the frequent trips to lunch. Derek, the many discussions, lunch breaks, and help with LaTeXwere always appreciated. Chris and Shashi, thank you for the visits to Virginia. It was nice to have you come down. My amateur radio friends, thank you for keeping me distracted and continually asking me if I was done writing yet.

And my wonderful family: Mom and Dad, thank you for the visits to Virginia and understanding the infrequency of my trips to Indiana. The good food you brought down, or filled my cooler with while I was home, was always appreciated. Adam and Gena, thank you for coming to visit me in Virginia. Thanks to all of you for keeping me motivated.

Contents

List of Figures

List of Tables

Chapter 1

Introduction

In any radio transmitter, and most radio receivers, an oscillator is an important part of the overall system. Oscillators provide a radio frequency (RF) signal source for the carrier of transmitted signals or a signal source that can be fed to a mixer to perform frequency translation. As W. P. Robins [26] states, ideally a signal source would consist of having an output at a single frequency; however, practical oscillators contain noise which creates amplitude and phase modulation of the carrier. Robins [26] also states that with unwanted amplitude or phase modulation, a baseband signal carrying information which is modulated on the carrier can result in degraded signal quality or bit errors in the communications link. Another effect of oscillator phase noise is reciprocal mixing. Reciprocal mixing is described by Ulrich L. Rohde [28] [29] as the process by which unwanted phase noise energy mixes with signals of adjacent channels resulting in interference at the intermediate frequency. This continues to become more important with the increased use of the frequency spectrum; therefore, there is an interest in understanding and reducing oscillator phase noise.

Understanding how an oscillator operates can give insight into the design process. Once one understands how changing a parameter will affect oscillator performance, one can make an informed decision on how to design an oscillator. Also, understanding the noise processes of an oscillator can give insight into what parameters can be adjusted to produce an oscillator with low phase noise. With these insights, one can go beyond relying on simulation software for design. Although simulation software can be helpful, the understanding of the oscillator operation is a valuable tool in the design process. It will be shown that although simulation software is a good tool, understanding the limits of the simulation is important.

Written as a few brief thoughts, an early letter by D. B. Leeson [16] provided a description of a simple model of oscillator noise spectrum that has been an important fixture in oscillator phase noise literature. Leeson [16] used a linear feedback oscillator model to develop a simple picture of the oscillator noise spectrum. Many discussions of oscillator phase noise provide models based on that of Leeson's letter. In 1968, Kaneyuki Kurokawa [14] discussed a noise analysis model based on a negative resistance approach. This approach is also discussed by

M. J. Buckingham [4]. Ali Hajimiri and Thomas H. Lee [9][10] present an alternate view of oscillator phase noise which utilizes a linear time-varying system model as opposed to the time-invariant Leeson derived models. The model of Hajimiri and Lee [9][10] involves an impulse sensitivity function to describe the time-varying properties of an oscillator circuit. Rohde discusses all of these models in *The Design of Modern Microwave Oscillators for Wireless Applications* [29].

While the insights gained by Hajimiri and Lee's impulse sensitivity function analysis are helpful to understand oscillator noise behavior, an approach will be discussed which represents the cyclostationary shot noise production as a physical process. Our oscillator noise analysis will give insight into the physical processes involved in the noise production and the noise transfer around the oscillator loop. This method will give a straightforward mathematical result for oscillator phase noise. The noise analysis will also be extended to the case in which the transistor saturates during a portion of the cycle and discuss the disadvantages resulting from saturation.

The dominant noise in an oscillator originates from the active device of the circuit. For detailed discussion of transistors and the noise associated with transistors, many texts can be considered–for example, those by Manasse [18], Thornton [30], Goldman [8], Pierret [24], Vasilescu [33], Robinson [27], Buckingham [4], Leach [15], van der Ziel [32], and many more. Many articles on the subject of device noise have also been written, some of which include the work of Johnson [12], Nyquist [21], van der Ziel [31], Nielsen [19], Fukui [7], Hawkins [11], Pucel and Rohde [25], Niu [20], and many others.

In Chapter 2 (*Basic Oscillator Design*), the nonlinear design principles discussed by Kenneth K. Clarke and Donald T. Hess [5] will be used to illustrate the oscillator design process as described by William A. Davis [6]. In Chapter 3 (*Example Oscillator Designs*), an oscillator will be designed and simulated using the Advanced Design System (ADS) [1] harmonic balance simulator. It will be shown that an oscillator can be designed so that the operation can be predicted fairly closely. The oscillator will then be modified so that the transistor saturates. The operation of this oscillator will then be predicted, and the results of the prediction will be compared to an ADS simulation.

In Chapter 4 (*Noise*), a treatment of noise sources will be covered with an emphasis on the shot noise production in a bipolar junction transistor (BJT). The BJT shot noise model will then be modified to account for saturation effects. In Section 4.4, a method of decomposing the noise power into in-phase and quadrature components will be discussed. The method used is a downconversion and detection process similar to the process one might use in the laboratory to measure the in-phase and quadrature noise power. The downconversion and detection process of computing in-phase and quadrature power will then be extended to the stochastic example of shot noise. The development is valid for shot noise produced by any periodic current waveform.

In Section 4.6, an expression for the in-phase and quadrature noise spectrum of an oscillator will be developed. A BJT as the active device will be used as an example; however, the development can be applied to oscillators utilizing other active devices.

In Chapter 5 (*Noise Performance of Examples*), the noise performance of the example oscillators of Chapter 3 will be analyzed and compared to ADS simulations of the noise. It will be shown that the noise prediction works well. It will also be shown that there are situations where the ADS simulation may be slightly off from the prediction but can be accounted for by adding external noise sources instead of using the noise model included with the generic BJT model.

Chapter 2

Basic Oscillator Design

In this chapter, the basic method of oscillator design will be discussed. Some consider basic oscillator design to be somewhat of an art [13]. However, using the nonlinear techniques of Clarke and Hess [5], and the three-terminal model from Davis [6], the process of designing an oscillator can be fairly straightforward.

We will start off with a basic description of an oscillator. We will then proceed to discuss the nonlinear sources that can be used to model the device used in an oscillator. The exponential source will be discussed in more detail because it can be used to model the Bipolar Junction Transistor (BJT). The BJT will be used throughout the thesis in examples; however, the concepts discussed can be applied to other devices. After discussing the nonlinear source, the three-terminal oscillator model is discussed. This allows for a short discussion on oscillator design and the effects of saturation on a design.

2.1 Basic Oscillator Description

One way to view an oscillator is as an active device with positive frequency dependent feedback. Figure 2.1 shows a diagram of this simplified model. Thermal noise and startup transients start the oscillation by providing a wide-band signal at the input of the active device. The positive feedback path is generally a frequency selective circuit, which filters the output of the active device and adds to the input signal at the desired frequency of oscillation. As this process of amplifying wide-band noise and feeding back the filtered output of the active device is repeated, a signal at the fundamental frequency emerges from the noise. The emerging oscillation continues to increase to the point where it is limited by some nonlinear characteristic of the active device or an automatic gain control circuit.

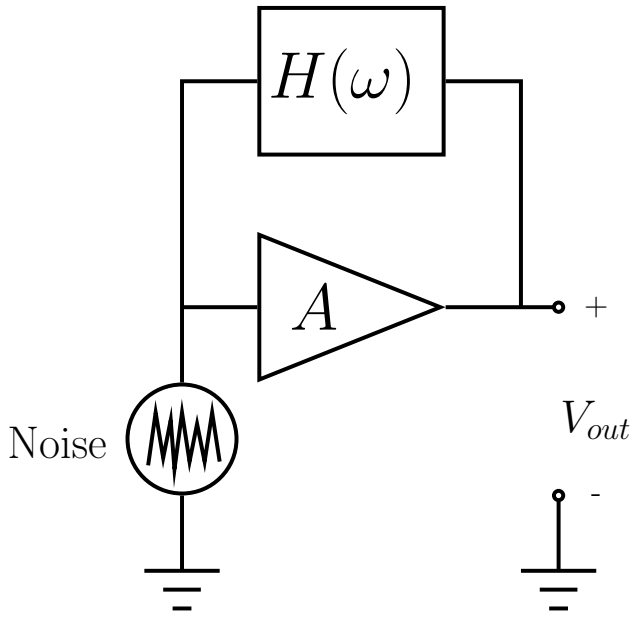

Figure 2.1: Feedback model of oscillator

2.2 Nonlinear Sources

The active device of an oscillator is generally a nonlinear device which produce currents as a result of an input voltage. A large signal analysis must be used to relate the input voltage to the output current. A sinusoidal input voltage will produce currents at the fundamental frequency and some harmonics, depending on the device. The nonlinear properties of the device can also shift the bias point depending on the amplitude of the driving voltage. The techniques used here can be used for any nonlinear characteristic. For the purposes of this thesis, we will focus on the exponential characteristic of the bipolar junction transistor (BJT). To see details of the analysis of circuits with other characteristics such as piecewise linear, square law, or differential, please refer to Chapter 4 of Clarke and Hess [5].

The exponential characteristic is the nonlinear characteristic of the P-N junction of a BJT. An approximate representation of the emitter current of a BJT is

$$i_e = I_S e^{\frac{qv_{be}}{kT}}, \tag{2.1}$$

where $\frac{kT}{q}$ is approximated by 26 mV at a temperature of 300 K [5]. The V-I relationship for the exponential characteristic is illustrated in Figure 2.2. For the purpose of an oscillator we may assume the base-emitter voltage is sinusoidal. This gives us

$$i_e = I_S e^{\frac{q}{kT}[V_{BE}+V_1\cos(\omega_o t)]} = I_S e^{\frac{qV_{BE}}{kT}} e^{\frac{qV_1\cos(\omega_o t)}{kT}} = I_S e^{\frac{qV_{BE}}{kT}} e^{x\cos(\omega_o t)}, \tag{2.2}$$

where $x = \frac{qV_1}{kT}$. As the drive, x, is increased, a sharper current pulse with a lower duty cycle is created, which can be seen in Figure 2.3.

For the large signal analysis of an oscillator, we would like to know the harmonic content of the current in the transistor. Since $e^{x\cos(w_o t)}$ is periodic, the emitter current can be represented as a Fourier Series of the form

$$i_e = I_S e^{\frac{qV_{BE}}{kT}} \sum_{n=0}^{\infty} a_n \cos(n\omega_o t), \tag{2.3}$$

where for $n = 0$

$$a_0 = \frac{1}{2\pi}\int_{-\pi}^{\pi} e^{x\cos\theta} d\theta = I_0(x), \tag{2.4}$$

and for $n > 0$

$$a_n = \frac{1}{\pi}\int_{-\pi}^{\pi} e^{x\cos\theta}\cos(n\theta) d\theta = 2I_n(x), \tag{2.5}$$

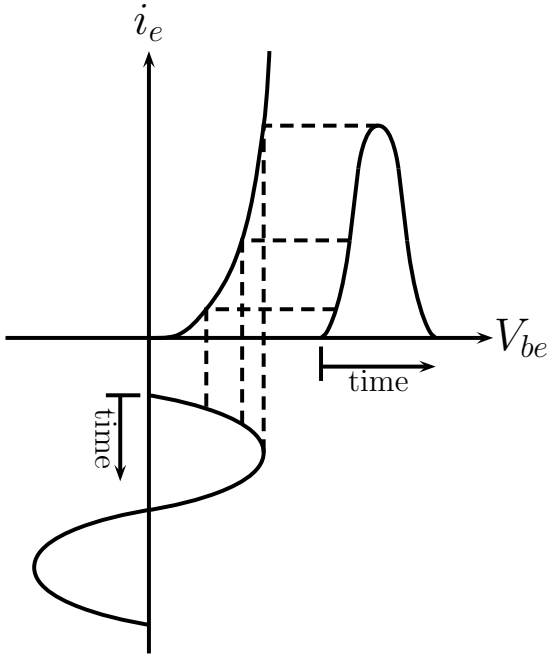

Figure 2.2: Exponential V-I characteristic of a BJT [5]

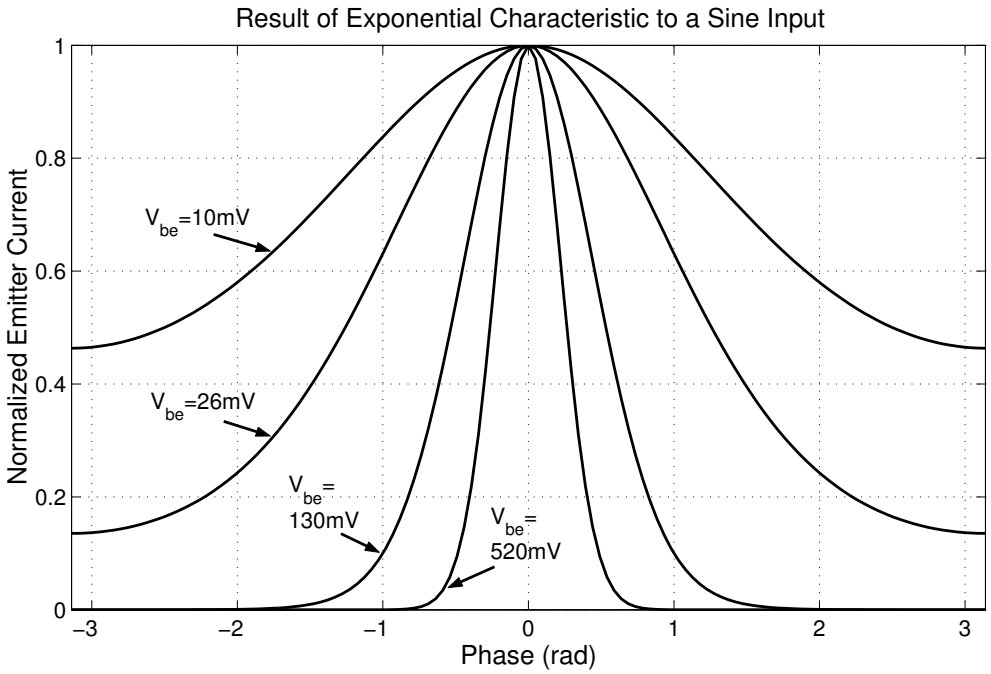

Figure 2.3: Result of sinusoidal input to a BJT [5]

and $I_n(x)$ is a modified Bessel function of the first kind, of order n and argument x. Substituting Equations 2.4 and 2.5 into Equation 2.3 results in

$$i_e = I_S e^{\frac{qV_{BE}}{kT}} \left[I_0(x) + \sum_{n=1}^{\infty} 2I_n(x) \cos(n\omega_o t) \right], \tag{2.6}$$

and with some rearranging gives

$$i_e = I_S e^{\frac{qV_{BE}}{kT}} I_0(x) \left[1 + \sum_{n=1}^{\infty} \frac{2I_n(x)}{I_0(x)} \cos(n\omega_o t) \right]. \tag{2.7}$$

Now, note that $I_S e^{\frac{qV_{BE}}{kT}} I_0(x)$ is the DC current; therefore Equation 2.7 becomes

$$i_e = I_{DC} \left[1 + \sum_{n=1}^{\infty} \frac{2I_n(x)}{I_0(x)} \cos(n\omega_o t) \right]. \tag{2.8}$$

A graphical representation of the harmonic content vs. drive level is shown in Figure 2.4. Notice that the harmonics asymptotically approach twice the DC current. Table 2.1 tabulates the values of $\frac{2I_n(x)}{I_0(x)}$ for $n = 1,$ and 2, and x from 0 to 20.

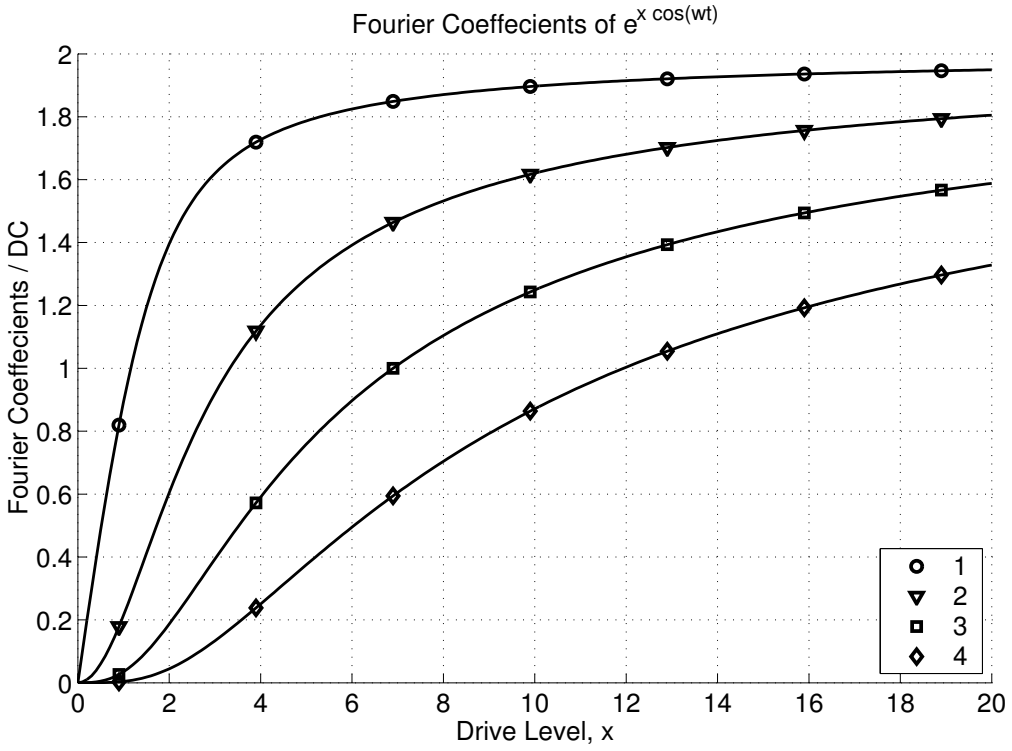

Figure 2.4: Harmonic content vs. drive level for exponential characteristic [5]

Table 2.1: $\frac{2I_n(x)}{I_0(x)}$ for $n = 1$ and 2, and x from 0 to 20 [5]

x	$\frac{2I_1(x)}{I_0(x)}$	$\frac{2I_2(x)}{I_0(x)}$
0.0	0.000	0.000
0.5	0.485	0.060
1.0	0.892	0.214
2.0	1.395	0.604
3.0	1.620	0.920
4.0	1.727	1.136
5.0	1.786	1.285
6.0	1.824	1.391
7.0	1.851	1.471
8.0	1.870	1.532
9.0	1.885	1.581
10.0	1.897	1.620
15.0	1.932	1.742
20.0	1.949	1.805

2.3 Three-Terminal Model

The three-terminal model method of oscillator design is a simple way of representing the feedback and active device in an oscillator circuit. This method requires drawing the model of the circuit at the fundamental frequency of oscillation. The tank capacitance and inductance are placed across the appropriate terminals in parallel with any conductances required for biasing. A model for the nonlinear device is then inserted in the circuit, and loop equations for the circuit can now be written.

For the purposes of this thesis, a bipolar junction transistor (BJT) will be used for the active device in the oscillator. However, the model can be used for other nonlinear characteristics by using a different nonlinear device model. When using the three-terminal model the common-collector, common-base, and common-emitter configurations all reduce to the same topology. The simplification to the three-terminal model is illustrated in Figure 2.5. A table relating the three-terminal model conductance values to the original circuit components is provided in Table 2.2. The common-collector topology will be used in this thesis.

For a BJT operating in a non-saturating environment the α-Model from Davis [6], shown in Figure 2.6, can be used. Once this model is inserted into the three-terminal model, the circuit can be rearranged and loop equations can be derived. Figure 2.7 shows the circuit with the α-model inserted, while Figure 2.8 has been rearranged to facilitate derivation of the loop equations. In Figure 2.8, the load has been represented as if it is included in the transistor model. With the basic case of an oscillator that does not saturate, the load resistance represented in Figure 2.8 is in series with a current source and has no effect on the design.

Let us first look at a couple of assumptions that make the design of an oscillator easier. First, we look at the impedance across the collector and emitter terminals. We have

$$Z_{ce} = \frac{1}{G_1 + j\omega C_1}. \tag{2.9}$$

If G_1 is small in comparison to ωC_1, then Z_{ce} can be approximated by $\frac{1}{j\omega C_1}$. The same high-Q assumption can be made for impedance across the base and emitter to give

$$Z_{be} = \frac{1}{G + G_2 + j\omega C_2} \simeq \frac{1}{j\omega C_2}. \tag{2.10}$$

Table 2.2: Equivalent conductances of three-terminal model for different oscillator topologies

	G_1	G_2	G_3	Load Resistance
Common-Collector	$\frac{1}{R_E}$	0	$\frac{1}{R_1} + \frac{1}{R_2}$	R_L
Common-Base	0	$\frac{1}{R_E}$	$\frac{1}{R_L}$	0
Common-Emitter	$\frac{1}{R_L} + \frac{1}{R_C}$	$\frac{1}{R_1} + \frac{1}{R_2}$	0	0

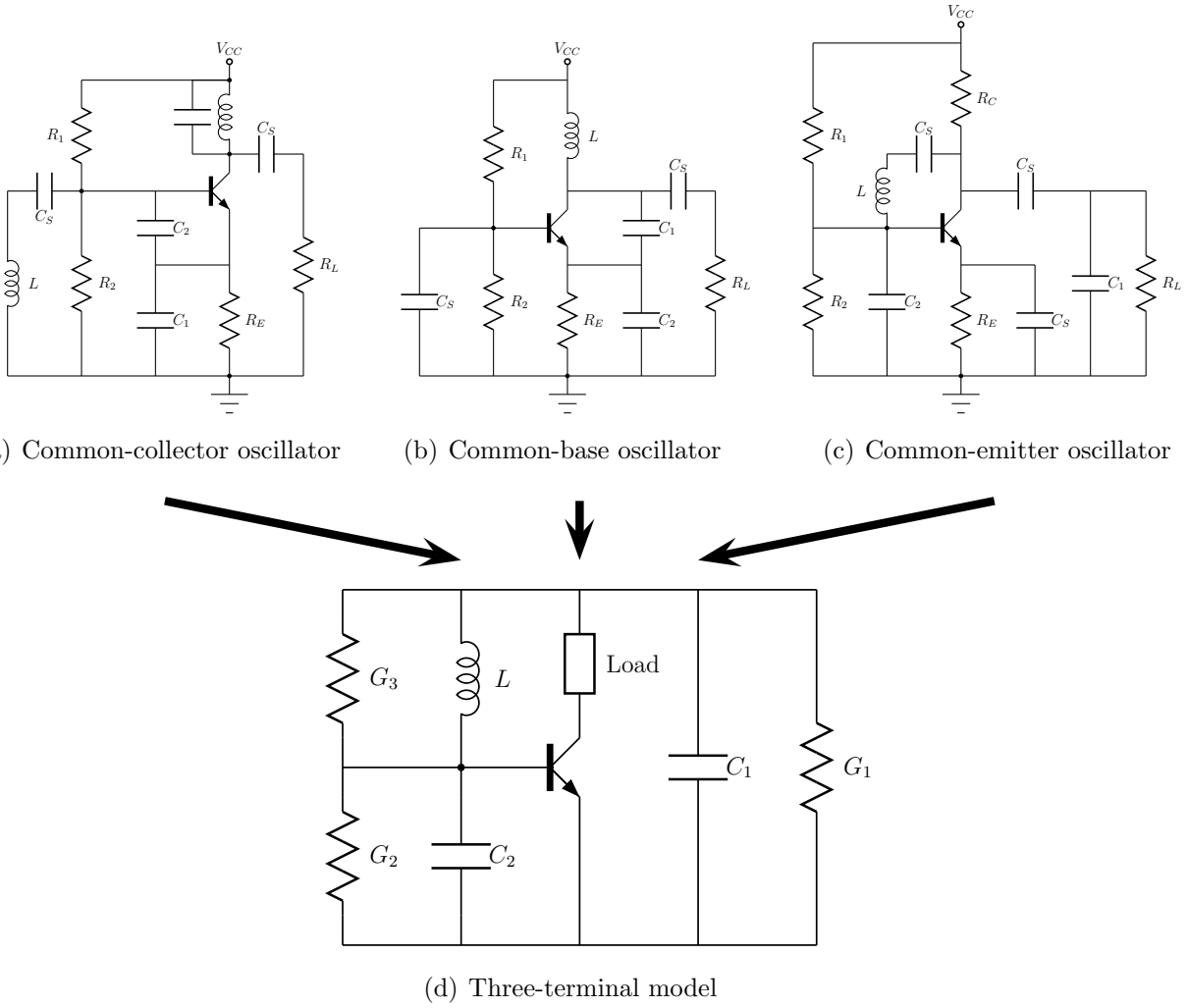

(a) Common-collector oscillator (b) Common-base oscillator (c) Common-emitter oscillator

(d) Three-terminal model

Figure 2.5: Three-terminal model simplifications (Used with permission of Dr. W. A. Davis [6])

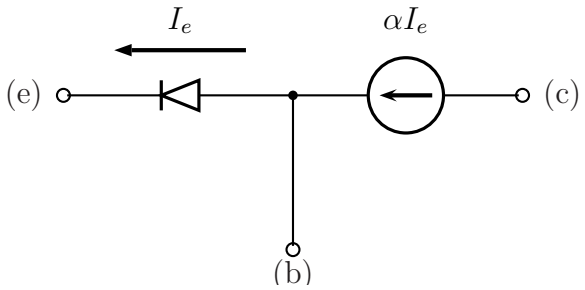

Figure 2.6: α-model of transistor (Used with permission of Dr. W. A. Davis [6])

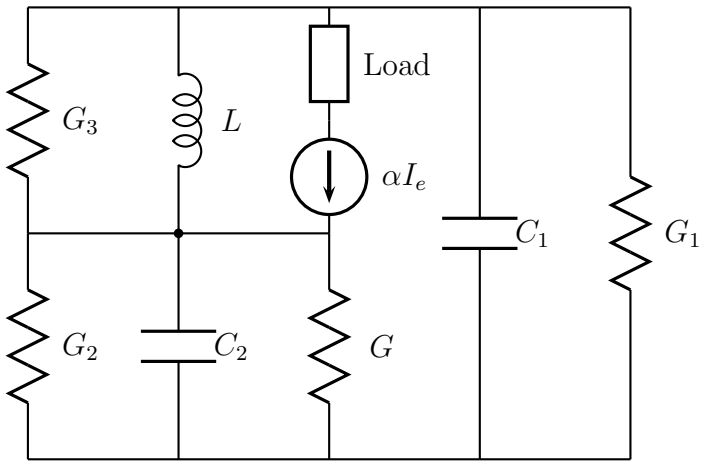

Figure 2.7: Three-terminal model with α transistor model inserted

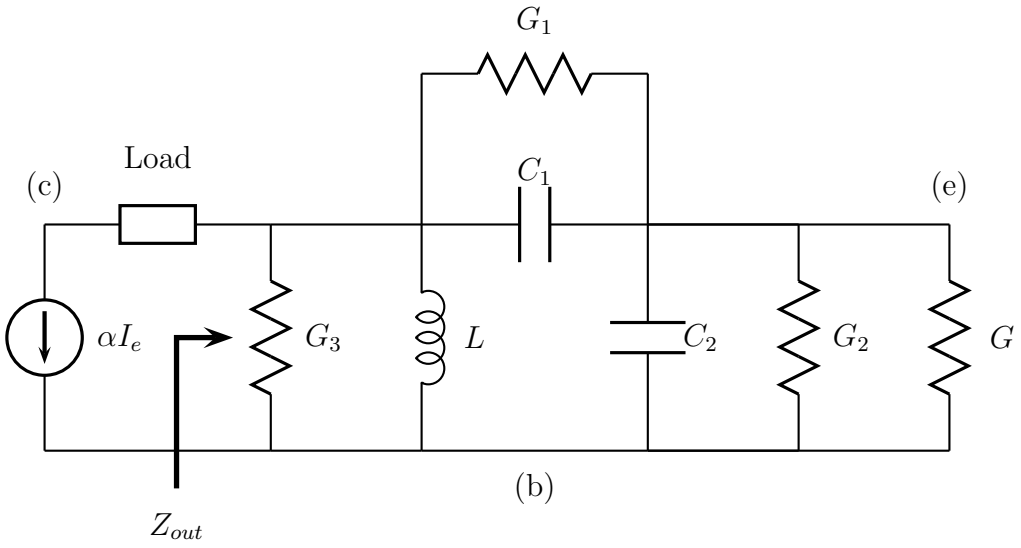

Figure 2.8: Rearranged three-terminal model (Used with permission of Dr. W. A. Davis [6])

Using these high-Q assumptions we can write

$$\frac{V_{eb}}{V_{cb}} \simeq \frac{\frac{1}{j\omega C_2}}{\frac{1}{j\omega C_2}+\frac{1}{j\omega C_1}} = \frac{\frac{1}{C_2}}{\frac{1}{C_2}+\frac{1}{C_1}} = \frac{C_1}{C_1+C_2} = \frac{1}{n}, \tag{2.11}$$

and

$$\frac{V_{ce}}{V_{cb}} \simeq \frac{\frac{1}{j\omega C_1}}{\frac{1}{j\omega C_2}+\frac{1}{j\omega C_1}} = \frac{C_2}{C_1+C_2} = \frac{n-1}{n}, \tag{2.12}$$

where

$$n = \frac{C_1+C_2}{C_1} = 1+\frac{C_2}{C_1} \tag{2.13}$$

resulting in a transformer-like circuit. Using these high-Q assumptions a loop equation for the oscillator can be derived. Note that

$$GV_{eb} = I_e, \tag{2.14}$$

which when multiplied by α results in

$$I_c = \alpha I_e = \alpha G V_{be}. \tag{2.15}$$

Multiplying by Z_{out} results in

$$I_c Z_{out} = V_{bc} = Z_{out}\alpha G V_{be}. \tag{2.16}$$

Dividing by n results in

$$\frac{1}{n}V_{bc} = V_{be} = \frac{1}{n}\alpha G Z_{out} V_{be}, \tag{2.17}$$

and dividing by V_{be} results in

$$1 = \frac{\alpha}{n} G Z_{out}. \tag{2.18}$$

Solving for G_{out} results in

$$G_{out} = \frac{\alpha G}{n}. \tag{2.19}$$

To find G_{out}, a combination of conservation of power and the high-Q assumption can be used. The power dissipated in G_{out} is the sum of the power dissipated in the individual conductances. Therefore we have

$$\begin{aligned} |V_{cb}|^2 G_{out} = |V_{cb}|^2 G_3 + |V_{ce}|^2 G_1 + |V_{eb}|^2 (G+G_2) \\ + |V_{cb}|^2 \left(\frac{1}{j\omega L}\right) + |V_{ce}|^2 j\omega C_1 + |V_{eb}|^2 j\omega C_2, \end{aligned} \tag{2.20}$$

and transforming the voltages results in

$$|V_{cb}|^2 G_{out} = |V_{cb}|^2 G_3 + \left(\frac{n-1}{n}\right)^2 |V_{cb}|^2 G_1 + \left(\frac{1}{n}\right)^2 |V_{cb}|^2 (G + G_2) + |V_{cb}|^2 \left(\frac{1}{j\omega L}\right) + \left(\frac{n-1}{n}\right)^2 |V_{cb}|^2 j\omega C_1 + \left(\frac{1}{n}\right)^2 |V_{cb}|^2 j\omega C_2. \quad (2.21)$$

Since α, n and G are real, the right side of Equation 2.21 must be real, with the imaginary part being 0. This requirement will give us a value for G_{out} and the frequency of oscillation.

For the real part of Equation 2.21 we have

$$G_{out} = G_3 + \left(\frac{n-1}{n}\right)^2 G_1 + \left(\frac{1}{n}\right)^2 (G + G_2)\,. \quad (2.22)$$

Substituting Equation 2.19 into Equation 2.22, a loop equation is formed which can give the required n for a specific drive level, or the drive level required by a specific n.

$$\frac{\alpha G}{n} = G_3 + \left(\frac{n-1}{n}\right)^2 G_1 + \left(\frac{1}{n}\right)^2 (G + G_2) \quad (2.23)$$

For the imaginary part of Equation 2.21 we have

$$0 = -\left(\frac{1}{\omega L}\right) + \left(\frac{n-1}{n}\right)^2 \omega C_1 + \left(\frac{1}{n}\right)^2 \omega C_2. \quad (2.24)$$

Solving Equation 2.24 for ω gives the frequency of oscillation as

$$\omega_o = \sqrt{\frac{C_1 + C_2}{L C_1 C_2}}. \quad (2.25)$$

Once a bias and drive level is decided on, Equations 2.23 and 2.25 are all that is needed to complete the basic oscillator design.

2.4 Oscillator Design

An oscillator is typically designed to deliver a required power into a specified load. To design the oscillator, the first step is to choose an oscillator topology and derive the three-terminal model and appropriate loop equations. The next step is to specify the drive level and bias required to produce the required power. Once a drive level and bias is specified, the loop equations can be solved, and the appropriate components can be selected for the

feedback. Parasitic effects of the transistor can be accounted for in the three-terminal model by including them as part of the feedback circuit.

2.5 Effects of Saturation on Design

Saturation can be used to provide a fixed output power level; however, the analysis becomes more difficult. When the base-collector junction of a BJT saturates, the simple α-model of Figure 2.6 is no longer correct. The model of Figure 2.9 must be used when saturation is involved. The saturation of the base-collector junction results in an added conductance between the base and collector terminals as well as another current source in the base-emitter junction.

Consider the three terminal model of Figure 2.10, which includes an ideal transformer and parallel RLC circuit representation of the feedback circuit. Also included are the extra source and conductance resulting from turning the base-collector junction on for a part of the cycle. Using Kirchhoff's Current Law (KCL) at the collector node results in

$$I_{FB}(\omega_m) = \alpha I_e(\omega_m) + G_C V_c(\omega_m) + \frac{1}{R}V_c(\omega_m) + \frac{1}{j\omega L}V_c(\omega_m) + j\omega C V_c(\omega_m), \tag{2.26}$$

where

$$\frac{1}{R} = G_3 + \frac{1}{n^2}G_2 + \left(\frac{n-1}{n}\right)^2 G_1. \tag{2.27}$$

We can also see from KCL at the emitter node that

$$I_{FB}(\omega_m) = \frac{1}{n}I_e(\omega_m) - \frac{\alpha_r}{n}I_r = -\frac{G}{n}V_e(\omega_m) + \frac{\alpha_r G_C}{n}V_c(\omega_m), \tag{2.28}$$

$$I_{FB}(\omega_m) = -\frac{G}{n^2}V_c(\omega_m) + \frac{\alpha_r G_C}{n}V_c(\omega_m). \tag{2.29}$$

Making some substitutions in Equation 2.26 results in

$$0 = \left(-\frac{\alpha_f G}{n} - \frac{\alpha_r G_C}{n} + \frac{G}{n^2} + G_C + \frac{1}{R} + \frac{1}{j\omega L} + j\omega C\right) V_c(\omega_m). \tag{2.30}$$

We can represent the gain of the device as a negative conductance of value $\alpha_f G/n + \alpha_r G_C/n$. To have a stable oscillation, note that we must have

$$\frac{\alpha_f G}{n} + \frac{\alpha_r G_C}{n} = \frac{G}{n^2} + G_C + \frac{1}{R}, \tag{2.31}$$

where G is the large signal conductance of I_{f1}/V_{be1} and G_C is the large signal conductance of I_{r1}/V_{bc1}. This equation is the saturating oscillator loop equation.

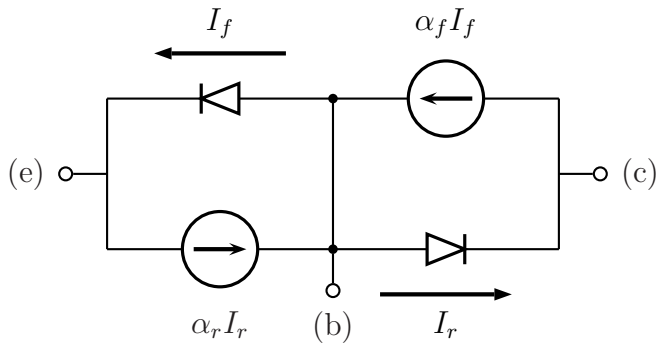

Figure 2.9: Large signal equivalent circuit based on Ebers-Moll equations

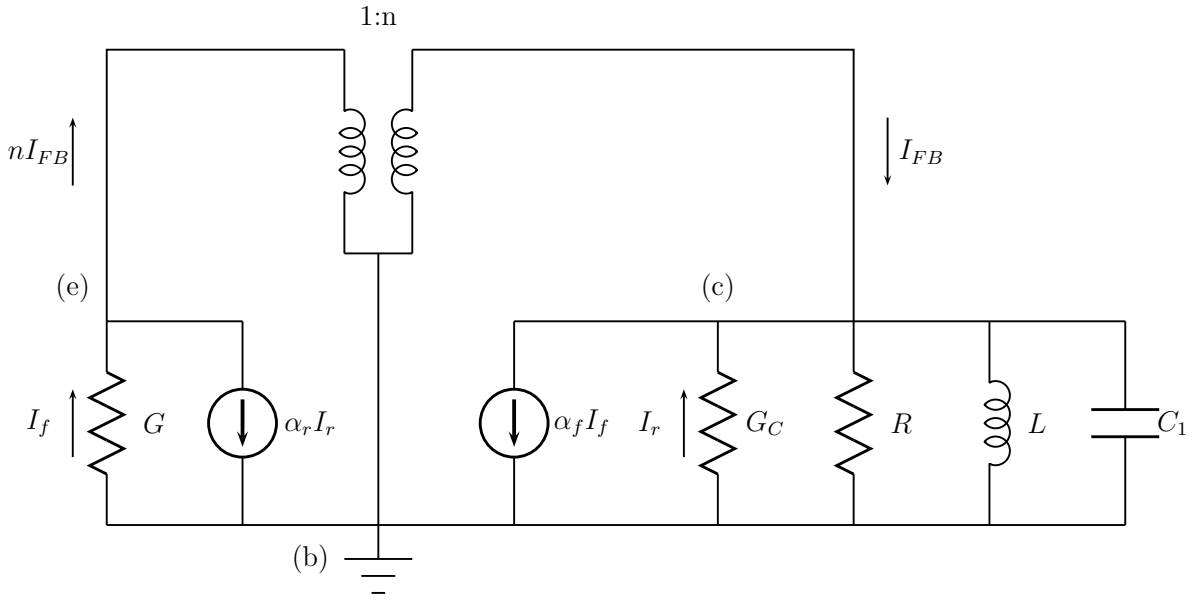

Figure 2.10: Three-terminal model with ideal transformer and parallel RLC circuit representing the feedback for a saturating oscillator

When saturating the transistor, the n does not change, yet a dynamic resistance appears across the base-collector junction that loads the output to control the output level to the clipped voltage of saturation. This results in a limited drive level, a lower Q and a change in the transistor bias. For biasing schemes such as a resistor bias, an iterative process or simulation tool must be used for the analysis of a saturating oscillator. If a constant current source bias is used, a reasonable approximation to the operation of a saturating oscillator can be made through the use of the nonlinear design concepts discussed in this chapter.

When designing a common collector oscillator, the load can be added between the collector terminal and ground. This can cause saturation if the voltage across this load becomes

large. A tuned circuit can help by providing a more sinusoidal voltage as opposed to a pulse the shape of the collector current pulses. This load resistor will also change the analysis of the oscillator if saturation occurs. Note that with a saturating transistor this load is no longer in series with a current source, but the load is in series with a parallel combination of a current source and the conductance of the base-collector junction. A transformation can be done to include the load in the source and conductance combination, but the details of this transformation will not be discussed here.

We will continue in the next chapter by showing some oscillator examples. We will see how our design process results in a close agreement with the results provided by the Advanced Design System (ADS) [1] harmonic balance simulation. We will also show the results of some ADS simulations which include a load resistor from the collector to ground.

Chapter 3

Example Oscillator Designs

Using the techniques of Chapter 2, two example oscillators will be designed. First, we will look at an oscillator that does not saturate. Then, we will modify the oscillator to make it saturate. We will use a current mirror biasing scheme for our examples. For the common-collector circuit topology, the load can be easily placed from the collector to ground. If one makes sure to keep the voltage across the load small enough so that the transistor does not saturate, the oscillator design and noise performance are not affected. The reason the load has no effect on the oscillator is that the load is in series with the current source of the transistor model. This isolation of the load is convenient to prevent changes in oscillator performance resulting from connection to a device, such as a mixer, that can have a varying load impedance across the frequency range of interest. If the transistor saturates, there is a further complication, because the load is in series with a parallel combination of a current source and the base-collector dynamic conductance, G_C, created from turning on the base-collector junction. Buffering of the load is no longer achieved with a dynamic base-collector conductance present. This complication can be dealt with using source transformations, but will not be discussed here. For other topologies, the load is a part of the three-terminal model and does not create this complication. In our development, we will use an ideal short for the load which will simplify the analysis of the saturating oscillator.

3.1 Non-Saturating Common-Collector Oscillator Example

Consider the oscillator circuit shown in Figure 3.1. An oscillator is normally designed to provide a specified output power to a load. Since we are assuming the load to be a short, we will design our oscillator to be biased with a DC emitter current of 10 mA. We will see that a larger drive level will reduce noise, so for our example let us pick a drive level of $x = 20$

corresponding to $V_{be1} = 520$ mV. This choice for x should provide decent noise performance. For illustration purposes a frequency of 1 GHz will be used.

For this oscillator topology, note that G_3 and G_2 are both zero. Furthermore, G can be computed to be

$$G = \frac{I_{e1}}{V_{be1}} = \frac{\frac{2I_1(x)}{I_0(x)} I_{e0}}{V_{be1}} = \frac{(1.95)(10 \text{ mA})}{520 \text{ mV}} = 37.5 \text{ mS}. \tag{3.1}$$

The emitter resistor, R_4 in Figure 3.1, is the resistor that makes up the G_1 of the three-terminal model. In order to choose a value for this resistor consider that too large a resistor will result in saturation. For this example we will choose R_1 to be 100Ω, which will give a DC emitter voltage of 1 V, and will result in a G_1 of 10 mS. We now have what we need to solve Equation 2.23. Substituting values into Equation 2.23 results in an n of 1.0101 or 4.7024. Using an n value near 1 should be avoided to avoid a small collector-emitter voltage which is near the noise level. Therefore, an n of 4.7024 will be used. The value of α will vary with different transistors. In general, the value of α will not change the outcome of the problem greatly. For this example a value of 0.99 will be used for α. Choosing a Q of

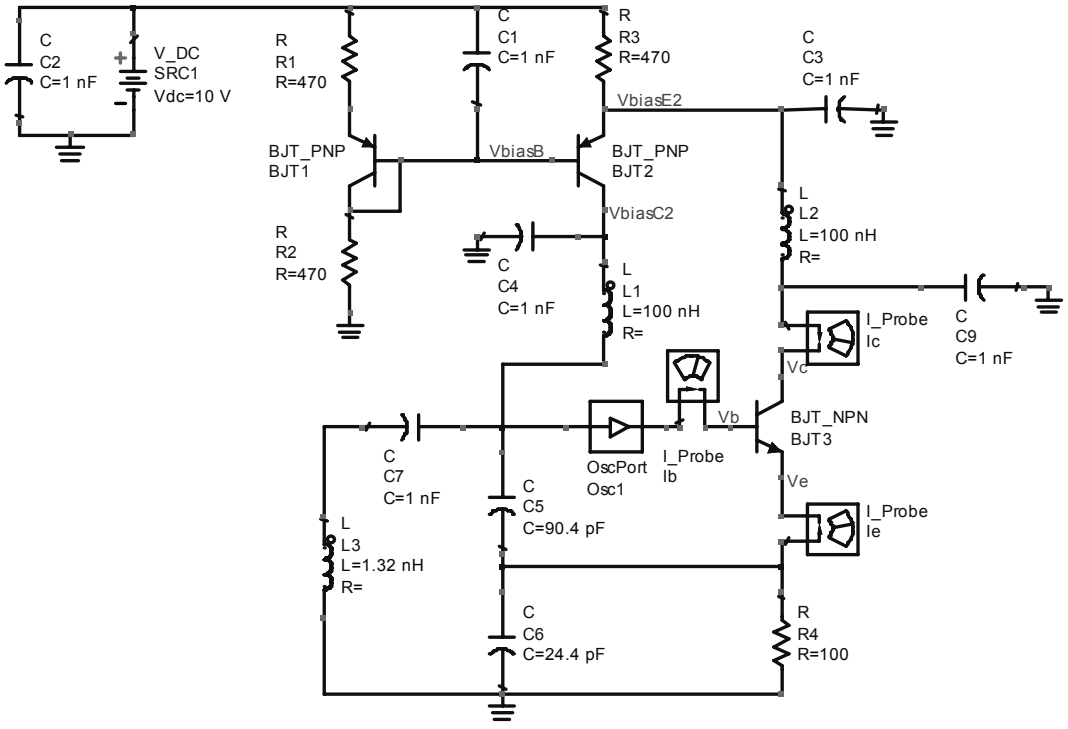

Figure 3.1: ADS circuit of non-saturating oscillator

15 for our feedback is a good compromise between noise performance and having reasonable component values. Using the Q we can compute the required inductance as

$$L = \frac{n\alpha}{G\omega Q} = 1.32 \text{ nH}. \tag{3.2}$$

Now values for C_2 and C_1 can be computed as

$$C_2 = \frac{n}{\omega^2 L} = 90.436 \text{ pF}, \tag{3.3}$$

and

$$C_1 = \frac{C_2}{n-1} = 24.427 \text{ pF}. \tag{3.4}$$

Using the Advanced Design System (ADS) [1], the oscillator can be simulated using a harmonic balance simulation. Figure 3.2 shows the harmonic content of the base-emitter voltage. It can be seen that the fundamental component is close to the value of 520 mV which we designed for. Also, note that the base-emitter voltage is fairly sinusoidal. A time domain plot of the base-emitter voltage is shown in Figure 3.3.

The harmonic content of the collector current is shown in Figure 3.4. The harmonic levels are approximately what would be calculated through the use of the modified Bessel functions. Figure 3.5 is a time domain plot of the collector, base, and emitter currents. Note that the current is of a pulse nature as described in Chapter 2.

Figure 3.6 shows the collector, base, and emitter voltage in the same plot. From this plot, we can see that there is enough of a separation of the base and collector voltage to prevent the base-collector junction from turning on.

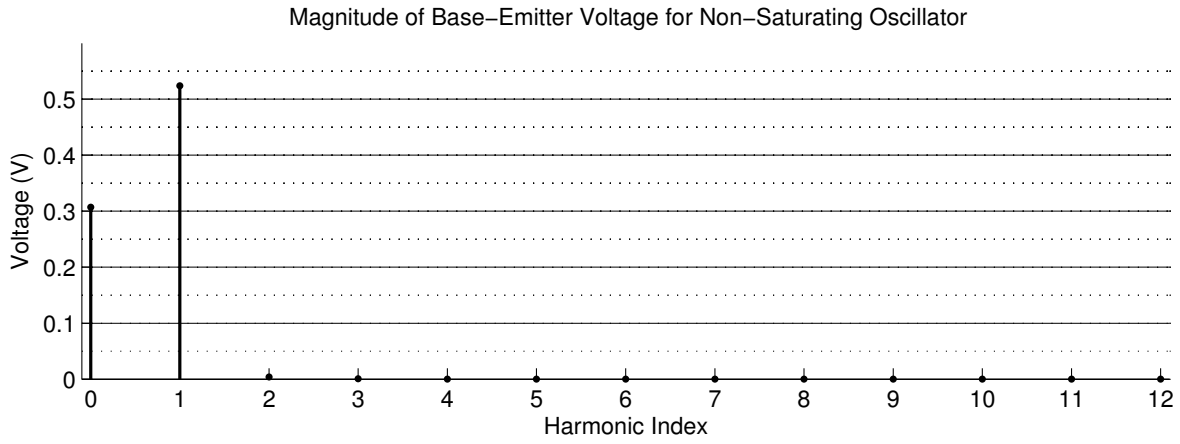

Figure 3.2: Harmonic content of base-emitter voltage for non-saturating oscillator

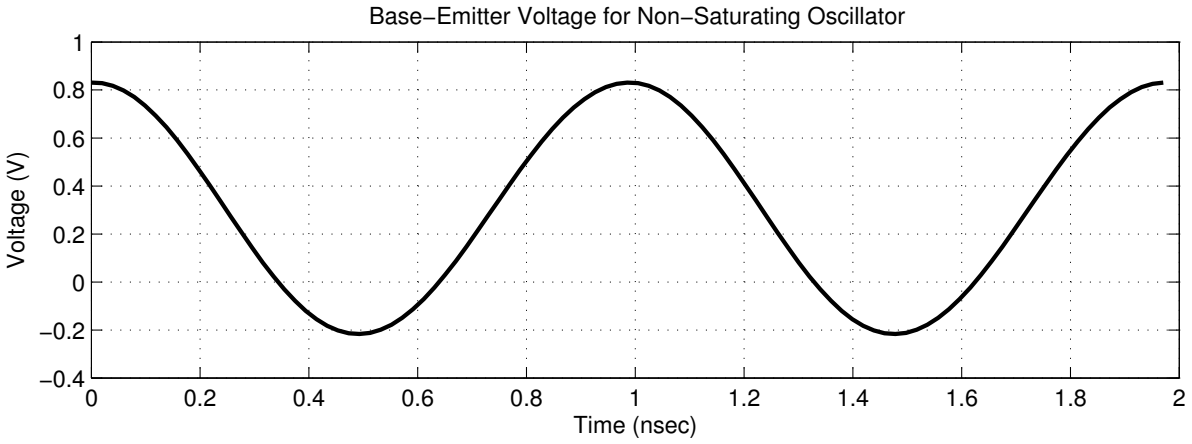

Figure 3.3: Time domain plot of base-emitter voltage for non-saturating oscillator

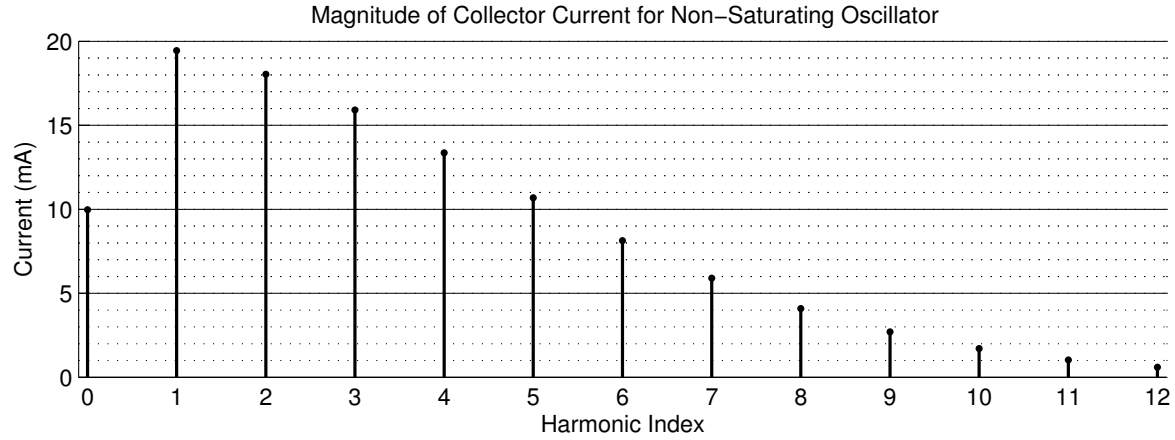

Figure 3.4: Harmonic content of collector current for non-saturating oscillator

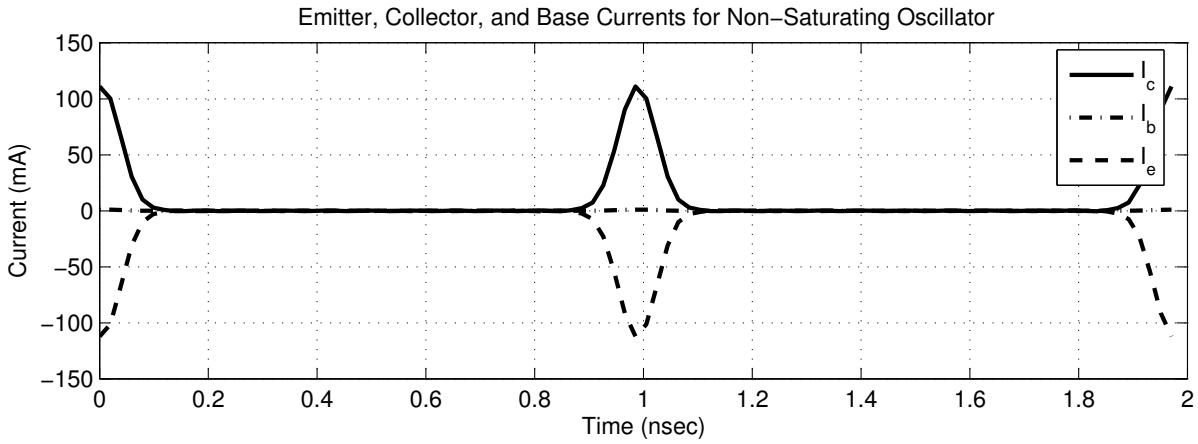

Figure 3.5: Time domain plot of collector, base, and emitter current for non-saturating oscillator

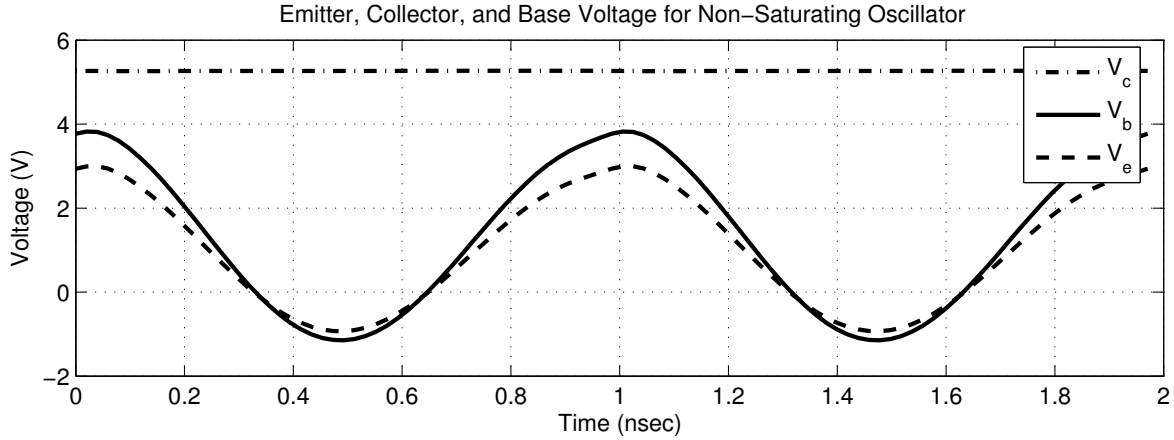

Figure 3.6: Time domain plot of collector, base, and emitter voltage for non-saturating oscillator

The design of an oscillator is fairly straight forward. We have seen that the design process can result in predicted voltage and current levels that agree closely with simulation tools. Understanding the design process and how oscillators work can give a designer a feel of what can be done to achieve the results they require. Now that we have seen a non-saturating oscillator designed, we can investigate what happens when an oscillator saturates.

3.2 Saturating Common-Collector Oscillator Example

For an example of an oscillator that saturates, let us modify the non-saturating oscillator of Section 3.1. Looking at Figure 3.6 we can see that if we lower the collector voltage below 4 V the transistor will begin to saturate. Changing the supply voltage to 4 V and setting the current to 10 mA in a DC simulation will result in an oscillator that saturates. Figure 3.7 is the ADS circuit for the saturating oscillator.

The biasing scheme of the oscillator results in a constant collector voltage and emitter current. This constant collector voltage and emitter current allows us to analyze the circuit

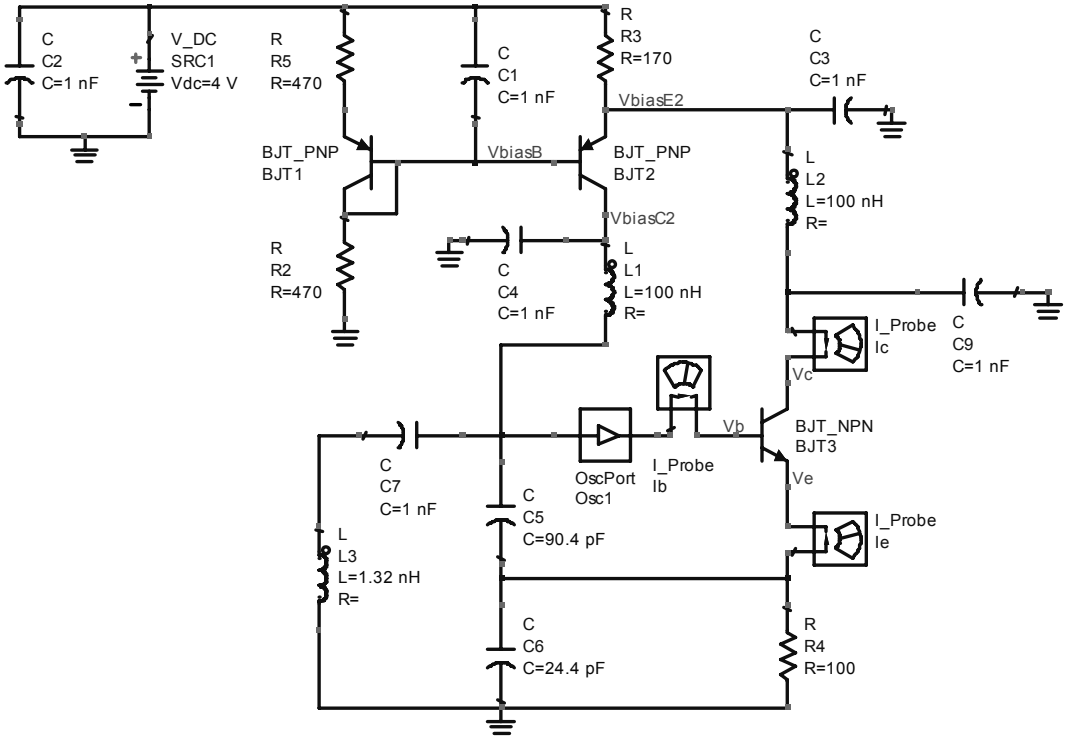

Figure 3.7: ADS circuit of saturating oscillator

without resorting to an iterative process due to a changing bias. We know that the collector voltage will be fixed at

$$V_c = 4 \text{ V} - (0.01\text{A})170\Omega = 2.3 \text{ V}. \tag{3.5}$$

We also know that with a constant emitter current, of 10 mA, the emitter voltage is fixed at 1 V. This gives us a DC collector-emitter voltage of 1.3 V. With the fundamental components of the tank voltage being sinusoidal, the transistor will saturate when $V_{ce1} = 1.3$ V. With an n of 4.7024, the base-emitter voltage is limited to

$$V_{be1} = \frac{V_{ce1}}{n-1} = 351 \text{ mV}. \tag{3.6}$$

Using the loop equation of Equation 2.31, we can note that

$$\frac{\alpha_f}{n}\left(\frac{I_{f1}}{V_{be1}}\right) + \frac{\alpha_r}{n}\left(\frac{I_{r1}}{V_{bc1}}\right) = \left(\frac{n-1}{n}\right)^2 G_1 + \frac{1}{n^2}\left(\frac{I_{f1}}{V_{be1}}\right) + \frac{I_{r1}}{V_{bc1}}, \tag{3.7}$$

or

$$I_{f1} = \frac{0.006 + 0.542 I_{r1}}{0.471}. \tag{3.8}$$

Writing the currents using Bessel functions and the DC current we can note that

$$I_{f0} = \frac{I_0(x_f)}{2I_1(x_f)}\left(\frac{0.006 + 1.08\left(\frac{I_1(x_r)}{I_0(x_r)}\right) I_{r0}}{0.471}\right). \tag{3.9}$$

We also know that

$$I_{f0} = \alpha_r I_{r0} + 0.010. \tag{3.10}$$

Using Equations 3.9 and 3.10, we can solve for I_{f0} and I_{r0} to get 12.3 mA and 4.6 mA.

If we look at the harmonic content of the collector current in Figure 3.8, the base current in Figure 3.9, and the emitter current in Figure 3.10, then we can see how these currents relate to the I_f and I_r currents of the transistor model of Figure 2.9. Note that

$$I_e = I_f - \alpha_r I_r, \tag{3.11}$$

$$I_c = \alpha_f I_f - I_r, \tag{3.12}$$

and

$$I_b = (1-\alpha_f) I_f + (1-\alpha_r) I_r. \tag{3.13}$$

From these equations we can compute I_f and I_r by noting that

$$I_f = \frac{2I_e - I_c}{2 - \alpha_f} \tag{3.14}$$

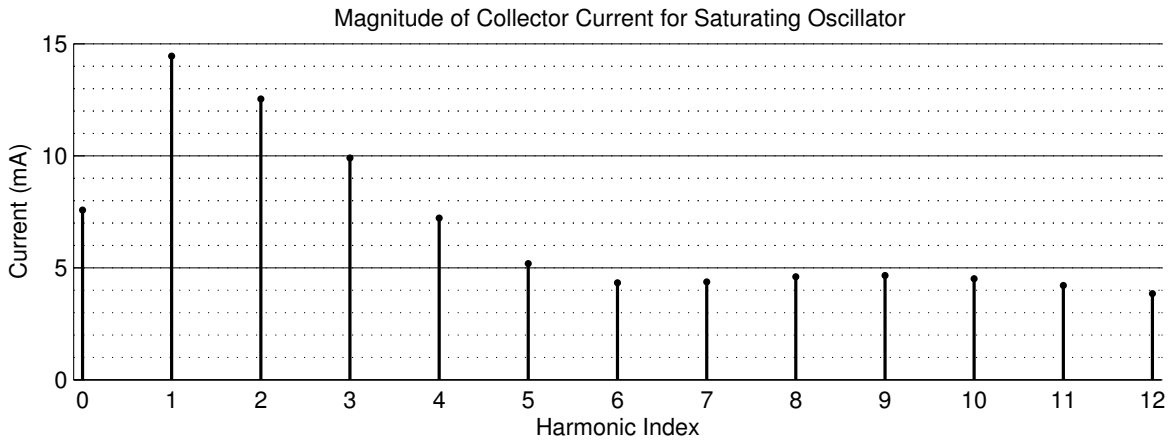

Figure 3.8: Harmonic content of collector current for saturating oscillator

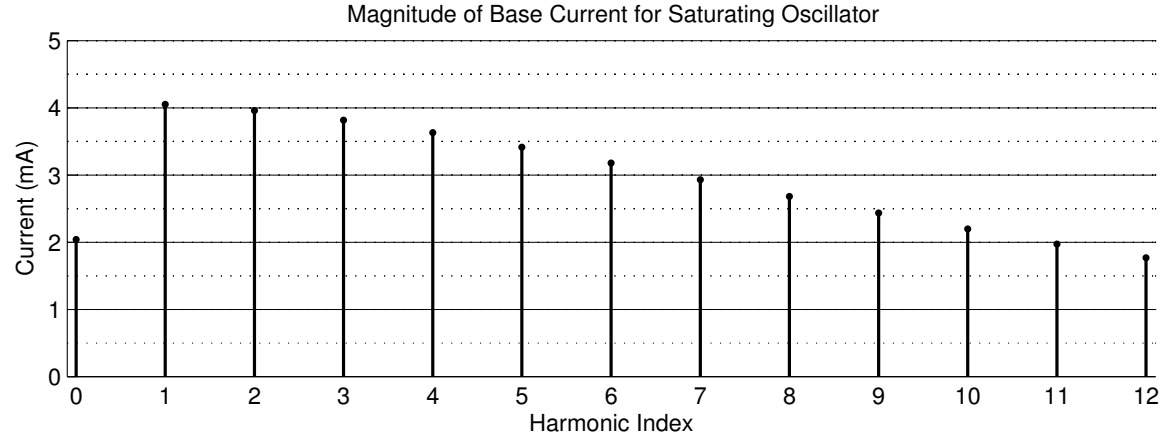

Figure 3.9: Harmonic content of base current for saturating oscillator

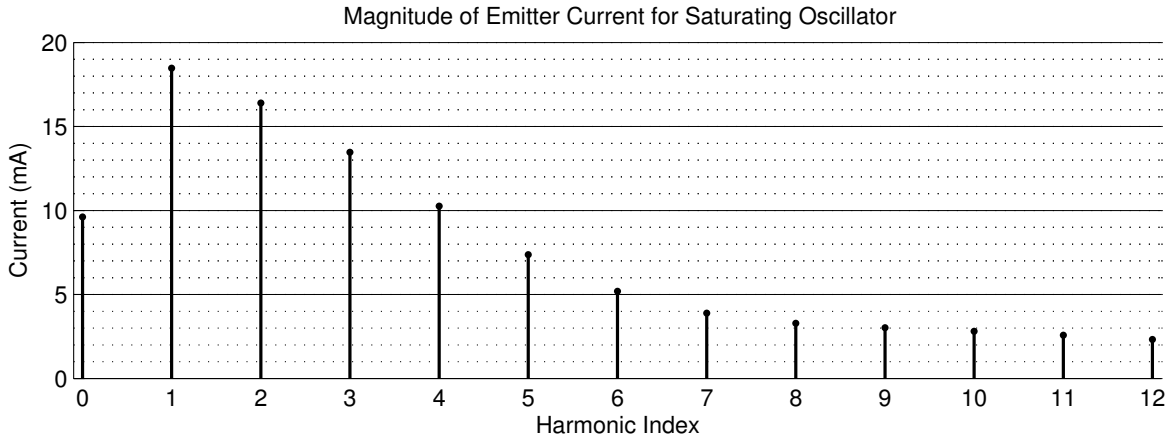

Figure 3.10: Harmonic content of emitter current for saturating oscillator

and

$$I_r = \frac{\alpha_f I_e - I_c}{1 - \alpha_r \alpha_f}. \tag{3.15}$$

Using Equations 3.14 and 3.15 we can compute I_f and I_r from the ADS simulation. The results of this computation are listed in Table 3.1.

From the ADS simulation we can see that the oscillator saturates. Figure 3.11 shows that the transistor base-collector junction is turning on for part of the cycle. This turning-on of the base-collector junction results in a dynamic resistance which limits the voltage levels of the oscillator. From Figure 3.12, we can see that the drive level has been reduced to a value of about 356 mV corresponding to $x = 13.8$. The base-emitter conductance has therefore been increased to

$$G = \frac{I_{f1}}{V_{be1}} \approx 62.6 \text{ mS}. \tag{3.16}$$

We can also see that the base-emitter voltage and the base-collector voltage are relatively sinusoidal.

Note that the DC component of the collector current, in Figure 3.8, is no longer 10 mA. This is because the saturation of the base-collector junction is creating a substantial current into the base. The harmonic content of the base current is shown in Figure 3.9. The oscillator is biased such that the sum of the base and collector currents is 10 mA. Also, note in the time domain plot of the transistor currents, Figure 3.13, there is a notch in the collector current. The current that produces this notch is split between the base current and the emitter current.

3.3 Effects of a Collector Load on Common-Collector Oscillator Performance

To illustrate the effects of adding a load on the collector of a common-collector oscillator, first consider the non-saturating oscillator of Section 3.1. If this oscillator is modified to include a resistive load, as illustrated in Figure 3.14, the result is a large enough voltage drop across the load to cause the oscillator to saturate. This is shown in Figure 3.15, a plot of the voltages at the transistor terminals. Note the pulse shape of the collector voltage. This pulse-shaped voltage is a result of the pulse-shaped current flowing through the load resistance, shown in Figure 3.16. Also note that the base current is not a sharp pulse like in

Table 3.1: Forward and reverse transistor currents for saturating oscillator

	$n = 0$	$n = 1$	$n = 2$
I_f	11.53 mA	22.29 mA	20.06 mA
I_r	3.85 mA	7.61 mA	7.32 mA

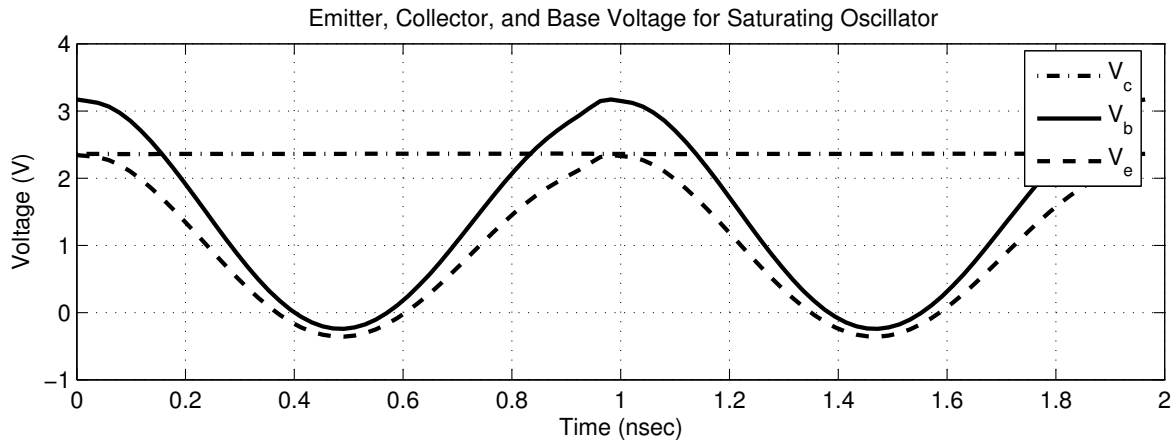

Figure 3.11: Time domain plot of collector, base, and emitter voltage for saturating oscillator

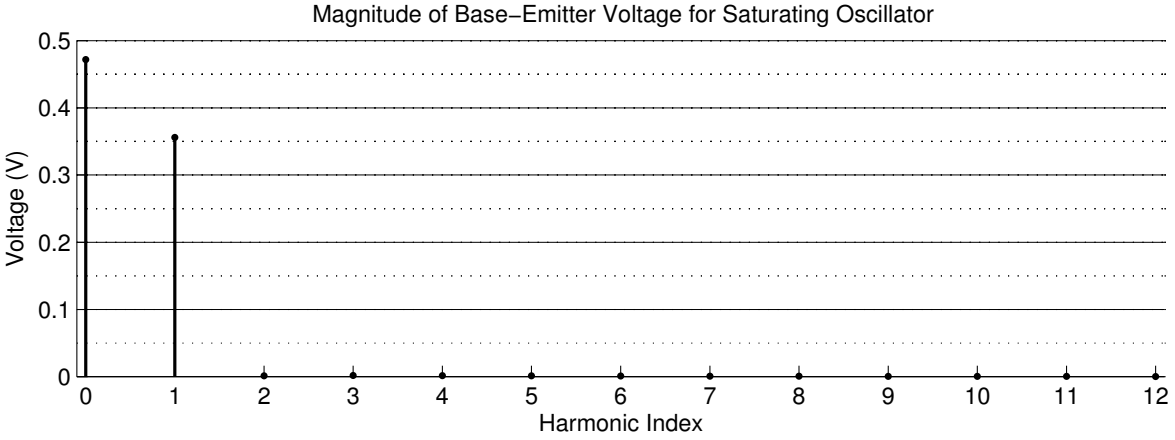

Figure 3.12: Harmonic content of base-emitter voltage for saturating oscillator

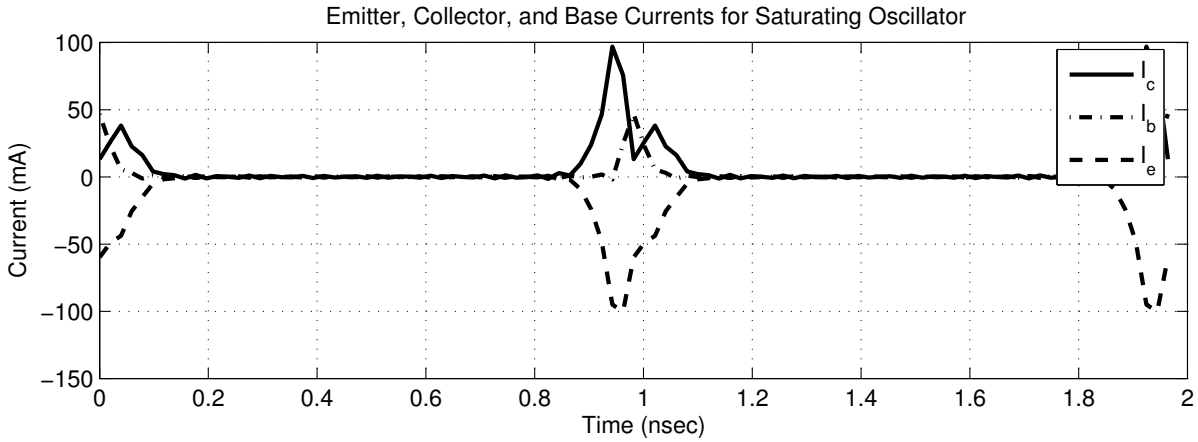

Figure 3.13: Time domain plot of collector, base, and emitter current for saturating oscillator

the saturating case of Section 3.2. This widening of the base current pulse is a result of the base-collector voltage no longer being sinusoidal.

Now consider adding a tuned circuit to the load to filter the output. An example is illustrated in Figure 3.17. Note, in Figure 3.18, that the oscillator does not saturate because the voltage across the load is now sinusoidal and does not become large enough for saturation to occur. We can also see, in Figure 3.19, that the current is back to the shape of the current in the non-saturating oscillator without a load.

Now consider the saturating oscillator of Section 3.2. If this oscillator is modified to include a resistive load, as illustrated in Figure 3.20, the result is an oscillator that saturates harder due to the voltage drop across the load. This is shown in Figure 3.21, which is a plot of the voltages at the transistor terminals. Note the pulse shape of the collector voltage. This pulse-shaped voltage is a result of the pulse-shaped current flowing through the load resistance, shown in Figure 3.22. Also note that the base current is not as sharp of a pulse as the base current pulse of the saturating oscillator without a load. This widening of the base current pulse is a result of the base-collector voltage no longer being sinusoidal.

Now consider adding a tuned circuit to the load to filter the output, as shown in Figure 3.23. Note, in Figure 3.24, that the oscillator still saturates about as hard as the case of

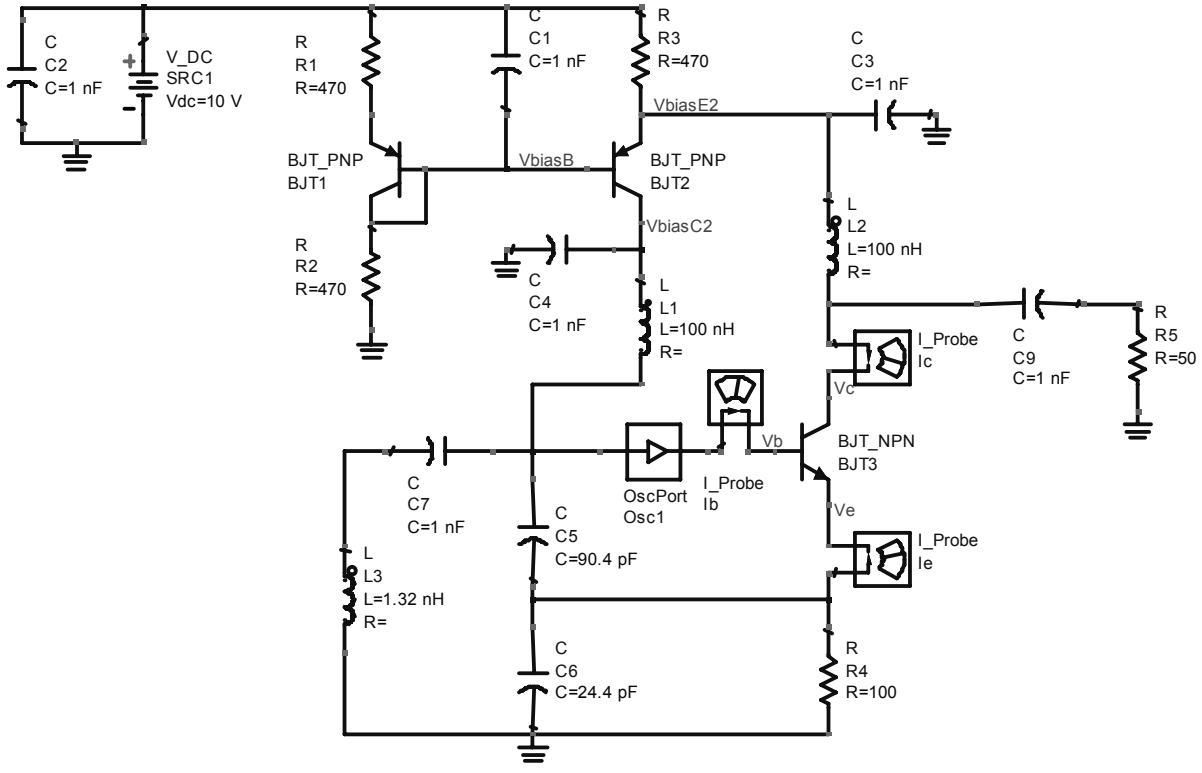

Figure 3.14: ADS circuit of a resistive load added to a non-saturating oscillator

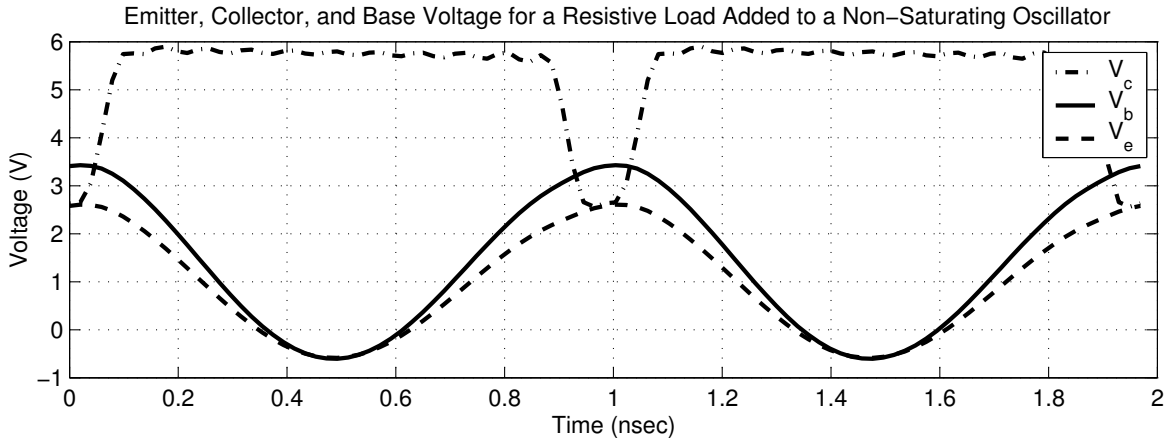

Figure 3.15: Emitter, collector, and base voltages for a resistive load added to a non-saturating oscillator

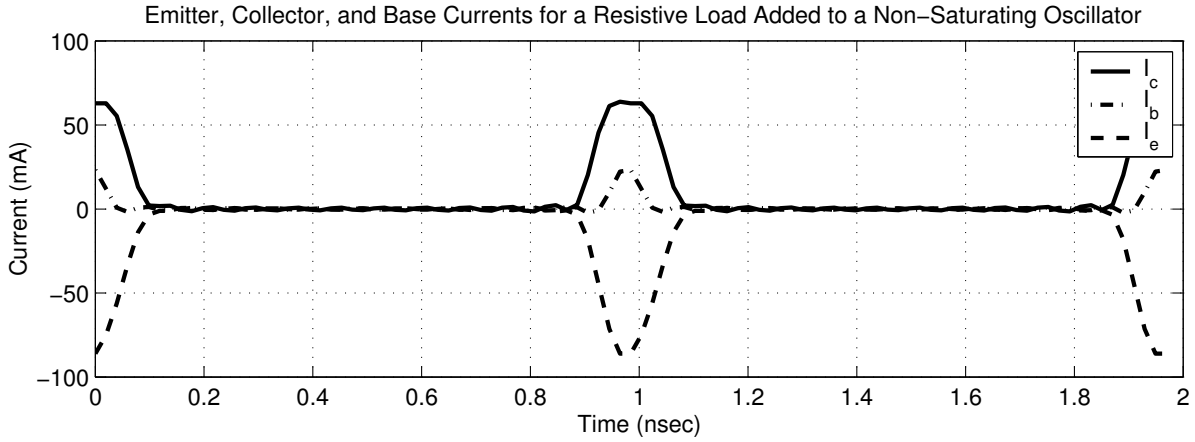

Figure 3.16: Emitter, collector, and base currents for a resistive load added to a non-saturating oscillator

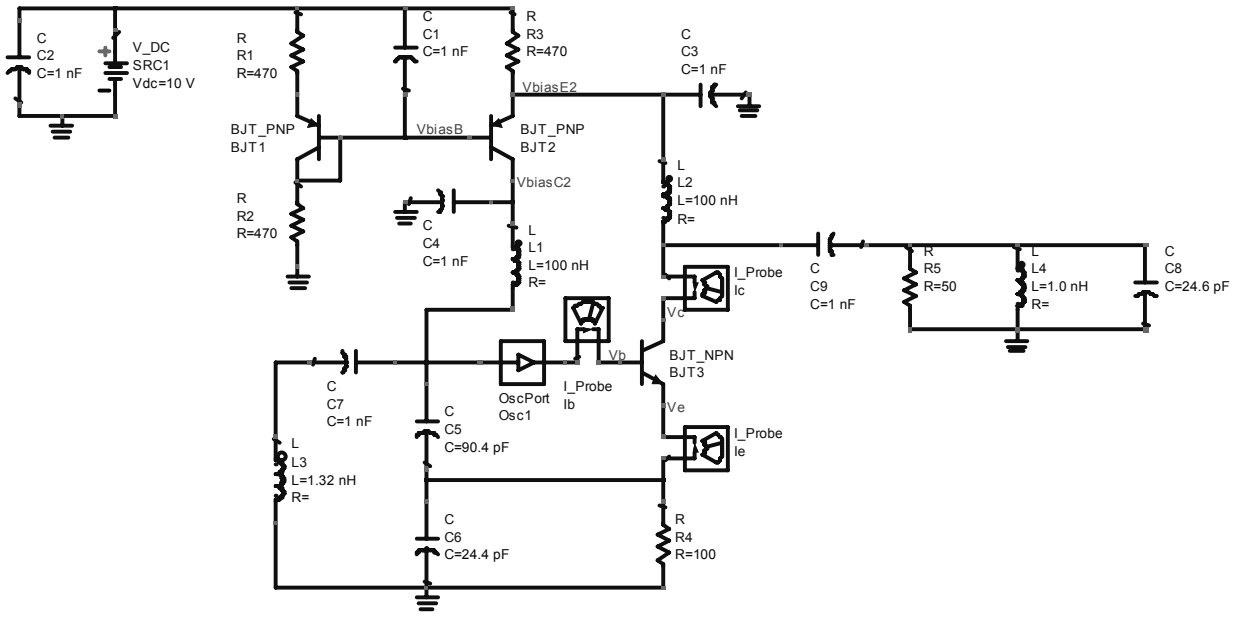

Figure 3.17: ADS circuit of a tuned load added to a non-saturating oscillator

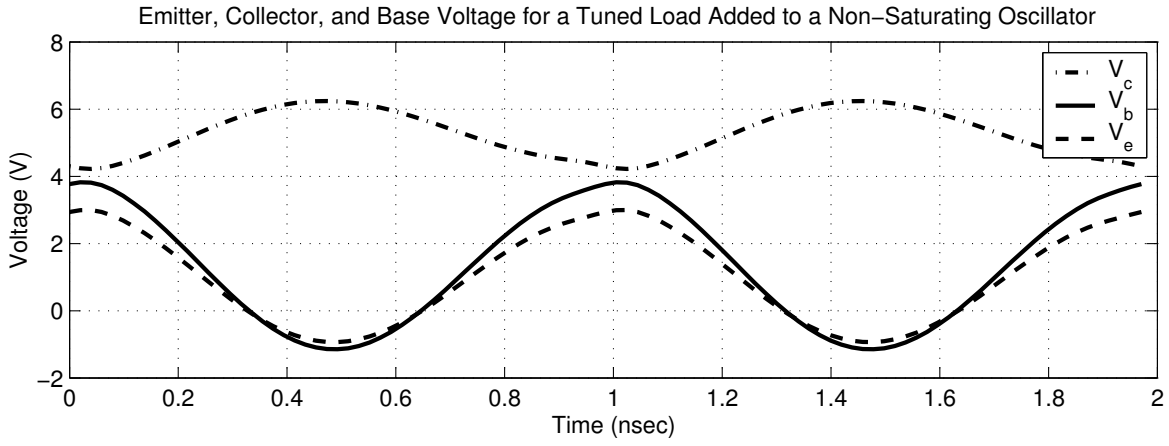

Figure 3.18: Emitter, collector, and base voltages for a tuned load added to a non-saturating oscillator

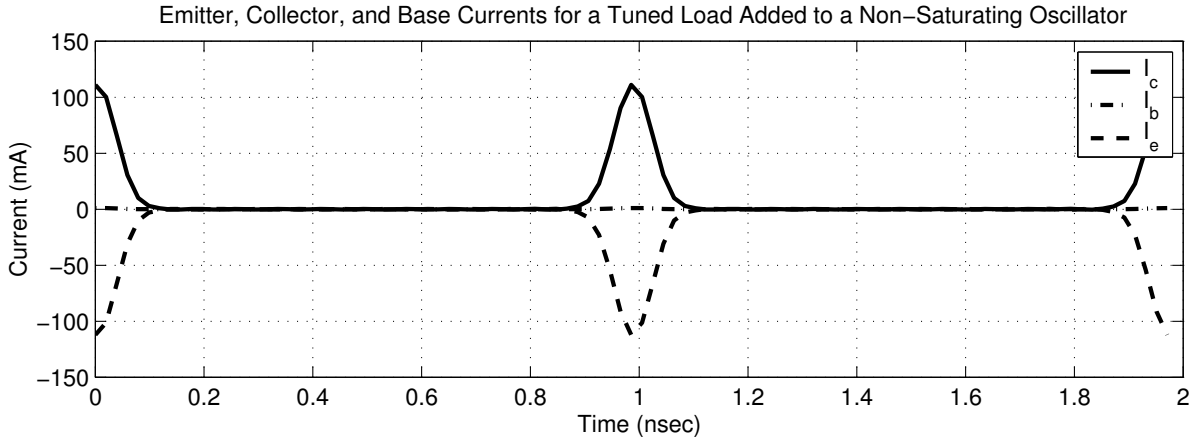

Figure 3.19: Emitter, collector, and base currents for a tuned load added to a non-saturating oscillator

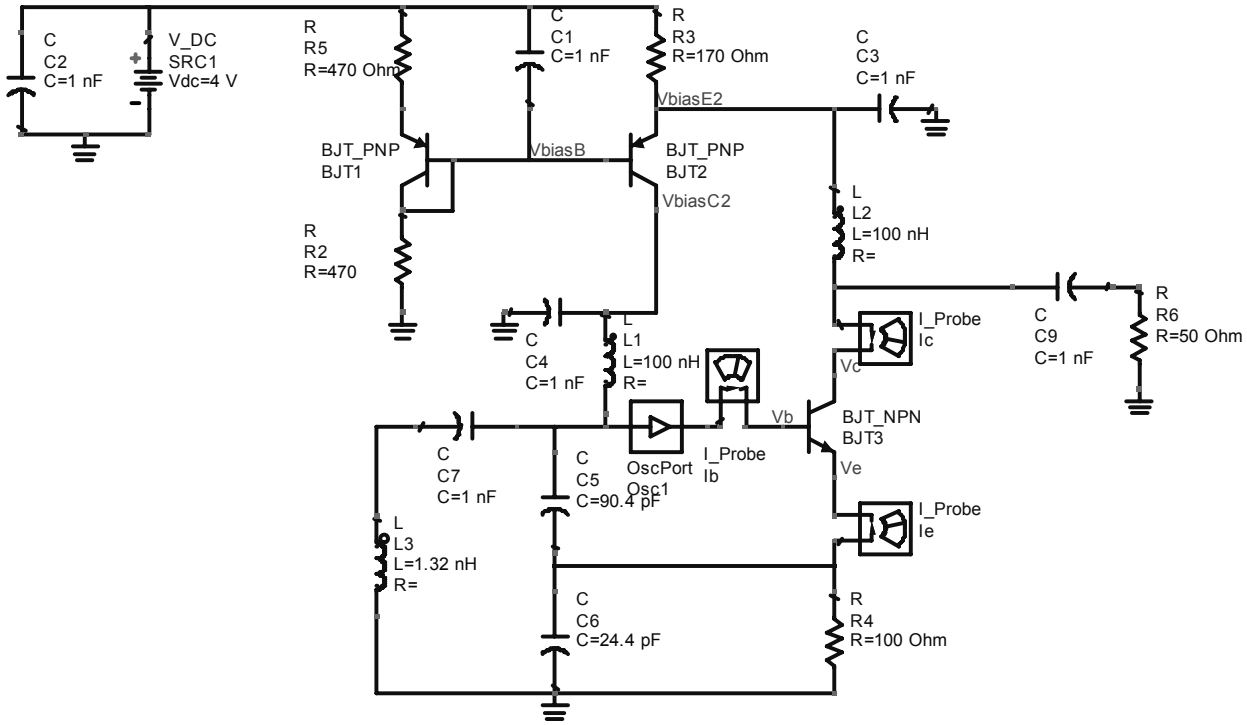

Figure 3.20: ADS circuit of a resistive load added to a saturating oscillator

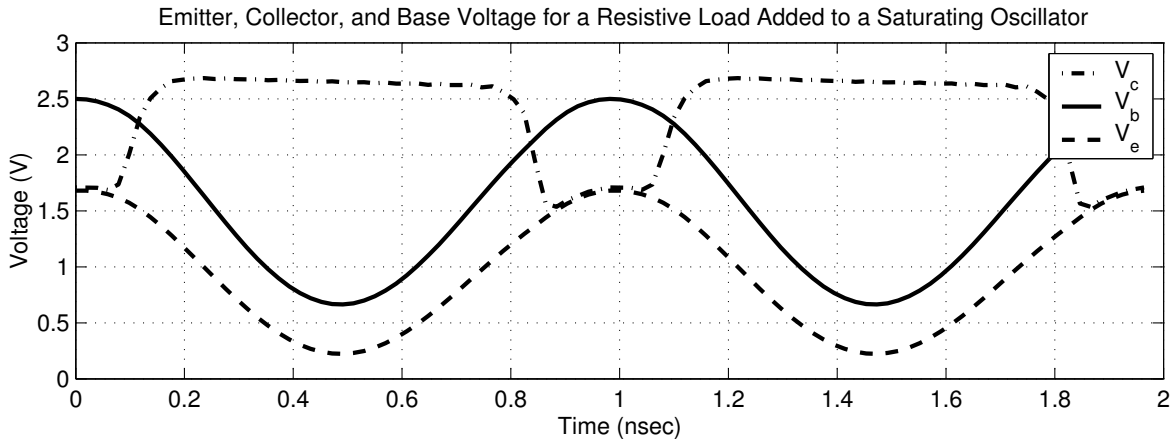

Figure 3.21: Emitter, collector, and base voltages for a resistive load added to a saturating oscillator

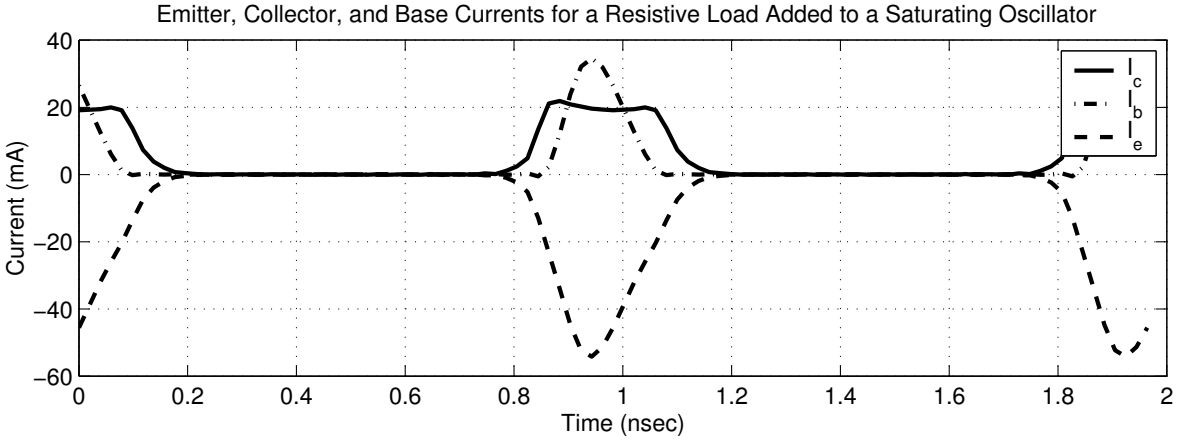

Figure 3.22: Emitter, collector, and base currents for a resistive load added to a saturating oscillator

a resistive load added to the saturating oscillator. Note that the difference between this case and the resistive load case is the shape of the current pulse, shown in Figure 3.25. In the case of a tuned load added to a saturating oscillator, the collector current is notched by a sharp base current pulse. This is the same behavior as the saturating oscillator without a load. The reason we have this notched current shape for the tuned load but not the resistive load is that the tuned load has a sinusoidal base-collector voltage. The sinusoidal base-collector voltage creates a sharper base current pulse than the non-sinusoidal voltage of the resistive load case.

The techniques used here to design and analyze oscillators are reasonably robust in predicting the behavior of an oscillator, even with saturation. With the knowledge of how an oscillator behaves, we can begin to look at how noise is produced in an oscillator and how to predict the noise level of the sidebands. With the knowledge of how to predict the noise level in a simple oscillator, one can gain insight about the situations with a collector load that were discussed in this section.

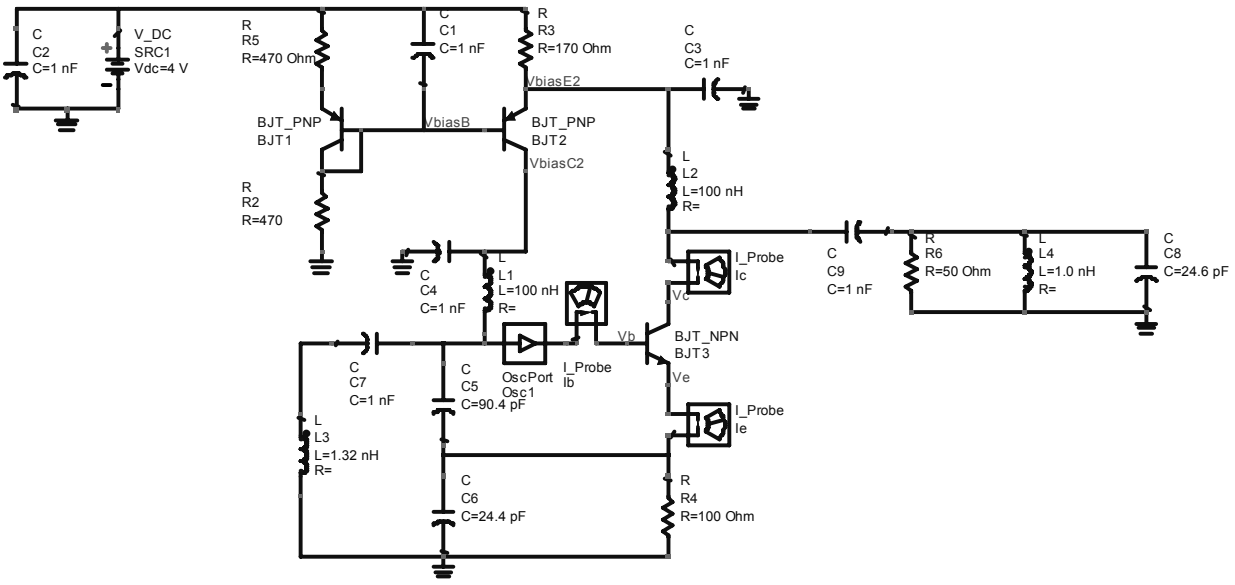

Figure 3.23: ADS circuit of a tuned load added to a saturating oscillator

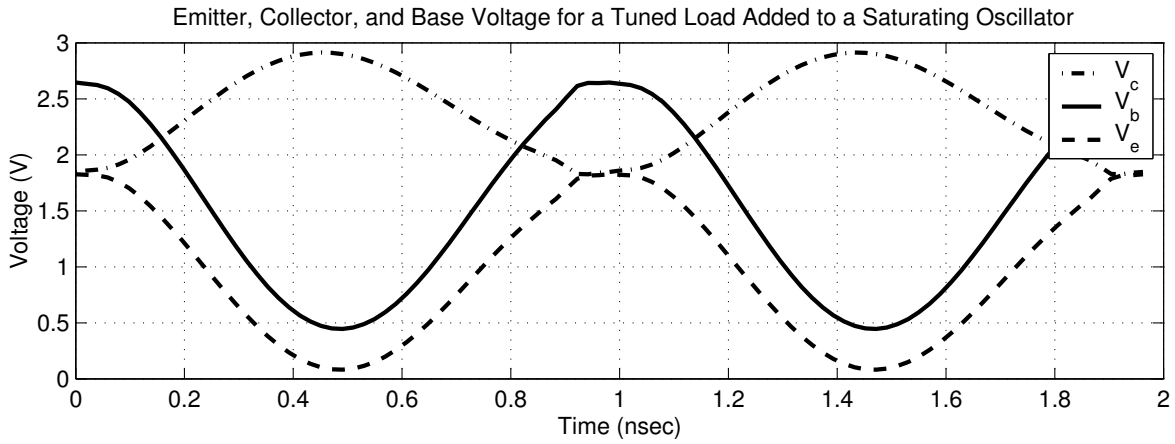

Figure 3.24: Emitter, collector, and base voltages for a tuned load added to a saturating oscillator

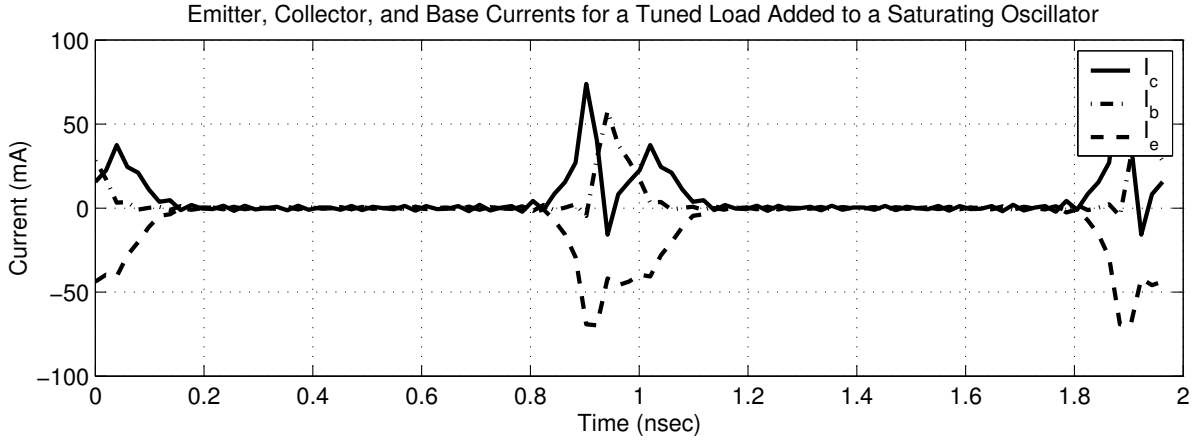

Figure 3.25: Emitter, collector, and base currents for a tuned load added to a saturating oscillator

Chapter 4

Noise

This chapter presents a brief overview of various noise sources. Shot noise generally dominates oscillator performance. Therefore, after the brief overview of noise sources, shot noise will be emphasized. Then, a method to decompose shot noise into in-phase and quadrature components will be discussed, and the result is used in an analysis of the transfer of the noise around the oscillator loop. The noise spectrum of a non-saturating oscillator as well as a saturating oscillator will be investigated.

4.1 Sources of Noise

The word noise, as it relates to electronic circuitry, refers to a random variation of a current or voltage. Aldert van der Ziel [32] describes the reason for the term noise by considering the hissing sound emitted from a loudspeaker after amplifying random variations of voltage or current.

Noise produced by different physical mechanisms can have different properties. A few different types of noise are discussed here. Shot noise generally dominates oscillator performance and will be the emphasis for the remainder of the chapter.

4.1.1 Thermal Noise

In 1827, R. Brown discovered random motion of pollen particles in a fluid [33]. This motion is now known as Brownian motion [33]. Then, in 1906, A. Einstein predicted that a piece of metal at thermal equilibrium would possess an electromotive force at each end due to the Brownian motion of the free electrons in the metal [33].

In 1928, J.B. Johnson [12] measured the current fluctuation of an amplifier created by the thermal agitation of electrons in varying resistors at varying temperatures. The same year H. Nyquist [21] used the principles of thermodynamics and statistical mechanics to obtain a theoretical expression for thermal noise of

$$E^2 df = 4RkTdf, \tag{4.1}$$

where $E^2 df$ is the average voltage squared within the frequency interval df, k is the Boltzmann constant, R is the resistance of the conductor, and T is the absolute temperature.

4.1.2 Flicker Noise

Flicker noise, sometimes called $1/f$ noise after the shape of its spectral density, can not be predicted reliably. Robinson [27] states that the corner frequency at which the flicker noise is equal to the white noise source spectrum can range from as low as 1 Hz to as high as 100 MHz. However, typical values are around a few kilohertz. The magnitude of flicker noise also varies widely with each device [27]. Furthermore, Robinson [27] states that in biased semiconductor devices, flicker noise is mainly associated with generation and recombination effects which produce and eliminate minority carriers. A definitive explanation and calculation of the source of this noise does not exist at present.

4.1.3 Partition Noise

W. Marshall Leach, Jr. [15] states that partition noise is created any time a current can possibly split between multiple paths. Leach [15] also states that in a BJT the emitter current can take one of two paths–the base or the collector. The emitter current has full shot noise, so the base and collector currents have full shot noise as well, but the base and collector noise currents are correlated as a result of the partition components. Treating the shot noise as two uncorrelated current sources, one from the collector to the emitter and another from the base to the emitter will account for the partition noise of a BJT [15].

4.1.4 Shot Noise

In 1918, W. Schottky pointed out that electric current emitted from a hot cathode is a combination of a large number of independently emitted electrons; therefore, the current will exhibit small fluctuations due to the finite charge of an electron and the randomness of the electron's emission [8]. These fluctuations became fluctuations in the plate-current of a vacuum tube and created noise in the final output, reminding Schottky of the sound created by a hail of shot striking a target; therefore, Schottky called the phenomenon the shot effect [8].

Estimating shot noise is classically accomplished using Carson's theorem [32], in which electrons are counted as they arrive at a collecting terminal and transit time is assumed to be negligible [33]. This approach to estimating shot noise results in a power spectral density (PSD) of

$$S(f) = 2qI_{DC} \ \mathrm{A}^2/\mathrm{Hz}. \tag{4.2}$$

A power spectral density is a real, even, nonnegative function which represents the distribution of signal power over the frequency spectrum; when integrated over the frequency domain, the power spectral density yields the total average power per ohm [33]. The power spectral density is also the Fourier transform of the autocorrelation function of the signal. [17] If the transit time of the electrons is considered, the spectrum will no longer be white but will have a cut-off frequency of approximately $\omega_c \approx 3.5/T_t$, where T_t represents the electron transit time [33].

4.2 BJT Noise Models

In early BJTs, $1/f$ noise was high and affected the quality of early transistor radio receivers; technological progress has reduced the $1/f$ noise level, and shot and thermal noise are now recognized as the limiting factors [33].

Some of the noise models of junction transistors include those developed and improved upon by Robinson [27], Buckingham [4], Niu [20], van der Ziel [31], Nielsen [19], Hawkins [11], Pucel and Rohde [25], and Fukui [7]. Robinson's model [27] uses power spectral densities to describe the transistor noise, taking into account transit time and electrons re-entering the emitter. Buckingham [4] corrected Robinson's model by accounting for charge-carrier recombination. Niu [20] states that intrinsic shot noise is a result of the diffusion currents across a pn junction. Nielsen [19], Hawkins [11], and Pucel and Rohde [25] all discuss noise figure using variations of a junction transistor noise model developed by van der Ziel [31]. Fukui [7] discussed a model for microwave bipolar transistors in which transistor parasitics were considered. The consideration of the parasitics accounted for discrepancies observed between theory and experiment at microwave frequencies.

Shot noise dominates oscillator noise; therefore, we will concentrate on shot noise in our discussion. Other noise sources can be added to the analysis without difficulty, if desired. The noise model used here is based on the model discussed by Niu [20]. The diffusion of carriers across a pn junction is a random event. Carriers which have sufficient energy to cross the potential barrier create a current pulse at the physical terminal. Due to the discrete nature of this current pulse, shot noise results. The shot noise in the emitter of a BJT biased in the forward active mode consists of two parts,

$$S_{i_{ne}}(f) = 2qI_C, \tag{4.3}$$

as a result of the electron injection across the emitter-base junction, and

$$S_{i_{pe}}(f) = 2qI_B, \tag{4.4}$$

as a result of the hole injection across the base-emitter junction. These two processes are independent due to the independence of the electron and hole injection. Physically, the shot noise in the collector is a delayed version of the shot noise induced by the emitter electron injection [20]. The noise can be modeled as a noise source connecting the collector and emitter, and a noise source connecting the base and emitter, as shown in Figure 4.1. This representation will also account for partition noise. The noise sources will be represented as a noise current density, I_N, with units $\mathrm{A}/\sqrt{\mathrm{Hz}}$, which is the square root of the power spectral density.

Since we are working with the three-terminal model and using a common base representation, it is convenient to have the noise sources appear across the base-collector junction. This can be done fairly easy for the three-terminal model. Consider the three-terminal model, of Figure 2.8, with uncorrelated noise sources added in accordance with Figure 4.1 to give Figure 4.2. We can represent the current source across the collector and emitter terminals as two correlated sources, one extending from the collector to the base, and one extending from the base to the emitter as shown in Figure 4.3. Then, using the transformer-like circuit approximation from Section 2.3, we can transform the two current sources across the base-emitter junction to be across the base-collector junction by multiplying them by $1/n$. The two correlated sources then combine to give a source with a value of $I_{N_{ce}}\left(1-\frac{1}{n}\right)$. This procedure is useful for the loop analysis and is illustrated by Figures 4.3 and 4.4. The noise sources in Figure 4.4 are uncorrelated and can be represented as a single noise source, I_N, by summing the noise powers to give

$$I_N = \sqrt{\left(\frac{1}{n}I_{N_{be}}\right)^2 + \left(\left(1-\frac{1}{n}\right)I_{N_{ce}}\right)^2}. \tag{4.5}$$

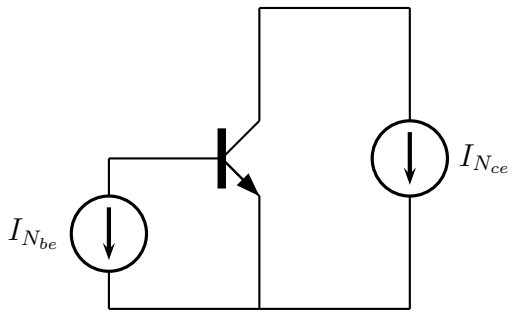

Figure 4.1: BJT noise model for non-saturating transistor

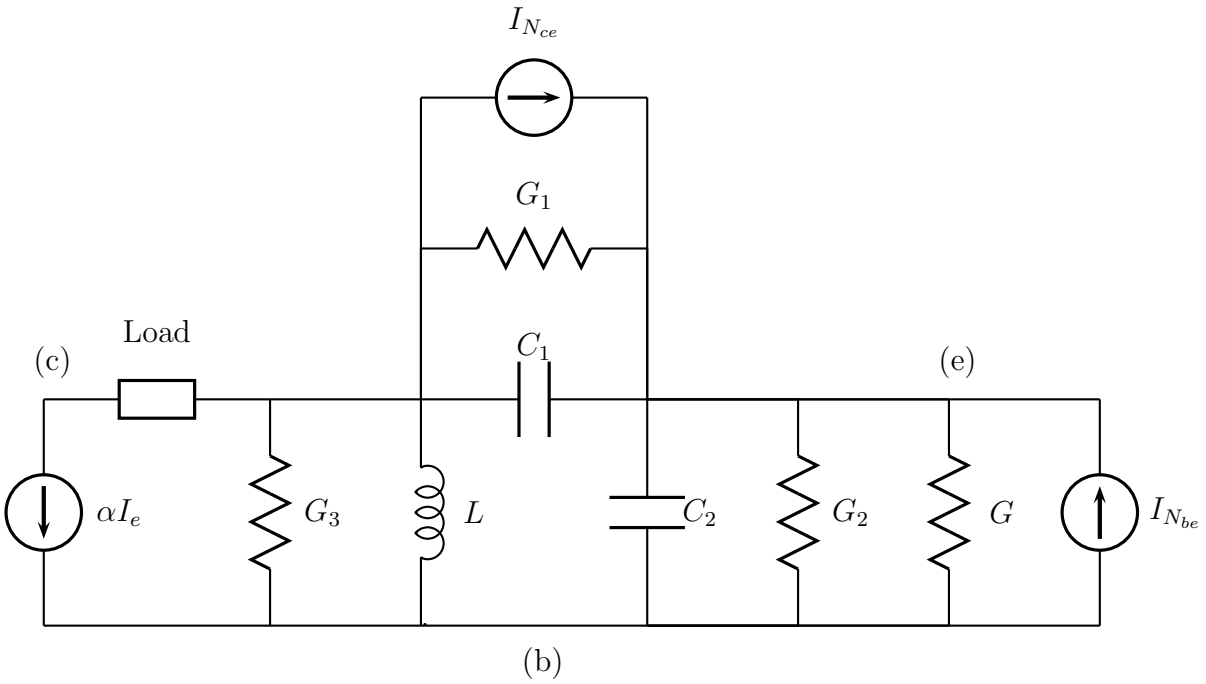

Figure 4.2: Three-terminal model with inclusion of noise sources for a non-saturating oscillator

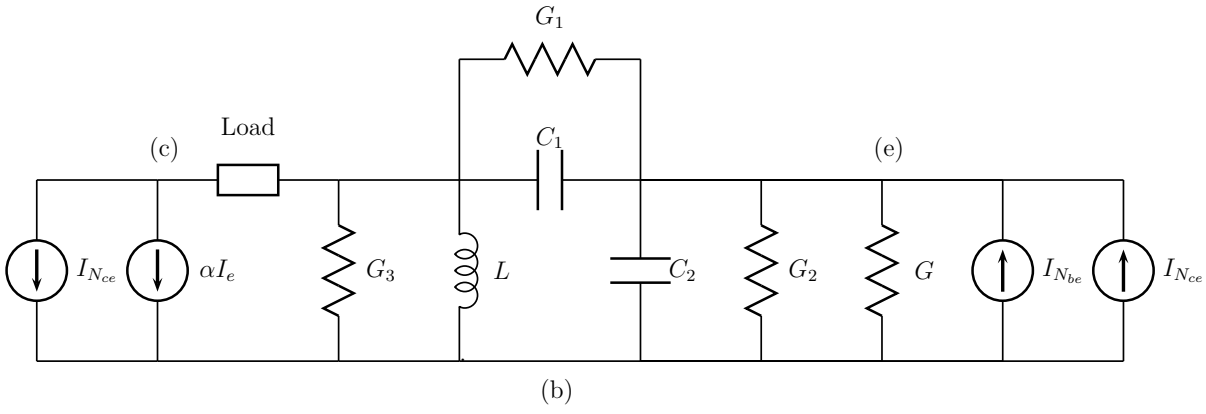

Figure 4.3: Three-terminal model with noise sources represented as sources across the base-collector and base-emitter junctions for a non-saturating oscillator

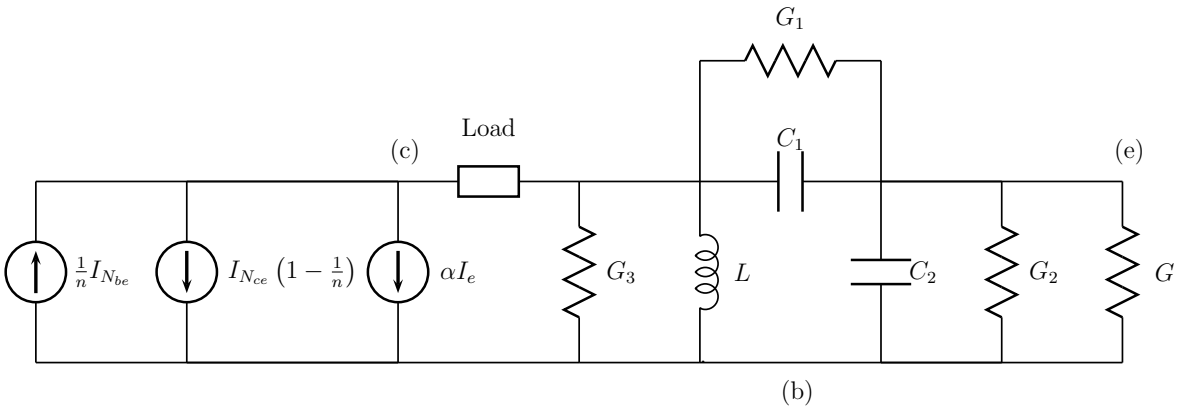

Figure 4.4: Three-terminal model with noise sources represented as sources across the base-collector junction for a non-saturating oscillator

4.3 Modification of BJT Noise Model to Include Saturation

In this section, the concepts of shot noise discussed by Niu [20] will be expanded on to include the effects of saturation. To understand how saturation changes the noise production, consider the BJT model shown in Figure 4.5 based on the Ebers-Moll equations. This model shows a diffusion current of I_f across the base-emitter pn junction as a result of the forward operation of the transistor. This model also shows a diffusion current of I_r across the base-collector pn junction as a result of the reverse operation of the transistor. While operating in saturation, the classic shot noise resulting from the hole injection from the base to the emitter is given by

$$S_{i_{pbe}}(f) = 2q\left(1-\alpha_f\right)I_f. \tag{4.6}$$

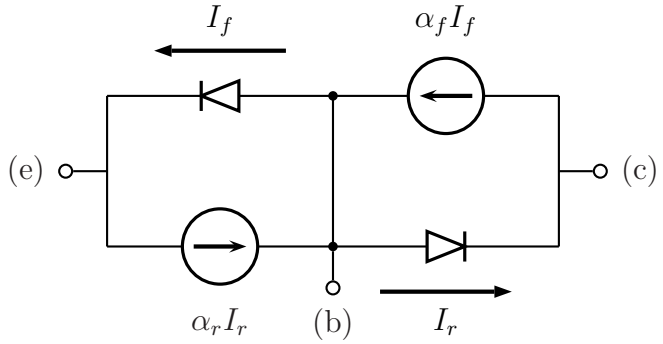

Figure 4.5: Large signal equivalent circuit based on Ebers-Moll equations

The classic shot noise resulting from the hole injection from the base to the collector is given by

$$S_{i_{pbc}}(f) = 2q\left(1 - \alpha_r\right) I_r. \tag{4.7}$$

For the shot noise generated due to the electron injection, the same electrons could be involved in the same process. Therefore, the net current will be used for computing the shot noise. The resulting classic shot noise power becomes

$$S_{i_{nce}}(f) = 2q\left(\alpha_f I_f - \alpha_r I_r\right). \tag{4.8}$$

The noise can be modeled as a noise source connecting the collector and emitter, a noise source connecting the base and emitter, and a noise source connecting the base and collector as shown in Figure 4.6. The noise sources can be transfered across the base-collector junction as explained in Section 4.2. The resulting noise sources are independent and can be represented as a single source, I_N. The result of this transformation is illustrated in Figure 4.7, where

$$I_N = \sqrt{I_{Nr_{bc}}^2 + \left(\frac{1}{n} I_{Nf_{be}}\right)^2 + \left(\left(1 - \frac{1}{n}\right) I_{N_{ce}}\right)^2}. \tag{4.9}$$

Note the modification of G_3 in the three-terminal model to include the base-collector conductance, G_C, resulting from turning on the base-collector junction. Also, note the emitter-base source resulting from the reverse operation of the transistor.

4.4 Computation of In-phase and Quadrature Power

In an oscillator, the noise that is in-phase with the signal will be transfered around the oscillator loop differently than noise that is not in-phase with the signal. If the shot noise is decomposed into an in-phase and a quadrature component, the loop transfer of the noise can be evaluated for each case separately. A concept of decomposing the signal into in-

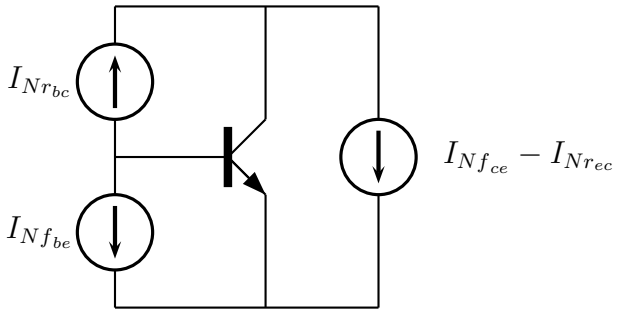

Figure 4.6: BJT noise model for saturating transistor

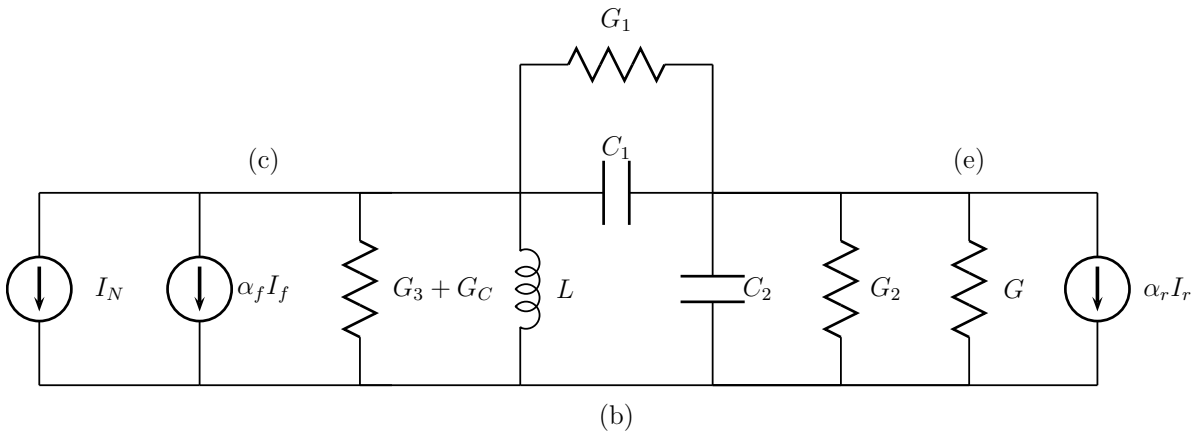

Figure 4.7: Three-terminal model with noise sources represented as sources across the base-collector junction for a saturating oscillator

phase and quadrature components by using a down-conversion and filtering process on the signal, similar to the process described in *Circuit Theory of Periodically Driven Nonlinear Systems* by Paul Penfield Jr. [23] , is used to decompose the standard shot noise spectrum into separate in-phase and quadrature shot noise spectra. Use of the autocorrelation process described by Paul Penfield Jr. [23] can also be used to arrive at the same result. However, the autocorrelation method is more involved and less intuitive.

Consider the current that would be produced by the nonlinear device in an oscillator without noise, referred to as the ideal current. This ideal current can be written as a Fourier series. In this oscillator application, one can assume that the fundamental component has a phase of zero, which results in the sum of the sine components to begin at the second harmonic. This ideal current can be written as

$$i_x(t) = \sum_{n=0}^{\infty} I_n \cos(n\omega_o t) + \sum_{n=2}^{\infty} A_n \sin(n\omega_o t). \tag{4.10}$$

The sine terms, of Equation 4.10, will allow for a signal in which the harmonics have a phase shift with respect to the fundamental term.

To represent the in-phase and quadrature noise separately, a down-conversion and detection process can be used. This process is similar to how in-phase and quadrature components would be experimentally measured. For the in-phase portion we will do the detection with a cosine, while for the quadrature portion we will use a sine, giving

$$i_a(t) = 2h(t) \otimes [\cos(\omega_o t) i(t)] \tag{4.11}$$

and

$$i_p(t) = 2h(t) \otimes [\sin(\omega_o t) i(t)] \,. \tag{4.12}$$

For our math purposes we will assume $h(t)$ to be an ideal low-pass filter defined in the frequency domain by

$$H(\omega) = \begin{cases} 1, & |\omega| < \frac{\Delta\omega}{2} \\ 0, & |\omega| > \frac{\Delta\omega}{2} \end{cases} \,, \tag{4.13}$$

where $\Delta\omega$ is the radian RF bandwidth. The bandwidth can also be represented as a Hertzian bandwidth, B, where

$$B = \frac{\Delta\omega}{2\pi} \tag{4.14}$$

Figure 4.8 is a graphical representation of this ideal low-pass filter.

For an example of the down-conversion and detection, let us look at the ideal current, i_x. Inserting Equation 4.10 in Equation 4.11 we obtain the in-phase component

$$i_{xa} = 2 \int_{-\infty}^{\infty} h(t-\lambda) \cos(\omega_o \lambda) i_x(\lambda) d\lambda, \tag{4.15}$$

$$i_{xa} = 2 \int_{-\infty}^{\infty} h(t-\lambda) \left[\cos(\omega_o \lambda) \sum_{n=0}^{\infty} I_n \cos(n\omega_o \lambda) + \cos(\omega_o \lambda) \sum_{n=2}^{\infty} A_n \sin(n\omega_o \lambda) \right] d\lambda. \tag{4.16}$$

Distributing the cosine to perform the in-phase down-conversion process results in

$$\begin{aligned} i_{xa} = 2 \int_{-\infty}^{\infty} h(t-\lambda) \Bigg[& \sum_{n=0}^{\infty} \left(\frac{I_n}{2} \cos((n-1)\omega_o \lambda) + \frac{I_n}{2} \cos((n+1)\omega_o \lambda) \right) \\ & + \sum_{n=2}^{\infty} \left(\frac{A_n}{2} \sin((n-1)\omega_o \lambda) + \frac{A_n}{2} \sin((n+1)\omega_o \lambda) \right) \Bigg] d\lambda. \end{aligned} \tag{4.17}$$

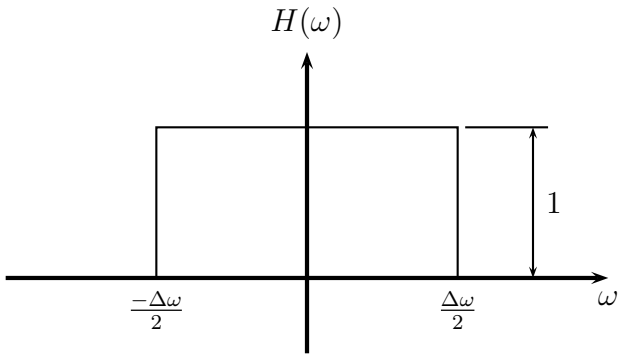

Figure 4.8: Graphical representation of ideal low-pass filter

Evaluating Equation 4.17 term-by-term in the frequency domain results in

$$i_{xa} = I_1 H(0) = I_1, \tag{4.18}$$

which is what is expected for the baseband representation of the in-phase fundamental component of the ideal current.

This process can also be completed for the quadrature component of the ideal current. Substituting Equation 4.10 in Equation 4.12 we obtain

$$i_{xp} = 2\int_{-\infty}^{\infty} h(t-\lambda)\sin(\omega_o\lambda) i_x(\lambda) d\lambda, \tag{4.19}$$

$$i_{xp} = 2\int_{-\infty}^{\infty} h(t-\lambda)\left[\sin(\omega_o\lambda)\sum_{n=0}^{\infty} I_n\cos(n\omega_o\lambda) + \sin(\omega_o\lambda)\sum_{n=2}^{\infty} A_n\sin(n\omega_o\lambda)\right] d\lambda. \tag{4.20}$$

Distributing the sine to perform the quadrature down-conversion process results in

$$\begin{aligned} i_{xp} = 2\int_{-\infty}^{\infty} h(t-\lambda)\Bigg[&\sum_{n=0}^{\infty}\left(\frac{I_n}{2}\sin((n+1)\omega_o\lambda) - \frac{I_n}{2}\sin((n-1)\omega_o\lambda)\right) \\ &+ \sum_{n=2}^{\infty}\left(\frac{A_n}{2}\cos((n-1)\omega_o\lambda) - \frac{A_n}{2}\cos((n+1)\omega_o\lambda)\right)\Bigg] d\lambda. \end{aligned} \tag{4.21}$$

Evaluating Equation 4.21 term by term in the frequency domain results in

$$i_{xp} = 0, \tag{4.22}$$

which is what is expected for the baseband representation of the quadrature component of the ideal current since we have assumed the phase reference is such that the fundamental component has a phase of zero.

When calculating the power using the down-conversion and detection method, one must be cautious because the down-conversion represents the peak values of the signal at ω_o in a baseband representation. Computing the power from this baseband representation will result in an error of a factor of two since the root mean square (RMS) value is not taken into account. Inserting a factor of one half in our power calculations will account for this error and result in the correct power. To illustrate this error, consider a cosine modulated by a single complex exponential

$$y(t) = \left(A + ae^{j\omega_m t}\right)\cos(\omega_o t). \tag{4.23}$$

To compute the power in $y(t)$ we have

$$P_{y(t)} = \lim_{T\to\infty} \frac{1}{T} \int_{-\frac{T}{2}}^{\frac{T}{2}} y(t)y^*(t)dt, \tag{4.24}$$

where $(*)$ represents the complex conjugate. Substituting $y(t)$ and $y^*(t)$ gives

$$P_{y(t)} = \lim_{T\to\infty} \frac{1}{T} \int_{-\frac{T}{2}}^{\frac{T}{2}} \left(\frac{A}{2}e^{j\omega_o t} + \frac{A}{2}e^{-j\omega_o t} + \frac{a}{2}e^{j(\omega_o+\omega_m)t} + \frac{a}{2}e^{-j(\omega_o-\omega_m)t}\right) \times \left(\frac{A}{2}e^{-j\omega_o t} + \frac{A}{2}e^{j\omega_o t} + \frac{a}{2}e^{-j(\omega_o+\omega_m)t} + \frac{a}{2}e^{j(\omega_o-\omega_m)t}\right) dt. \tag{4.25}$$

The result of this calculation is

$$P_{y(t)} = \frac{A^2}{2} + \frac{a^2}{2}, \tag{4.26}$$

which is what we expect for the power of the signal $y(t)$.

Now consider the power computed from a down-converted version of $y(t)$. Since $y(t)$ contains only in-phase components, let us use the down-conversion represented in Equation 4.11. This down-conversion results in

$$y_a(t) = A + ae^{-j\omega_m t}. \tag{4.27}$$

Computing the power of $y_a(t)$ results in

$$P_{y_a(t)} = \lim_{T\to\infty} \frac{1}{T} \int_{-\frac{T}{2}}^{\frac{T}{2}} \left(A + ae^{-j\omega_m t}\right)\left(A + ae^{j\omega_m t}\right) dt, \tag{4.28}$$

which simplifies to

$$P_{y_a(t)} = \lim_{T\to\infty} \frac{1}{T} \int_{-\frac{T}{2}}^{\frac{T}{2}} \left(A^2 + 2Aa\cos(\omega_m t) + a^2\right) dt = A^2 + a^2. \tag{4.29}$$

This power computation results in a power twice that of what is expected due to the mixing process. Therefore, when computing the in-phase and quadrature shot noise power we must remember to correct for the factor of two error.

4.5 I/Q Decomposition of Shot Noise

In reality, the current through a transistor is composed of a series of K discrete charges flowing at times, τ_k, over a period, T, where $\tau_k \in \left(-\frac{T}{2}, \frac{T}{2}\right)$, and $I_0 = \frac{Kq}{T}$, referred to here as the non-ideal current. This non-ideal current can be represented as

$$i(t) = \sum_{k=1}^{K} q\delta(t - \tau_k), \quad \tau_k \in \left(-\frac{T}{2}, \frac{T}{2}\right), \tag{4.30}$$

where the probability density function (pdf) of a given electron flowing at time τ is given by

$$pdf = p(\tau) = \frac{i_x(\tau)}{TI_0}. \tag{4.31}$$

The pdf represents the probability an electron will cross a two-dimensional boundary in the nonlinear device at a specific time, τ. It is possible for two electrons to flow at the same time through a two dimensional surface, and we can assume that there will not be so many electrons flowing at time τ that the two dimensional surface is saturated with electrons limiting the flow. Therefore, we can assume that the flow of one electron is independent from all other electrons. If we let $i_x(\tau) = I_0$ in Equation 4.31, then the result is the standard shot noise form of Equation 4.2. Using $i_x(\tau)$ provides for a general extension to provide in-phase and quadrature components of the noise to be derived below.

To illustrate the down-conversion process with inclusion of the stochastic process of the non-ideal current representation illustrated in Equation 4.30, the expected value of the in-phase and quadrature components of the non-ideal discrete charge version of the current will be computed. For the in-phase component, inserting Equation 4.30 in Equation 4.11 and taking the expected value results in

$$\mathrm{E}\left[i_a\right] = \mathrm{E}\left[2h(t) \otimes \sum_{k=1}^{K} q\delta(t - \tau_k)\cos(\omega_o t)\right]. \tag{4.32}$$

Rewriting Equation 4.32 in integral form results in

$$\mathrm{E}\left[i_a\right] = \mathrm{E}\left[2\int_{-\infty}^{\infty} h(t - \lambda)\sum_{k=1}^{K} q\delta(\lambda - \tau_k)\cos(\omega_o \lambda)d\lambda\right], \tag{4.33}$$

and interchanging the order of the summation and integration for independent events results in

$$\mathrm{E}\left[i_a\right] = 2q\sum_{k=1}^{K} \mathrm{E}\left[\int_{-\infty}^{\infty} h(t - \lambda)\delta(\lambda - \tau_k)\cos(\omega_o \lambda)d\lambda\right]. \tag{4.34}$$

Using the sifting property of the delta function, the integral can be easily evaluated, giving

$$\mathrm{E}\left[i_a\right] = 2q \sum_{k=1}^{K} \mathrm{E}\left[h(t-\tau_k)\cos(\omega_o \tau_k)\right]. \tag{4.35}$$

If we assume that each electron flows at a time independent of all other electrons, then the expected value is the same for the case of each electron. The assumption of independence allows for the replacment of the summation by a multiplication by K. We can evaluate the expected value by integrating the product of the function in question and the probability density function. The result of the independence assumption and the integral representation of the expected value is

$$\mathrm{E}\left[i_a\right] = 2qK \int_{-\frac{T}{2}}^{\frac{T}{2}} h(t-\tau)\cos(\omega_o \tau)\frac{i_x(\tau)}{TI_0} d\tau. \tag{4.36}$$

If we let the observation window, T, become large and note that $\frac{qK}{TI_0} = 1$, Equation 4.36 becomes identical to Equation 4.15 to give

$$\mathrm{E}\left[i_a\right] = I_1 = i_{xa}. \tag{4.37}$$

The expected value of the in-phase component of the realistic current agrees with what we expected from the ideal current.

The same procedure may be applied to the quadrature component, i_p. Inserting Equation 4.30 in Equation 4.12 and taking the expected value results in

$$\mathrm{E}\left[i_p\right] = \mathrm{E}\left[2h(t) \otimes \sum_{k=1}^{K} q\delta(t-\tau_k)\sin(\omega_o t)\right]. \tag{4.38}$$

Rewriting Equation 4.38 in integral form results in

$$\mathrm{E}\left[i_p\right] = \mathrm{E}\left[2\int_{-\infty}^{\infty} h(t-\lambda)\sum_{k=1}^{K} q\delta(\lambda-\tau_k)\sin(\omega_o \lambda)d\lambda\right], \tag{4.39}$$

and interchanging the order of the summation and integration results in

$$\mathrm{E}\left[i_p\right] = 2q \sum_{k=1}^{K} \mathrm{E}\left[\int_{-\infty}^{\infty} h(t-\lambda)\delta(\lambda-\tau_k)\sin(\omega_o \lambda)d\lambda\right]. \tag{4.40}$$

Making the same assumption about independence that was made in the in-phase case results in

$$\mathrm{E}\left[i_p\right] = 2qK \int_{-\frac{T}{2}}^{\frac{T}{2}} h(t-\tau)\sin(\omega_o\tau)\frac{i_x(\tau)}{TI_0}d\tau. \tag{4.41}$$

If we let the observation window, T, become large and note that $\frac{qK}{TI_0} = 1$, Equation 4.5 becomes identical to Equation 4.19 to give

$$\mathrm{E}\left[i_p\right] = 0 = i_{xp}. \tag{4.42}$$

Again, this result is what is expected given the form of the ideal current.

The noise power, which we are interested in finding, is the mean squared value of the actual current. This noise power can be found using the same down-conversion method previously illustrated. However, we must remember to account for the RMS value by dividing by two. Consider the in-phase component of the mean squared value and we have

$$\sigma_a^2 = \frac{1}{2}\mathrm{E}\left[(i_a - \mathrm{E}\left[i_a\right])^2\right] = \frac{1}{2}\mathrm{E}\left[i_a^2\right] - \frac{1}{2}i_{xa}^2. \tag{4.43}$$

Substituting the expression for the in-phase current using the down-conversion process of Equation 4.11 and the current model of Equation 4.30 results in

$$\sigma_a^2 = \frac{1}{2}\mathrm{E}\left[\left(\int_{-\infty}^{\infty} 2h(t-\lambda)\sum_{k=1}^{K} q\delta(\lambda-\tau_k)\cos(\omega_o\lambda)d\lambda\right) \times \left(\int_{-\infty}^{\infty} 2h(t-\lambda)\sum_{l=1}^{K} q\delta(\lambda-\tau_l)\cos(\omega_o\lambda)d\lambda\right)\right] - \frac{1}{2}i_{xa}^2. \tag{4.44}$$

Changing the order of the summation and integration and using the sifting property of the delta function results in

$$\sigma_a^2 = \frac{q^2}{2}\mathrm{E}\left[\left(\sum_{k=1}^{K} h(t-\tau_k)2\cos(\omega_o\tau_k)\right)\left(\sum_{l=1}^{K} h(t-\tau_l)2\cos(\omega_o\tau_l)\right)\right] - \frac{1}{2}i_{xa}^2. \tag{4.45}$$

In Equation 4.45 there is an expected value of a product of two sums. If we look at each term of the product, we will see that there are K^2 terms. Each of these terms contains an expected value of a product of two random variables which have identical pdfs. If we assume the two random variables are independent of each other, we can write each term as a product of two expected values, which would simplify to K^2 times the square of the expected value of one random variable. However, for $k = l$ the two random variables are not independent since they represent the same electron. The $k = l$ cases can be accounted for by subtracting K of the expected value squared terms back out and adding the correct representation of these K

terms as K times the expected value of the random variable squared. This procedure results in

$$\sigma_a^2 = \frac{q^2}{2}(K^2 - K)\mathrm{E}^2\left[2h(t-\tau)\cos(\omega_o\tau)\right] + \frac{q^2K}{2}\mathrm{E}\left[4h^2(t-\tau)\cos^2(\omega_o\tau)\right] - \frac{1}{2}i_{xa}^2. \quad (4.46)$$

Rewriting these expected values in integral form results in

$$\sigma_a^2 = \frac{q^2(K^2-K)}{2T^2I_0^2}\left[\int_{-\frac{T}{2}}^{\frac{T}{2}} 2h(t-\tau)\cos(\omega_o\tau)i_x(\tau)d\tau\right]^2 + \frac{q^2K}{2TI_0}\int_{-\frac{T}{2}}^{\frac{T}{2}} 4h^2(t-\tau)\cos^2(\omega_o\tau)i_x(\tau)d\tau - \frac{1}{2}i_{xa}^2. \quad (4.47)$$

The bracketed term in Equation 4.47 is the equivalent of Equation 4.15. Making this substitution, and with some canceling of terms, gives

$$\sigma_a^2 = \frac{1}{2}i_{xa}^2 - \frac{1}{2K}i_{xa}^2 + \frac{q^2K}{2TI_0}\int_{-\frac{T}{2}}^{\frac{T}{2}} 4h^2(t-\tau)\cos^2(\omega_o\tau)i_x(\tau)d\tau - \frac{1}{2}i_{xa}^2. \quad (4.48)$$

The i_{xa}^2 terms can now be canceled and $i_x(\tau)$, of Equation 4.10, can be substituted to give

$$\sigma_a^2 = 2q\int_{-\frac{T}{2}}^{\frac{T}{2}} h^2(t-\tau)\cos^2(\omega_o\tau)\left(\sum_{n=0}^{\infty} I_n\cos(n\omega_o\tau) + \sum_{n=2}^{\infty} A_n\sin(n\omega_o\tau)\right)d\tau - \frac{1}{2K}i_{xa}^2. \quad (4.49)$$

Expanding the cosine squared term using trigonometric identities results in

$$\sigma_a^2 = 2q\int_{-\frac{T}{2}}^{\frac{T}{2}} h^2(t-\tau)\frac{1}{2}\left(\sum_{n=0}^{\infty} I_n\cos(n\omega_o\tau) + \sum_{n=2}^{\infty} A_n\sin(n\omega_o\tau)\right)d\tau + 2q\int_{-\frac{T}{2}}^{\frac{T}{2}} h^2(t-\tau)\frac{1}{2}\cos(2\omega_o\tau)\left(\sum_{n=0}^{\infty} I_n\cos(n\omega_o\tau) + \sum_{n=2}^{\infty} A_n\sin(n\omega_o\tau)\right)d\tau - \frac{1}{2K}i_{xa}^2, \quad (4.50)$$

and distributing the cosine term results in

$$\sigma_a^2 = 2q\int_{-\frac{T}{2}}^{\frac{T}{2}} h^2(t-\tau)\frac{1}{2}\left(\sum_{n=0}^{\infty} I_n\cos(n\omega_o\tau) + \sum_{n=2}^{\infty} A_n\sin(n\omega_o\tau)\right)d\tau + 2q\int_{-\frac{T}{2}}^{\frac{T}{2}} h^2(t-\tau)\frac{1}{4}\left(\sum_{n=0}^{\infty}\left(I_n\cos((n+2)\omega_o\tau) + I_n\cos((n-2)\omega_o\tau)\right)\right)d\tau + 2q\int_{-\frac{T}{2}}^{\frac{T}{2}} h^2(t-\tau)\frac{1}{4}\left(\sum_{n=2}^{\infty}\left(A_n\sin((n+2)\omega_o\tau) + A_n\sin((n-2)\omega_o\tau)\right)\right)d\tau - \frac{1}{2K}i_{xa}^2. \quad (4.51)$$

As the observation window, T, becomes large, Equation 4.51 becomes a convolution with the square of the ideal low-pass filter of Equation 4.13. The multiplication property, which is the dual of the convolution property, states that multiplication in the time domain corresponds to a convolution in the frequency domain, which can be represented more specifically by [22]

$$r(t) = s(t)p(t) \xleftrightarrow{\mathscr{F}} R(j\omega) = \frac{1}{2\pi}\left[S(j\omega) \otimes P(j\omega)\right]. \tag{4.52}$$

The convolution of the frequency domain representation of the ideal low-pass filter with itself results in a triangle shaped low-pass response. The height of the triangle response is $\frac{\Delta\omega}{2\pi}$ at $\omega = 0$ and slopes down to zero at $\omega = \pm\Delta\omega$. The division by 2π results in the peak of the triangle to be the Hertzian bandwidth, B. The result of the convolution of the ideal low-pass filter with itself is shown graphically in Figure 4.9. Considering this frequency domain response of the filter, the result of the convolution is

$$\sigma_a^2 = qBI_0 + \frac{1}{2}qBI_2 - \frac{1}{2K}i_{xa}^2. \tag{4.53}$$

Since the observation window has been assumed to be large, it can also assumed that $2K$ is large enough such that the last term in Equation 4.53 is small, giving

$$\sigma_a^2 = qB\left(I_0 + \frac{I_2}{2}\right). \tag{4.54}$$

The resulting noise power has a white spectrum and Equation 4.54 can be represented as a PSD by dividing by the bandwidth. We will represent this PSD as

$$I_{Na}^2 = q\left(I_0 + \frac{I_2}{2}\right) \ \text{A}^2/\text{Hz}. \tag{4.55}$$

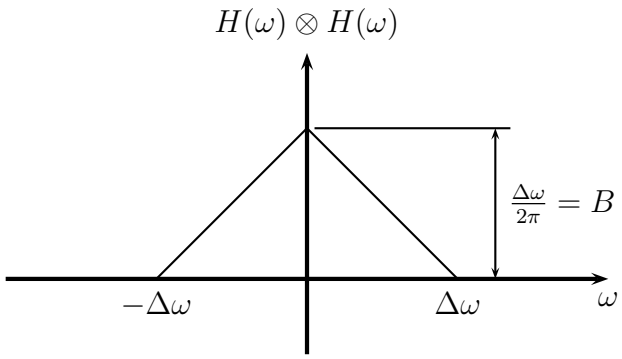

Figure 4.9: Graphical representation of the convolution of the ideal low-pass filter with itself

The same procedure can be followed for the quadrature component of the noise power. Looking at the quadrature component of the mean squared value, we have

$$\sigma_p^2 = \frac{1}{2}\mathrm{E}\left[(i_p - \mathrm{E}\left[i_p\right])^2\right] = \frac{1}{2}\mathrm{E}\left[i_p^2\right] - \frac{1}{2}i_{xp}^2. \tag{4.56}$$

Substituting the expression for the quadrature current using the down conversion process of Equation 4.12 and the current model of Equation 4.30 results in

$$\sigma_p^2 = \frac{1}{2}\mathrm{E}\left[\left(\int_{-\infty}^{\infty} 2h(t-\lambda)\sum_{k=1}^{K} q\delta(\lambda-\tau_k)\sin(\omega_o\lambda)d\lambda\right) \times \left(\int_{-\infty}^{\infty} 2h(t-\lambda)\sum_{l=1}^{K} q\delta(\lambda-\tau_l)\sin(\omega_o\lambda)d\lambda\right)\right]. \tag{4.57}$$

Changing the order of the summation and integration, and using the sifting property of the delta function results in

$$\sigma_p^2 = \frac{q^2}{2}\mathrm{E}\left[\left(\sum_{k=1}^{K} 2h(t-\tau_k)\sin(\omega_o\tau_k)\right)\left(\sum_{l=1}^{K} 2h(t-\tau_l)\sin(\omega_o\tau_l)\right)\right]. \tag{4.58}$$

Assuming all electrons have an independent τ results in

$$\sigma_p^2 = \frac{q^2}{2}(K^2-K)\mathrm{E}^2\left[2h(t-\tau)\sin(\omega_o\tau)\right] + \frac{q^2}{2}K\mathrm{E}\left[4h^2(t-\tau)\sin^2(\omega_o\tau)\right]. \tag{4.59}$$

Rewriting the expected values in integral form results in

$$\sigma_p^2 = \frac{q^2(K^2-K)}{2T^2I_0^2}\left[\int_{-\frac{T}{2}}^{\frac{T}{2}} 2h(t-\tau)\sin(\omega_o\tau)i_x(\tau)d\tau\right]^2 + \frac{q^2K}{2TI_0}\int_{-\frac{T}{2}}^{\frac{T}{2}} 4h^2(t-\tau)\sin^2(\omega_o\tau)i_x(\tau)d\tau. \tag{4.60}$$

The bracketed term in Equation 4.60 is the equivalent of Equation 4.19. Making this substitution, and canceling some terms results in

$$\sigma_p^2 = \frac{1}{2}i_{xp}^2 - \frac{1}{2K}i_{xp}^2 + \frac{2q^2K}{TI_0}\int_{-\frac{T}{2}}^{\frac{T}{2}} h^2(t-\tau)\sin^2(\omega_o\tau)i_x(\tau)d\tau, \tag{4.61}$$

and since i_{xp}^2 is zero Equation 4.61 becomes

$$\sigma_p^2 = \frac{2q^2K}{TI_0}\int_{-\frac{T}{2}}^{\frac{T}{2}} h^2(t-\tau)\sin^2(\omega_o\tau)i_x(\tau)d\tau. \tag{4.62}$$

Equation 4.10 can now be substituted for $i_x(\tau)$ to give

$$\sigma_p^2 = 2q\int_{-\frac{T}{2}}^{\frac{T}{2}} h^2(t-\tau)\sin^2(\omega_o\tau)\left(\sum_{n=0}^{\infty} I_n\cos(n\omega_o\tau) + \sum_{n=2}^{\infty} A_n\sin(n\omega_o\tau)\right)d\tau. \tag{4.63}$$

Expanding the sine squared term using trigonometric identities results in

$$\begin{aligned}\sigma_p^2 = q\int_{-\frac{T}{2}}^{\frac{T}{2}} h^2(t-\tau)\left(\sum_{n=0}^{\infty} I_n\cos(n\omega_o\tau) + \sum_{n=2}^{\infty} A_n\sin(n\omega_o\tau)\right)d\tau \\ - q\int_{-\frac{T}{2}}^{\frac{T}{2}} h^2(t-\tau)\cos(2\omega_o\tau)\left(\sum_{n=0}^{\infty} I_n\cos(n\omega_o\tau) + \sum_{n=2}^{\infty} A_n\sin(n\omega_o\tau)\right)d\tau,\end{aligned} \tag{4.64}$$

and distributing the resulting cosine term gives

$$\begin{aligned}\sigma_p^2 = q\int_{-\frac{T}{2}}^{\frac{T}{2}} h^2(t-\tau)\left(\sum_{n=0}^{\infty} I_n\cos(n\omega_o\tau) + \sum_{n=2}^{\infty} A_n\sin(n\omega_o\tau)\right)d\tau \\ - \frac{q}{2}\int_{-\frac{T}{2}}^{\frac{T}{2}} h^2(t-\tau)\left(\sum_{n=0}^{\infty}\left(I_n\cos((n+2)\omega_o\tau) + I_n\cos((n-2)\omega_o\tau)\right)\right)d\tau \\ - \frac{q}{2}\int_{-\frac{T}{2}}^{\frac{T}{2}} h^2(t-\tau)\left(\sum_{n=2}^{\infty}\left(A_n\sin((n+2)\omega_o\tau) + A_n\sin((n-2)\omega_o\tau)\right)\right)d\tau.\end{aligned} \tag{4.65}$$

As the observation window, T, becomes large Equation 4.65 becomes a convolution with the square of the ideal low-pass filter of Equation 4.13. Considering the frequency domain representation of Equation 4.65, the result of the filtering action of the convolution is

$$\sigma_p^2 = qBI_0 - \frac{1}{2}qBI_2 = qB\left(I_0 - \frac{I_2}{2}\right). \tag{4.66}$$

The resulting noise power has a white spectrum and Equation 4.66 can be represented as a PSD by dividing by the bandwidth. We will represent this PSD as

$$I_{Np}^2 = q\left(I_0 - \frac{I_2}{2}\right) \ \text{A}^2/\text{Hz}. \tag{4.67}$$

The discussion of the I/Q decomposition of the shot noise has been presented in a manner that is independent of the nonlinear device in which the shot noise is produced. If in-phase noise power and the quadrature noise power are summed, the result is

$$\sigma^2 = \sigma_a^2 + \sigma_p^2 = qB\left(I_0 + \frac{I_2}{2}\right) + qB\left(I_0 - \frac{I_2}{2}\right) = 2qBI_0. \tag{4.68}$$

This result is the classic shot noise power of Equation 4.2. This classic result is commonly used in analysis and simulation, but offers an incomplete description of the amplitude and phase noise sources. The more complete form of Equations 4.55 and 4.67 will be used in the remainder of this work and offer a major contribution to current analysis techniques.

Applying these decomposition results to the noise sources of the non-saturating three-terminal model, shown in Figure 4.4, results in the amplitude/phase noise powers of

$$I_{N_{be}}^2 = q\left(I_{b0} \pm \frac{I_{b2}}{2}\right) \ \text{A}^2/\text{Hz}, \tag{4.69}$$

and

$$I_{N_{ce}}^2 = q\left(I_{c0} \pm \frac{I_{c2}}{2}\right) \ \text{A}^2/\text{Hz}, \tag{4.70}$$

for a total noise power through the base-collector junction of

$$I_N^2 = \frac{q}{n^2}\left(I_{b0} \pm \frac{I_{b2}}{2}\right) + q\left(1 - \frac{1}{n}\right)^2\left(I_{c0} \pm \frac{I_{c2}}{2}\right) \ \text{A}^2/\text{Hz}, \tag{4.71}$$

where we use the sum when computing the in-phase component and the difference when computing the quadrature component. If α is sufficiently close to 1, the base current will be small and Equation 4.71 can be approximated by

$$I_N^2 \approx q\left(1 - \frac{1}{n}\right)^2\left(I_{c0} \pm \frac{I_{c2}}{2}\right) \ \text{A}^2/\text{Hz}. \tag{4.72}$$

Applying the decomposition results to the noise sources of the saturating case, shown in Figure 4.7, results in the amplitude/phase noise powers of

$$I_{N_{rbc}}^2 = q\left(1 - \alpha_r\right)\left(I_{r0} \pm \frac{I_{r2}}{2}\right) \ \text{A}^2/\text{Hz}, \tag{4.73}$$

$$I_{N_{fbe}}^2 = q\left(1 - \alpha_f\right)\left(I_{f0} \pm \frac{I_{f2}}{2}\right) \ \text{A}^2/\text{Hz}, \tag{4.74}$$

$$I_{N_{ce}}^2 = q\left[\left(\alpha_f I_{f0} \pm \frac{\alpha_f I_{f2}}{2}\right) - \left(\alpha_f I_{r0} \pm \frac{\alpha_r I_{r2}}{2}\right)\right] \ \text{A}^2/\text{Hz}, \tag{4.75}$$

for a total noise power through the base-collector junction of

$$I_N^2 = q\left[(1-\alpha_r)\left(I_{r0} \pm \frac{I_{r2}}{2}\right) + \frac{1}{n^2}(1-\alpha_f)\left(I_{f0} \pm \frac{I_{f2}}{2}\right) + \left(1-\frac{1}{n}\right)^2\left[\alpha_f\left(I_{f0} \pm \frac{I_{f2}}{2}\right) - \alpha_r\left(I_{r0} \pm \frac{I_{r2}}{2}\right)\right]\right] \text{ A}^2/\text{Hz} \quad (4.76)$$

or

$$I_N^2 = q\left[1 - 2\alpha_r + \frac{2\alpha_r}{n} - \frac{\alpha_r}{n^2}\right]\left(I_{r0} \pm \frac{I_{r2}}{2}\right) + q\left[\frac{1}{n^2} + \alpha_f - \frac{2\alpha_f}{n}\right]\left(I_{f0} \pm \frac{I_{f2}}{2}\right) \text{ A}^2/\text{Hz}, \quad (4.77)$$

where we use the sum when computing the in-phase component and the difference when computing the quadrature component. If α_f is sufficiently close to 1, the base-emitter noise source can again be neglected, and Equation 4.77 can be approximated by

$$I_N^2 \approx q\left[1 - 2\alpha_r + \frac{2\alpha_r}{n} - \frac{\alpha_r}{n^2}\right]\left(I_{r0} \pm \frac{I_{r2}}{2}\right) + q\left[1 - \frac{1}{n}\right]^2\left(\alpha_f I_{f0} \pm \alpha_f \frac{I_{f2}}{2}\right) \text{ A}^2/\text{Hz}. \quad (4.78)$$

4.6 Loop Transfer of Noise

In this section, we will investigate the transfer of noise around the oscillator loop. First, we will look at how noise is transfered through the device. We will look at a generalization first, followed by the specific example of a BJT. We can then look at the closed loop equation for the noise transfer. We will look at the non-saturating case first, followed by the case in which the base-collector junction conducts due to saturation.

4.6.1 Device Transfer

In the general case of a nonlinear device

$$i(t) = f(v(t)), \quad v_x(t) + v_n(t) \quad (4.79)$$

where $v(t)$ is an ideal input voltage, $v_x(t)$, with an added noise component, $v_n(t)$. In an oscillator environment, we can write the ideal input voltage as

$$v_x(t) = V_0 + V_1\cos(\omega_o t), \quad (4.80)$$

and we can represent the input noise voltage as

$$v_n(t) = v_{n0}(t) + v_{n1a}(t)\cos(\omega_o t) + v_{n1p}\sin(\omega_o t). \tag{4.81}$$

Higher order harmonics could be added; however, the filtering of the oscillator feedback circuit will reduce the magnitude of the higher order harmonics to a negligible level. The nonlinear transfer of noise can be approximated by a performing a Taylor series on Equation 4.79 with respect to the noise voltage resulting in

$$i(t) = f(v_x(t)) + g(t)v_n(t), \tag{4.82}$$

where

$$g(t) = \left.\frac{\partial f(v(t))}{\partial v(t)}\right|_{v(t)=v_x(t)}. \tag{4.83}$$

We can write $g(t)$ as a Fourier series to give

$$g(t) = g_0 + \sum_{m=1}^{\infty}\left(g_{ma}\cos(m\omega_o t) + g_{mp}\sin(m\omega_o t)\right). \tag{4.84}$$

We can now write the noise component of the current as

$$\begin{aligned} i_n(t) = &\left(g_0 + \sum_{m=1}^{\infty}\left(g_{ma}\cos(m\omega_o t) + g_{mp}\sin(m\omega_o t)\right)\right)v_{n0}(t) \\ &+ \left(g_0 + \sum_{m=1}^{\infty}\left(g_{ma}\cos(m\omega_o t) + g_{mp}\sin(m\omega_o t)\right)\right)v_{n1a}(t)\cos(\omega_o t) \\ &+ \left(g_0 + \sum_{m=1}^{\infty}\left(g_{ma}\cos(m\omega_o t) + g_{mp}\sin(m\omega_o t)\right)\right)v_{n1p}\sin(\omega_o t) \end{aligned} \tag{4.85}$$

Combining the harmonics of $g(t)$ and $v_n(t)$ results in

$$\begin{aligned} i_n(t) = &\left[g_o v_{n0}(t) + \frac{g_{1a}}{2}v_{n1a} + \frac{g_{1p}}{2}v_{n1p}(t)\right] \\ &+ \left[g_{1a}v_{n0}(t) + \left(g_o + \frac{g_{2a}}{2}\right)v_{n1a} + \frac{g_{2p}}{2}v_{n1p}(t)\right]\cos(\omega_o t) \\ &+ \left[g_{1p}v_{n0}(t) + \frac{g_{2p}}{2}v_{n1a} + \left(g_o - \frac{g_{2a}}{2}\right)v_{n1p}(t)\right]\sin(\omega_o t) + \ldots, \end{aligned} \tag{4.86}$$

which can also be written as

$$\begin{aligned} i_n(t) = &[G_{0,0}v_{n0}(t) + G_{0,1a}v_{n1a}(t) + G_{0,1p}v_{n1p}(t)] \\ &+ [G_{1a,0}v_{n0}(t) + G_{1a,1a}v_{n1a}(t) + G_{1a,1p}v_{n1p}(t)]\cos(\omega_o t) \\ &+ [G_{1p,0}v_{n0}(t) + G_{1p,1a}v_{n1a}(t) + G_{1p,1p}v_{n1p}(t)]\sin(\omega_o t) + \ldots \end{aligned} \quad (4.87)$$

Equation 4.87 can be represented as a DC component, an in-phase component, and a quadrature component in the frequency domain which results in

$$i_{n0}(\omega_m) = G_{0,0}v_{n0}(\omega_m) + G_{0,1a}v_{n1a}(\omega_m) + G_{0,1p}v_{n1p}(\omega_m), \quad (4.88)$$

$$i_{n1a}(\omega_m) = G_{1a,0}v_{n0}(\omega_m) + G_{1a,1a}v_{n1a}(\omega_m) + G_{1a,1p}v_{n1p}(\omega_m), \quad (4.89)$$

and

$$i_{n1p}(\omega_m) = G_{1p,0}v_{n0}(\omega_m) + G_{1p,1a}v_{n1a}(\omega_m) + G_{1p,1p}v_{n1p}(\omega_m) \quad (4.90)$$

respectively. In addition to the circuit feedback, the device transfer represented by Equations 4.88, 4.89, and 4.90 can be used to solve for the transfer of the noise around the oscillator loop.

Consider the Bipolar Junction Transistor (BJT) as the non-linear device. The BJT has an exponential I-V relationship, which can be represented by

$$i_e(t) = I_s e^{\frac{qv_{be}}{kT}}, \quad (4.91)$$

where k is Boltzmann's constant, T is the temperature in Kelvin, and q is the charge of an electron.

Consider the situation where the base-emitter voltage is represented by

$$v_{be} = V_{BE} + V_{be1}\cos(\omega_o t) + v_{ben}(t), \quad (4.92)$$

with $v_{ben}(t)$ representing noise, or a variation about the operating point. The operating point consists only of a DC and a fundamental component. Furthermore, consider the noise voltage, $v_{ben}(t)$, to be represented by

$$v_{ben}(t) = v_{ben0}(t) + v_{ben1a}(t)\cos(\omega_o t) + v_{ben1p}(t)\sin(\omega_o t), \quad (4.93)$$

with higher order harmonics not included for the same reasoning used for excluding the harmonics from the operating point. Combining Equations 4.91, 4.92, and 4.93 results in

$$i_e(t) = I_s e^{\frac{q}{kT}(V_{BE} + v_{ben0}(t) + (V_{be1} + v_{ben1a}(t))\cos(\omega_o t) + v_{ben1p}(t)\sin(\omega_o t))}, \quad (4.94)$$

which can be rewritten as

$$i_e(t) = I_s e^{\frac{q}{kT}(V_{BE} + V_{be1}\cos(\omega_o t))} e^{\frac{q}{kT}(v_{ben0}(t) + v_{ben1a}(t)\cos(\omega_o t) + v_{ben1p}(t)\sin(\omega_o t))}. \quad (4.95)$$

Using a Taylor series approximation on Equation 4.95 results in

$$i_e(t) = I_s e^{\frac{q}{kT}(V_{BE}+V_{be1}\cos(\omega_o t))}\left(1 + \frac{qv_{ben0}(t)}{kT} + \frac{qv_{ben1a}(t)}{kT}\cos(\omega_o t) + \frac{qv_{ben1p}(t)}{kT}\sin(\omega_o t)\right). \quad (4.96)$$

Using a Fourier series representation for the remaining exponential, Equation 4.96 can be written as

$$i_e(t) = \sum_{m=0}^{\infty} I_{em}\cos(m\omega_o t)\left[1 + \frac{qv_{ben0}(t)}{kT} + \frac{qv_{ben1a}(t)}{kT}\cos(\omega_o t) + \frac{qv_{ben1p}(t)}{kT}\sin(\omega_o t)\right]. \quad (4.97)$$

Expanding and combining terms results in

$$\begin{aligned} i_e(t) = I_{e0} &+ \frac{qI_{e0}}{kT}v_{ben0}(t) + \frac{qI_{e1}}{2kT}v_{ben1a}(t) \\ &+ \left[I_{e1} + \frac{qI_{e1}}{kT}v_{ben0}(t) + \frac{q}{kT}\left(I_{e0} + \frac{I_{e2}}{2}\right)v_{ben1a}(t)\right]\cos(\omega_o t) \\ &+ \frac{q}{kT}\left(I_{e0} - \frac{I_{e2}}{2}\right)v_{ben1p}(t)\sin(\omega_o t) + \ldots \end{aligned} \quad (4.98)$$

Equation 4.98 gives the values of $G_{i,j}$ for the case of a BJT, which are tabulated in Table 4.1, where $1a$ is refers to the in-phase component of the first harmonic and $1p$ refers to the quadrature component of the first harmonic.

4.6.2 Derivation of Loop Transfer for a Non-Saturating Oscillator

To compute the modulation transfer around the loop, the in-phase and quadrature components will be considered separately. The in-phase noise modulation must include the perturbations about both the fundamental and DC operating points. Adding more harmonics to the base-emitter voltage would result in even more complicated interactions between

Table 4.1: Values of $G_{i,j}$ for a BJT

i \ j	0	1a	1p
0	$\frac{qI_{e0}}{kT}$	$\frac{qI_{e1}}{2kT}$	0
1a	$\frac{qI_{e1}}{kT}$	$\frac{q}{kT}\left(I_{e0} + \frac{I_{e2}}{2}\right)$	0
1p	0	0	$\frac{q}{kT}\left(I_{e0} - \frac{I_{e2}}{2}\right)$

the harmonics and the fundamental. However, as mentioned earlier, the harmonic content of the base-emitter voltage is negligible due to the filtering effect of the feedback circuit.

Consider the DC current approximated by

$$i_{ne0}(\omega_m) = -Y_{DC}(\omega_m)v_{ben0}(\omega_m) = G_{0,0}v_{ben0}(\omega_m) + G_{0,1a}v_{ben1a}(\omega_m), \tag{4.99}$$

where $Y_{DC}(\omega_m)$ represents the circuit and the $G_{i,j}$ represent the device. Solving Equation 4.99 for $v_{ben0}(\omega_m)$ results in

$$v_{ben0}(\omega_m) = -\frac{G_{0,1a}v_{ben1a}(\omega_m)}{Y_{DC}(\omega_m) + G_{0,0}}. \tag{4.100}$$

Equation 4.100 can now be used in Equation 4.89 to solve for the modulation transfer of the device about the fundamental. The result of this substitution is

$$i_{ne1a}(\omega_m) = \left[\frac{-G_{0,1a}G_{1a,0}}{Y_{DC}(\omega_m) + G_{0,0}} + G_{1a,1a}\right] v_{ben1a}(\omega_m). \tag{4.101}$$

Around DC, $Y_{DC}(\omega_m)$ is dominated by the bias resistance which is large compared to the resistance looking into the device. Therefore, it is reasonable to neglect Y_{DC} in Equation 4.101. Substituting the values of $G_{i,j}$, from Table 4.1, gives

$$i_{ne1a}(\omega_m) = \left[\frac{-\left(\frac{qI_{e1}}{kT}\right)\left(\frac{qI_{e1}}{2kT}\right)}{\frac{qI_{e0}}{kT}} + \frac{q}{kT}\left(I_{e0} + \frac{I_{e2}}{2}\right)\right] v_{ben1a}(\omega_m), \tag{4.102}$$

or

$$i_{ne1a}(\omega_m) = \left[-\left(\frac{q}{2kT}\right)\left(\frac{I_{e1}^2}{I_{e0}}\right) + \frac{q}{kT}\left(I_{e0} + \frac{I_{e2}}{2}\right)\right] v_{ben1a}(\omega_m). \tag{4.103}$$

Equation 4.103 can be written in terms of the modified Bessel function to give

$$i_{ne1a}(\omega_m) = \left[-\left(\frac{2qI_{e0}}{kT}\right)\left(\frac{I_1(x)}{I_0(x)}\right)^2 + \frac{qI_{e0}}{kT}\left(1 + \frac{I_2(x)}{I_0(x)}\right)\right] v_{ben1a}(\omega_m). \tag{4.104}$$

By using the modified Bessel function approximation for large x, from Clarke and Hess [5], of

$$I_n(x) \approx \frac{e^x}{\sqrt{2\pi x}}\left(1 - \frac{n^2}{2x}\right), \tag{4.105}$$

we can write

$$i_{ne1a}(\omega_m) \approx \left[-\left(\frac{2qI_{e0}}{kT}\right)\left(1 - \frac{1}{2x}\right)^2 + \frac{qI_{e0}}{kT}\left(1 + 1 - \frac{4}{2x}\right)\right] v_{ben1a}(\omega_m), \tag{4.106}$$

or

$$i_{ne1a}(\omega_m) \approx \left[-\left(\frac{2qI_{e0}}{kT}\right)\left(1 - \frac{1}{x} + \frac{1}{4x^2}\right) + \frac{2qI_{e0}}{kT}\left(1 - \frac{1}{x}\right)\right] v_{ben1a}(\omega_m), \tag{4.107}$$

which simplifies to

$$i_{ne1a}(\omega_m) \approx -\left(\frac{2qI_{e0}}{kT}\right)\left(\frac{1}{4x^2}\right) v_{ben1a}(\omega_m). \tag{4.108}$$

Since x is large, we can see that the in-phase noise does not get transferred through the device. Therefore, the output in-phase noise power is due to only the in-phase noise source and not the feedback, resulting in a noise to signal power ratio of

$$\left|\frac{P_{i_{nouta}}(\omega_m)}{P_{I_{c1}}}\right|_{dB} \approx 10\log_{10}\left(\frac{I_{Na}^2}{\frac{1}{2}I_{c1}^2}\right) \quad \text{dBc/Hz}. \tag{4.109}$$

Substituting Equation 4.72 for I_{Na}^2 results in

$$\left|\frac{P_{i_{nouta}}(\omega_m)}{P_{I_{c1}}}\right|_{dB} \approx 10\log_{10}\left(\frac{2q\left(1-\frac{1}{n}\right)^2\left(I_{c0}+\frac{I_{c2}}{2}\right)}{I_{c1}^2}\right) \quad \text{dBc/Hz}. \tag{4.110}$$

Since there is no DC interaction with the quadrature component of the transfer, the three-terminal model can be used to show the loop transfer of the quadrature noise. Note that for the noise transfer of the device $G_{1p,1p}$ is used instead of the large signal conductance of G. However, for a BJT, the currents can be represented with modified Bessel functions which follow a recursive relationship of the form [5]

$$2nI_n(x) = x\left[I_{n-1}(x) - I_{n+1}(x)\right]. \tag{4.111}$$

Therefore, Equation 4.111 can be used to make some simplifications by noting that

$$\frac{I_{c0}-\frac{I_{c2}}{2}}{I_{c1}} = \frac{I_0(x)-I_2(x)}{2I_1(x)} = \frac{1}{x}. \tag{4.112}$$

Using the relationship of Equation 4.112, we can note that

$$G_{1p,1p} = \frac{q}{kT}\left(I_{e0}-\frac{I_{e2}}{2}\right) = \frac{qI_{e1}}{xkT} = \frac{I_{e1}}{V_{be1}}, \tag{4.113}$$

which is equivalent to the large signal G.

To compute the loop transfer of the quadrature component of the noise, consider the three-terminal model of Figure 4.10 which includes an ideal transformer and parallel RLC circuit representation of the feedback circuit. Using Kirchhoff's Current Law (KCL) at the collector node results in

$$I_{FB}(\omega_m) = \alpha I_e(\omega_m) + \frac{1}{R}V_c(\omega_m) + \frac{1}{j\omega L}V_c(\omega_m) + j\omega C V_c(\omega_m) + I_N, \tag{4.114}$$

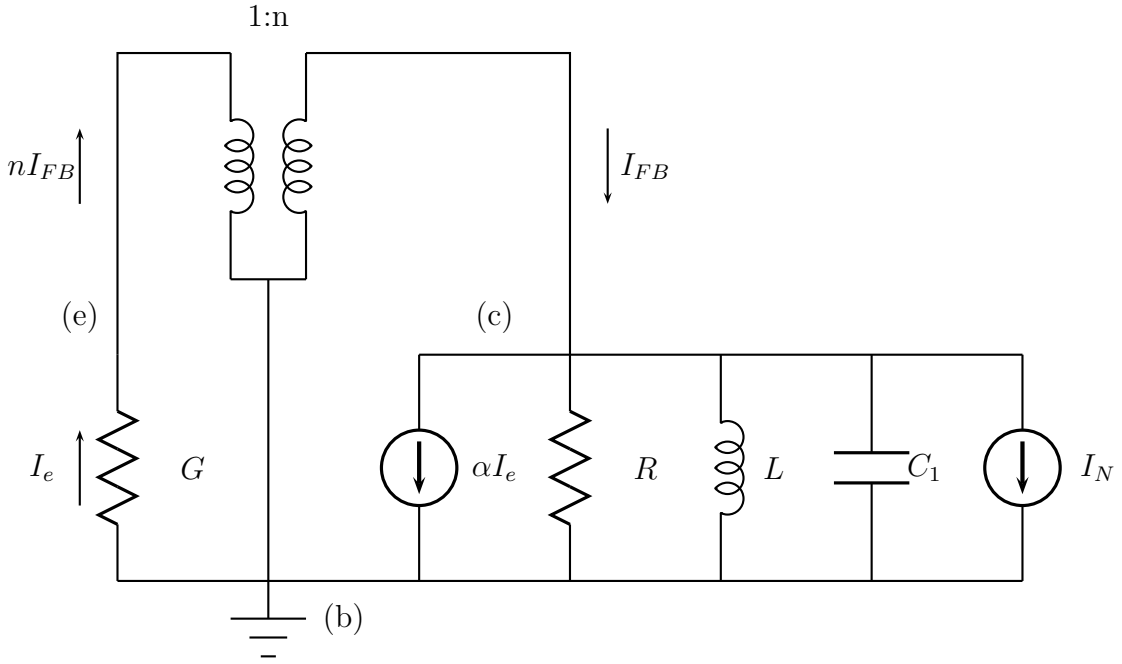

Figure 4.10: Three-terminal model with ideal transformer and parallel RLC circuit representing the feedback for a non-saturating oscillator

where

$$\frac{1}{R} = G_3 + \frac{1}{n^2}G_2 + \left(\frac{n-1}{n}\right)^2 G_1. \tag{4.115}$$

We can also see from KCL at the emitter node that

$$I_{FB}(\omega_m) = \frac{1}{n}I_e(\omega_m) = -\frac{G}{n}V_e(\omega_m) = -\frac{G}{n^2}V_c(\omega_m). \tag{4.116}$$

Making some substitutions in Equation 4.114 results in

$$-I_N = \left(-\frac{\alpha G}{n} + \frac{G}{n^2} + \frac{1}{R} + \frac{1}{j\omega L} + j\omega C\right) V_c(\omega_m). \tag{4.117}$$

We can see the gain of the device as a negative conductance of value $\alpha G/n$. Since the conductance for the quadrature component of the noise is equivalent to the large signal conductance, and to have a stable oscillation the loop equation must satisfy

$$\frac{\alpha G}{n} = \frac{G}{n^2} + \frac{1}{R}, \tag{4.118}$$

we can note that the real parts of the denominator of Equation 4.117 will cancel to give

$$V_{nc}(\omega_m) = \frac{-I_{Np}}{\frac{1}{j\omega L} + j\omega C} \approx \frac{-I_{Np}}{j2\omega_o C\left(\frac{\omega_m}{\omega_o}\right)}. \tag{4.119}$$

Taking the magnitude squared gives the quadrature noise power density of

$$P_{V_{nc}} = \frac{I_{Np}^2}{4\left(\omega_o C\right)^2\left(\frac{\omega_m}{\omega_o}\right)^2}. \tag{4.120}$$

We are interested in the output noise power to signal power ratio. The noise power to signal power ratio can be represented, in units of dBc/Hz, as

$$\left|\frac{P_{V_{nc}}(\omega_m)}{P_{V_{bc1}}}\right|_{\text{dB}} = 10\log_{10}\left(\frac{I_{Np}^2}{\frac{1}{2}V_{bc1}^2 4\left(\omega_o C\right)^2\left(\frac{\omega_m}{\omega_o}\right)^2}\right) \quad \text{dBc/Hz}, \tag{4.121}$$

or

$$\left|\frac{P_{V_{nc}}(\omega_m)}{P_{V_{bc1}}}\right|_{\text{dB}} = 10\log_{10}\left(\frac{I_{Np}^2}{2V_{bc1}^2\left(\omega_o C\right)^2\left(\frac{\omega_m}{\omega_o}\right)^2}\right) \quad \text{dBc/Hz}. \tag{4.122}$$

Substituting Equation 4.72 for I_{Np}^2 results in

$$\left|\frac{P_{V_{nc}}(\omega_m)}{P_{V_{bc1}}}\right|_{\text{dB}} = 10\log_{10}\left(\frac{q\left(1-\frac{1}{n}\right)^2\left(I_{c0}-\frac{I_{c2}}{2}\right)}{2V_{bc1}^2\left(\omega_o C\right)^2\left(\frac{\omega_m}{\omega_o}\right)^2}\right) \quad \text{dBc/Hz}. \tag{4.123}$$

Representing the base-collector voltage in the denominator of Equation 4.123 as

$$|V_{bc1}|^2 = I_{c1}^2 R_T^2, \tag{4.124}$$

where

$$R_T = \left(\frac{G}{n^2} + \frac{1}{R}\right)^{-1} \tag{4.125}$$

represents the impedance seen by the collector current at resonance, results in a noise to signal power ratio of

$$\left|\frac{P_{V_{nc}}(\omega_m)}{P_{V_{bc1}}}\right|_{\text{dB}} = 10\log_{10}\left(\frac{q\left(1-\frac{1}{n}\right)^2\left(I_{c0}-\frac{I_{c2}}{2}\right)}{2I_{c1}^2 Q^2\left(\frac{\omega_m}{\omega_o}\right)^2}\right) \quad \text{dBc/Hz}. \tag{4.126}$$

Now, using the relationship of Equation 4.112, Equation 4.126 can be simplified to give

$$\left|\frac{P_{V_{nc}}(\omega_m)}{P_{V_{bc1}}}\right|_{\text{dB}} = 10\log_{10}\left(\frac{q\left(1-\frac{1}{n}\right)^2}{2xI_{c1}Q^2\left(\frac{\omega_m}{\omega_o}\right)^2}\right) \quad \text{dBc/Hz.} \tag{4.127}$$

This expression for the phase noise spectrum illustrates that the noise performance can be improved by increasing the Q of the tank circuit, increasing the bias current (approximately half of the fundamental current), and increasing the drive level, x.

In good design, a current consistent with the required output level generally would be selected for power considerations and good over-all performance. That leaves the drive level and tank Q as the additional constraints for minimizing the phase-noise produced within the oscillator. For other devices, one would expect similar results, but not necessarily as dramatic. The effects of parasitics and other variations in the problem will likely reduce the effectiveness of this result, but the general concept of bias current, Q, and drive level should still apply to minimizing noise produced by an oscillator.

The next section addresses saturation and the detrimental effects of saturation on noise production. We will show that, though the output level may be stabilized versus frequency, the tradeoff is an increase in produced noise. Thus care should be taken in using saturation for amplitude control and design for the amplitude control with the device as much as possible without saturation.

4.6.3 Derivation of Loop Transfer for a Saturating Oscillator

For the situation in which the oscillator saturates, the loop transfer becomes slightly more complicated. When the transistor saturates there is an added noise current due to the base collector junction.

As we saw in the case where the transistor did not saturate, the transfer through the device for the in-phase component will be small and dominated by the noise source itself at a relatively constant level. The same result applies to the saturating oscillator. This leaves the shot noise produced by the forward and reverse operation of the transistor as the significant output noise power. Using the shot noise power for a saturating oscillator of Equation 4.78 results in

$$\left|\frac{P_{i_{nouta}}(\omega_m)}{P_{I_{c1}}}\right|_{dB} \approx 10\log_{10}\left(\frac{q\left[1-2\alpha_r+\frac{2\alpha_r}{n}-\frac{\alpha_r}{n^2}\right]\left(I_{r0}+\frac{I_{r2}}{2}\right)}{\frac{1}{2}\left(\alpha_f I_{f1}-I_{r1}\right)^2}+\right.$$
$$\left.\frac{q\left[1-\frac{1}{n}\right]^2\left(\alpha_f I_{f0}+\alpha_f\frac{I_{f2}}{2}\right)}{\frac{1}{2}\left(\alpha_f I_{f1}-I_{r1}\right)^2}\right) \quad \text{dBc/Hz.} \tag{4.128}$$

Since there is no DC interaction with the quadrature component of the transfer, the three-terminal model can be used to show the loop transfer of the quadrature noise as we did for the non-saturating case. To represent the transfer of the quadrature component of the noise, $G_{1p,1p}$ will replace G in the three-terminal model, and $G_{C1p,1p}$ will replace G_C. In the saturation case, the values of Table 4.1 have the subscript of e replaced with f to represent the forward operation of the transistor. The value of $G_{C1p,1p}$ are the same as that of $G_{1p,1p}$ except all subscripts of f become subscripts of r to represent the reverse operation of the transistor. Using the relationship of Equation 4.112, we can note that

$$G_{1p,1p} = \frac{q}{kT}\left(I_{f0} - \frac{I_{f2}}{2}\right) = \frac{qI_{f1}}{x_f kT} = \frac{I_{f1}}{V_{be1}}, \tag{4.129}$$

which is the large signal G. Similarly,

$$G_{C1p,1p} = \frac{q}{kT}\left(I_{r0} - \frac{I_{r2}}{2}\right) = \frac{qI_{r1}}{x_r kT} = \frac{I_{r1}}{V_{bc1}}, \tag{4.130}$$

which is the large signal G_C.

To compute the loop transfer of the quadrature component of the noise, consider the three-terminal model of Figure 4.11, which includes an ideal transformer and parallel RLC circuit representation of the feedback circuit. Also included are the extra source and conductance resulting from turning the base-collector junction on for part of the cycle. Using

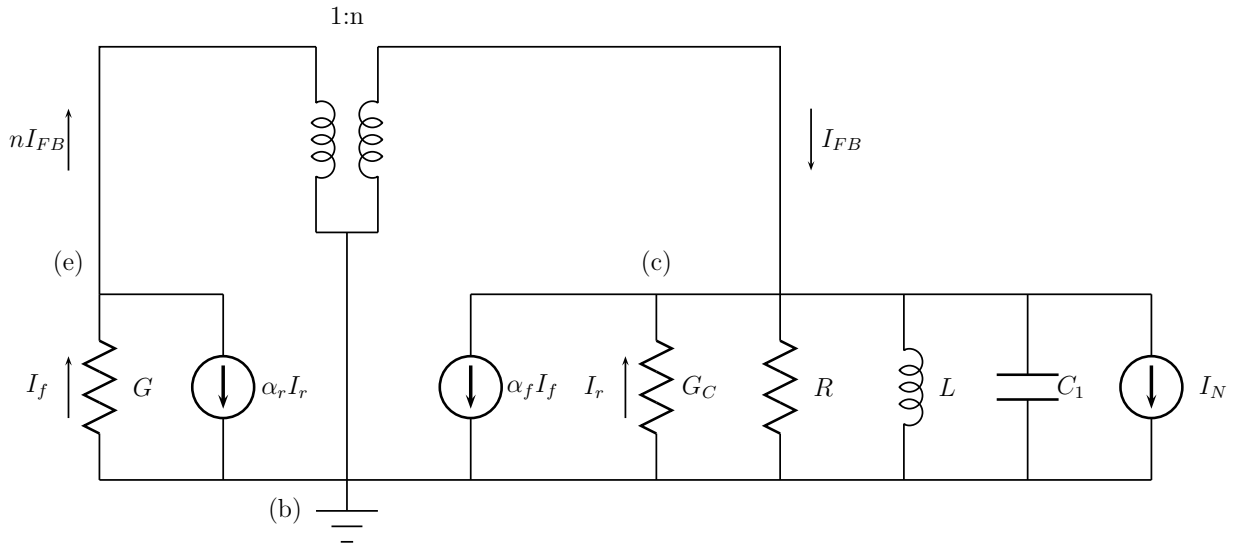

Figure 4.11: Three-terminal model with ideal transformer and parallel RLC circuit representing the feedback for a saturating oscillator

Kirchhoff's Current Law (KCL) at the collector node results in

$$I_{FB}(\omega_m) = \alpha I_e(\omega_m) + G_C V_c(\omega_m) + \frac{1}{R} V_c(\omega_m) + \frac{1}{j\omega L} V_c(\omega_m) + j\omega C V_c(\omega_m) + I_N, \quad (4.131)$$

where

$$\frac{1}{R} = G_3 + \frac{1}{n^2} G_2 + \left(\frac{n-1}{n}\right)^2 G_1. \quad (4.132)$$

We can also see from KCL at the emitter node that

$$I_{FB}(\omega_m) = \frac{1}{n} I_e(\omega_m) - \frac{\alpha_r}{n} I_r = -\frac{G}{n} V_e(\omega_m) + \frac{\alpha_r G_C}{n} V_c(\omega_m), \quad (4.133)$$

$$I_{FB}(\omega_m) = -\frac{G}{n^2} V_c(\omega_m) + \frac{\alpha_r G_C}{n} V_c(\omega_m). \quad (4.134)$$

Making some substitutions in Equation 4.131 results in

$$-I_N = \left(-\frac{\alpha_f G}{n} - \frac{\alpha_r G_C}{n} + \frac{G}{n^2} + G_C + \frac{1}{R} + \frac{1}{j\omega L} + j\omega C\right) V_c(\omega_m). \quad (4.135)$$

We can see the gain of the device as a negative conductance of value $\alpha_f G/n + \alpha_r G_C/n$. If we briefly consider the large signal steady state solution of Equation 4.135 where I_N is zero, we can see that to have a stable oscillation

$$\frac{\alpha_f G}{n} + \frac{\alpha_r G_C}{n} = \frac{G}{n^2} + G_C + \frac{1}{R}, \quad (4.136)$$

where G is the large signal conductance of I_{f1}/V_{be1} and G_C is the large signal conductance of I_{r1}/V_{bc1}. Since the conductance for the quadrature component of the noise is equivalent to the large signal conductance, we can note that the real parts of the denominator of Equation 4.135 will cancel to give

$$V_{nc}(\omega_m) = \frac{-I_{Np}}{\frac{1}{j\omega_o L} + j\omega_o C} \approx \frac{-I_{Np}}{j2\omega_o C\left(\frac{\omega_m}{\omega_o}\right)}. \quad (4.137)$$

This is the same result we found for the non-saturating oscillator. From Subsection 4.6.2, we can write the noise to signal power ratio as

$$\left|\frac{P_{V_{cn}}(\omega_m)}{P_{V_{bc1}}}\right|_{\text{dB}} = 10\log_{10}\left(\frac{I_{Np}^2}{2V_{bc1}^2\left(\omega_o C\right)^2\left(\frac{\omega_m}{\omega_o}\right)^2}\right) \quad \text{dBc/Hz}. \quad (4.138)$$

The difference here is that the noise power, I_{Np}^2, is different. Substituting Equation 4.78 for I_{Np}^2 results in

$$\left|\frac{P_{V_{cn}}(\omega_m)}{P_{V_{bc1}}}\right|_{\text{dB}} = 10\log_{10}\left(\frac{q\left[1-2\alpha_r+\frac{2\alpha_r}{n}-\frac{\alpha_r}{n^2}\right]\left(I_{r0}-\frac{I_{r2}}{2}\right)}{2V_{bc1}^2\left(\omega_o C\right)^2\left(\frac{\omega_m}{\omega_o}\right)^2}\right.$$
$$\left.+\frac{q\alpha_f\left[1-\frac{1}{n}\right]^2\left(I_{f0}-\frac{I_{f2}}{2}\right)}{2V_{bc1}^2\left(\omega_o C\right)^2\left(\frac{\omega_m}{\omega_o}\right)^2}\right) \quad \text{dBc/Hz.} \quad (4.139)$$

Using the relationship of Equation 4.112 results in

$$\left|\frac{P_{V_{cn}}(\omega_m)}{P_{V_{bc1}}}\right|_{\text{dB}} = 10\log_{10}\left(\frac{q\left[1-2\alpha_r+\frac{2\alpha_r}{n}-\frac{\alpha_r}{n^2}\right]\frac{I_{r1}}{x_r}}{2V_{bc1}^2\left(\omega_o C\right)^2\left(\frac{\omega_m}{\omega_o}\right)^2}\right.$$
$$\left.+\frac{q\alpha_f\left[1-\frac{1}{n}\right]^2\frac{I_{f1}}{x_f}}{2V_{bc1}^2\left(\omega_o C\right)^2\left(\frac{\omega_m}{\omega_o}\right)^2}\right) \quad \text{dBc/Hz.} \quad (4.140)$$

If the transistor is saturating, then the base-collector voltage will be fixed. While this may provide for a fixed output level, the noise advantage of having a higher current level goes away. In the non-saturating oscillator, the noise power is proportional to the fundamental signal current, but the signal level is proportional to the square of the fundamental signal current. In the saturating oscillator, the noise power is still increased in proportion to the current, but the signal level becomes fixed. Therefore, the advantage of a higher bias current is lost. Also, since increasing the drive level, x_f, will decrease the base-collector voltage and x_r the advantage of having a high drive level is reduced. The remaining parameter that can be used to control the phase-noise is the oscillator Q, which can be seen indirectly in Equation 4.140 as $\omega_o C$.

Chapter 5

Noise Performance of Examples

In this chapter, we will evaluate the noise performance of the examples from Chapter 3 using the analysis of Chapter 4 and then compare them to simulations of noise in Advanced Design System (ADS [1]). For analysis use, it will be shown that ADS correctly predicts the phase noise of an oscillator that does not saturate. ADS procuces an apparent error in the phase noise of a saturating oscillator. However, we will also show that ADS can predict the phase noise of an oscillator that saturates by turning off the transistor's noise source and adding noise sources across the collector-emitter terminals and the base-collector terminals.

5.1 Advanced Design System Phase Noise Simulation

There are two methods to simulate phase noise in ADS. One uses the frequency sensitivity to noise and one uses small-signal mixing of noise. These two methods are represented with the abbreviations pnfm and pnmx respectively. The ADS documentation [3] does not give a detailed description of how the noise analysis is performed. The documentation does note that the mixing analysis is more accurate for large offset frequencies, and the frequency sensitivity method is more accurate for close-in phase noise.

The documentation for the BJT model being used [2] refers to the shot noise produced by the BJT as being the standard shot noise of $2qI_B$ and $2qI_c$. This model appears not to account for the shaping of the noise due to the current having a pulse nature; however, the result of the phase noise simulations for non-saturating oscillators is the correct value. For saturating oscillators, it appears that the ADS simulation continues to treat the noise currents in the same manner as a non-saturating oscillator. Due to the forward bias of the base-collector junction, the transistor currents have additional components in the collector relative to the non-saturating oscillator. This difference in current flow results in an error when using the BJT noise model for the phase noise simulation. This limitation can be overcome by turning off the internal noise source of the BJT model and adding an external noise source. The

external noise source is a white noise source which the ADS simulation treats as half in-phase noise and half quadrature noise. Since the in-phase noise is not transfered around the loop, we can simulate the phase noise using our computed noise power, from Section 4.5, by computing the noise current from twice the value of our computed noise power. This factor of two in the noise power will correct for the ADS simulation treating only half the power of the noise source as quadrature noise. Additional noise sources such as thermal noise or $1/f$ noise can be used in the simulation as well; however, the simulations in this thesis will be restricted to the dominant shot noise.

5.2 Non-Saturating Common-Collector Oscillator Example

Looking at the non-saturating oscillator designed in Chapter 3, the parameters needed for the noise analysis of Chapter 4 are listed in Table 5.1. Using the values of Table 5.1 and the in-phase noise spectrum of Equation 4.110, the in-phase noise spectrum was computed and is plotted in Figure 5.1. Also plotted in Figure 5.1 are ADS noise simulations using the noise model of a generic BJT and a noise model using added noise sources. The two simulation methods and the prediction of the in-phase noise are not in very close agreement; however, the level of the noise is low enough it is not significant and the error may be a result of numerical limitation in the simulation.

Using the values of Table 5.1 and the phase noise spectrum of Equation 4.127, the phase noise spectrum was computed and is plotted in Figures 5.2 and 5.3. Also plotted in Figures 5.2 and 5.3 are the ADS simulation results using the noise model of a generic BJT and a noise model using added noise sources. Figure 5.3 shows that the predicted phase noise spectrum is close to that of the ADS simulation. This result was seen on other oscillators simulated as well. This close agreement shows that the ADS can be be a good tool for simulating phase noise in a non-saturating oscillator; however, an understanding of the noise analysis gives a feel for what can be done to improve the noise performance of an oscillator.

Table 5.1: Parameters needed for noise analysis of non-saturating oscillator

α	0.99
n	4.7
x	20
Q	15.3
f_o	1.0 GHz
I_{e0}	10.0 mA
I_{e1}	19.5 mA
I_{e2}	18.1 mA

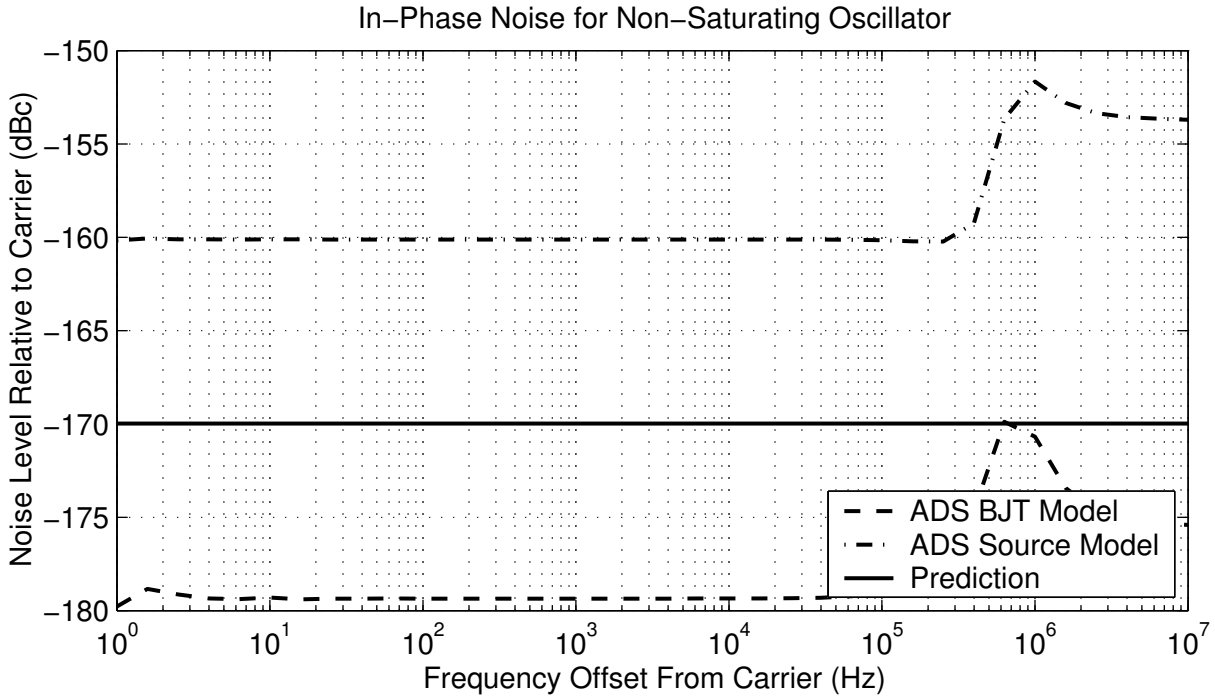

Figure 5.1: In-phase noise of non-saturating oscillator

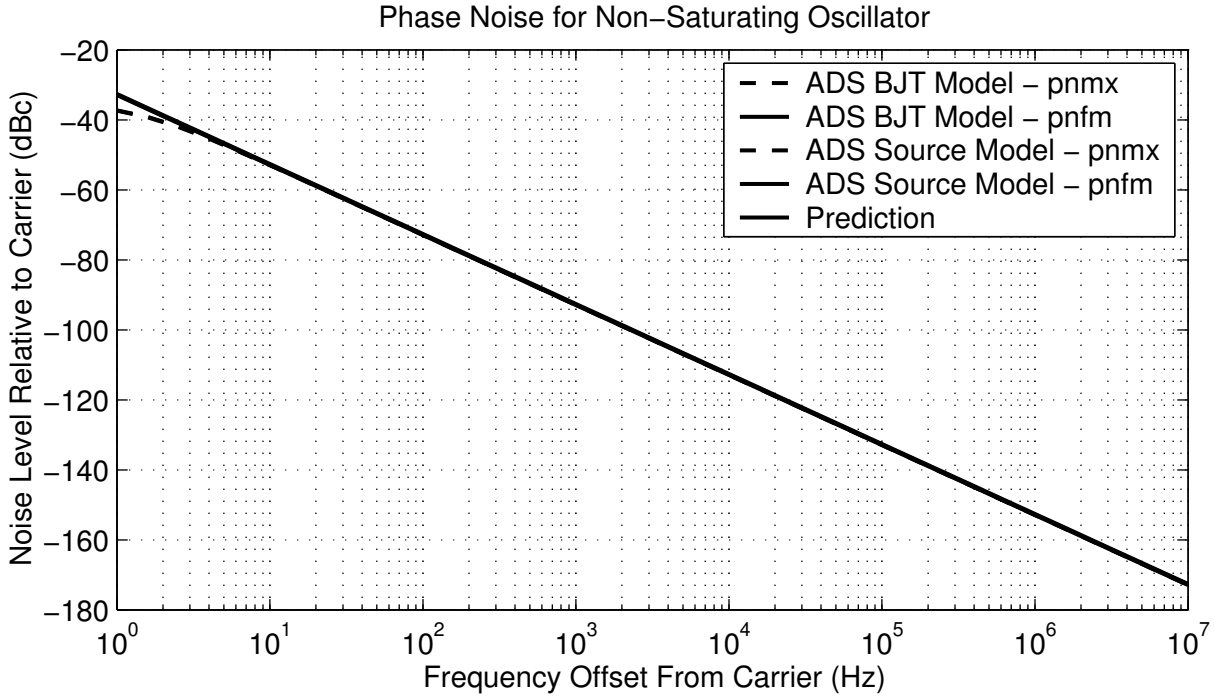

Figure 5.2: Phase noise of non-saturating oscillator

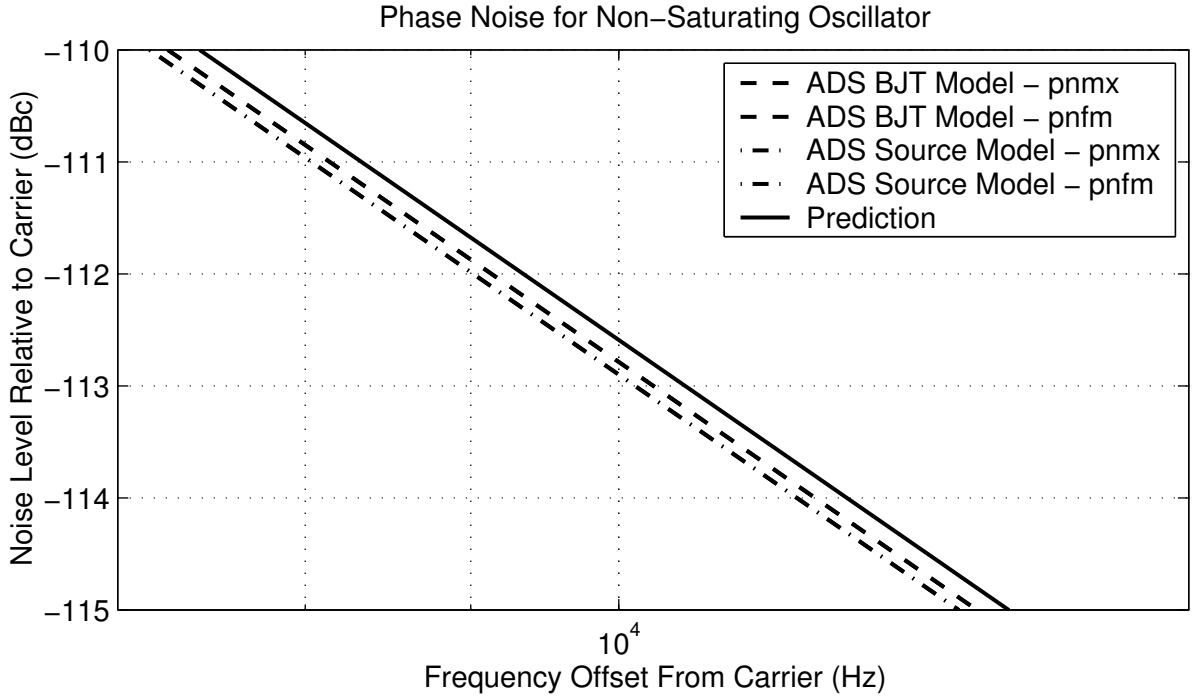

Figure 5.3: Phase noise of non-saturating oscillator (expanded)

5.3 Saturating Common-Collector Oscillator Example

If we look at the saturating oscillator designed in Chapter 3, the parameters needed for the noise analysis of Chapter 4 are listed in Table 5.2. Using the values of Table 5.2 and the in-phase noise spectrum of Equation 4.128, the in-phase noise spectrum was computed and is plotted in Figure 5.4. Also plotted in Figure 5.4 are ADS noise simulations using the noise model of a generic BJT and a noise model using added noise sources. As with the non-saturating case, the prediction of the in-phase noise does not agree very closely with the simulation; however, the level of the noise is low enough it is not significant and may be a result of numerical limitation in the simulation.

Using the values of Table 5.2 and the phase noise spectrum of Equation 4.140, the phase noise spectrum was computed and is plotted in Figures 5.5 and 5.6. Also plotted in Figures 5.5 and 5.6 are the ADS simulation results using the noise model of a generic BJT and a noise model using added noise sources. It can be seen in Figure 5.6 that the predicted phase noise is in close agreement with the noise source model simulation, but the BJT noise model simulation results in a lower phase noise. It appears that the ADS BJT model computes the noise sources using the total collector current to give a collector-emitter noise source and the total base current to give a base-emitter noise source. The fact that a majority of the base current is actually going to the collector is not accounted for. Simulating the phase noise using flawed external noise sources calculated in this manner results in a closer agreement

Table 5.2: Parameters needed for noise analysis of saturating oscillator

α_f	0.99
α_r	0.5
n	4.7
x_f	13.8
x_r	64.8
V_{bc1}	1.68 V
C	19.2 pF
f_o	1.0 GHz
I_{f0}	12.3 mA
I_{f1}	23.7 mA
I_{f2}	21.1 mA
I_{r0}	4.6 mA
I_{r1}	9.1 mA
I_{r2}	8.9 mA

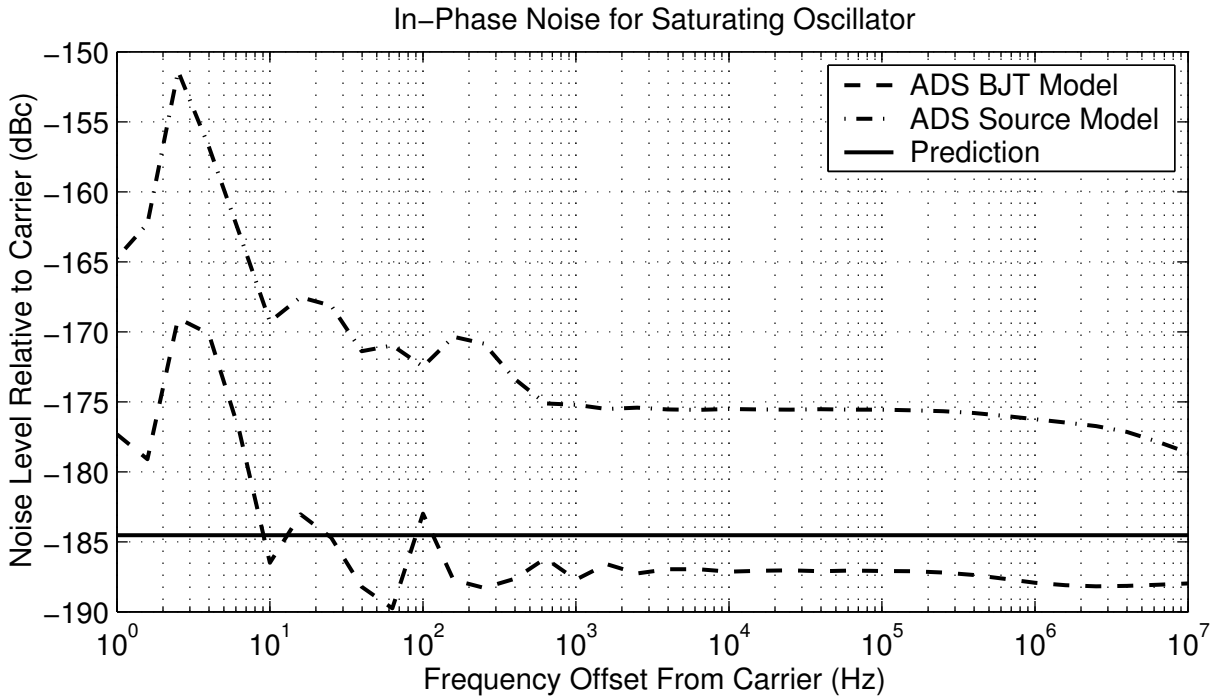

Figure 5.4: In-phase noise of saturating oscillator

with the ADS BJT noise model, as can be seen in Figures 5.7 and 5.8. This shows that if the proper noise sources are added to the ADS circuit, the simulation tool can provide an improved noise simulation. It should be noted that, although the generic transistor model correctly simulates the large signal operation of the circuit in saturation, the noise model included with the generic transistor model does not correctly take into consideration the shot noise produced by saturation.

From the plots of oscillator noise we can see that ADS can be a good tool for phase noise analysis if care is taken for the case where the oscillator saturates. Having a simulation tool can be convenient, but it should not be used blindly. Understanding oscillator phase noise can give important insights on how to design an oscillator to achieve a low phase noise and what can be changed to improve the phase noise performance.

5.4 Effects of a Collector Load on Common-Collector Oscillator Phase Noise

To illustrate the effect on phase noise of adding a collector load, simulations were performed on the oscillators of Chapter 3 with resistive and tuned loads added. Although it appears that the ADS simulation does not correctly account for phase noise of an oscillator that is

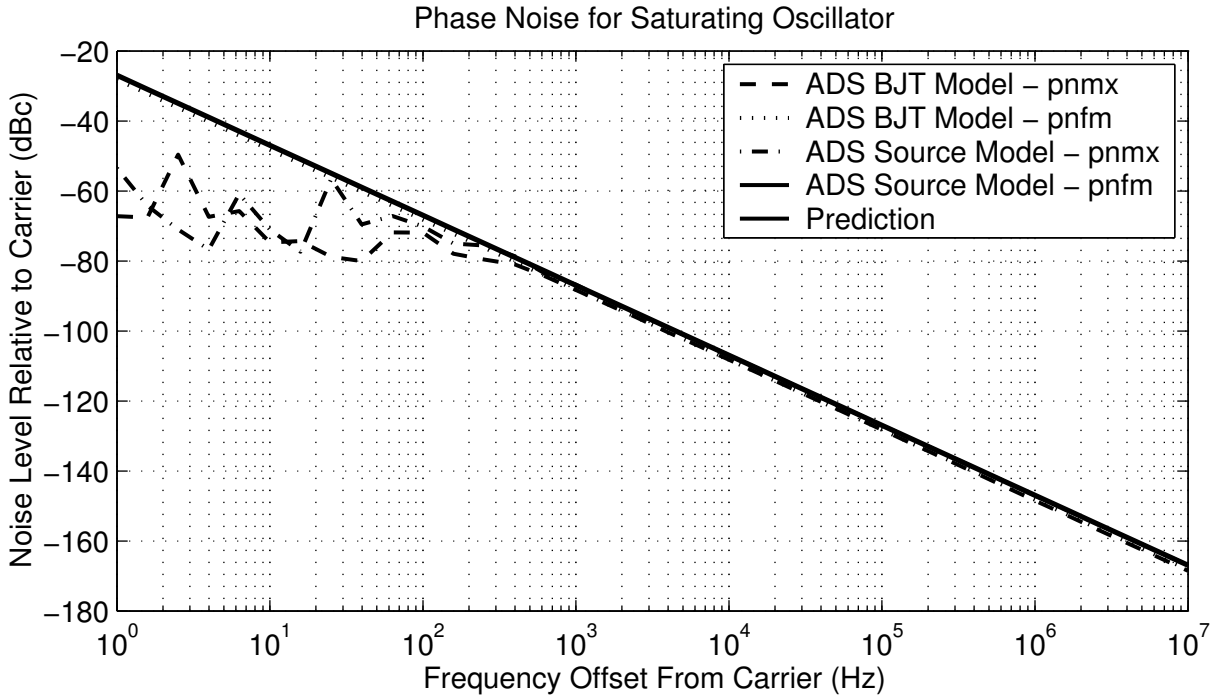

Figure 5.5: Phase noise of saturating oscillator

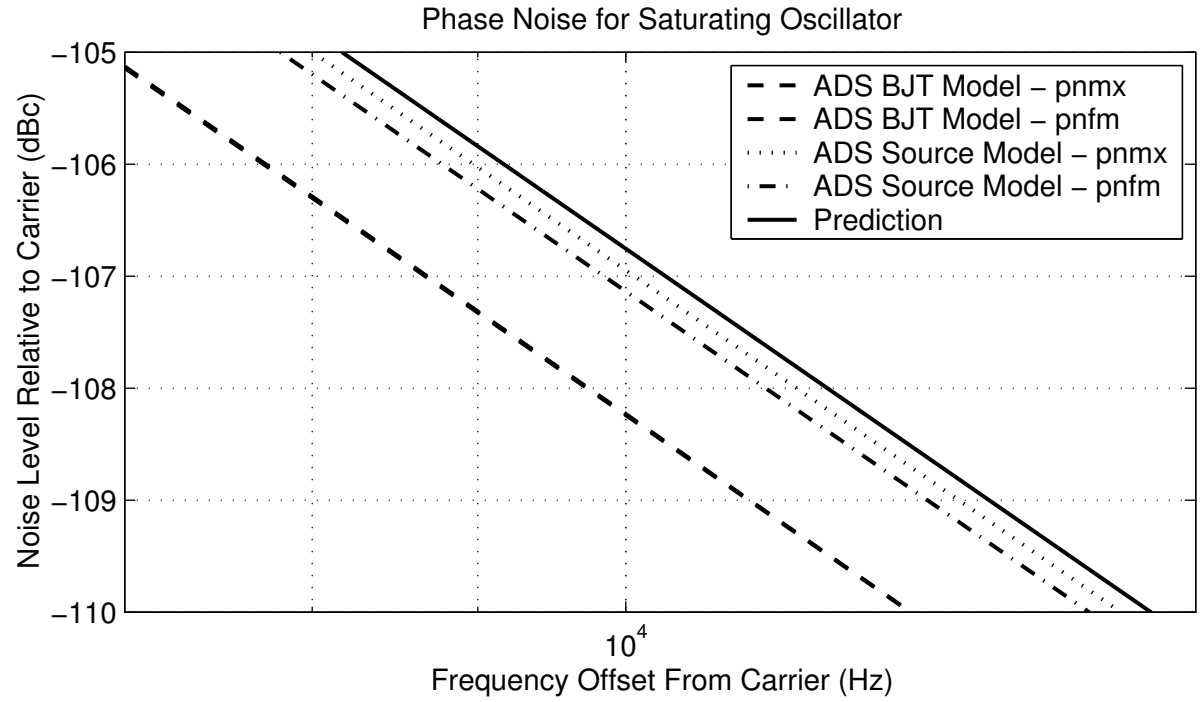

Figure 5.6: Phase noise of saturating oscillator (expanded)

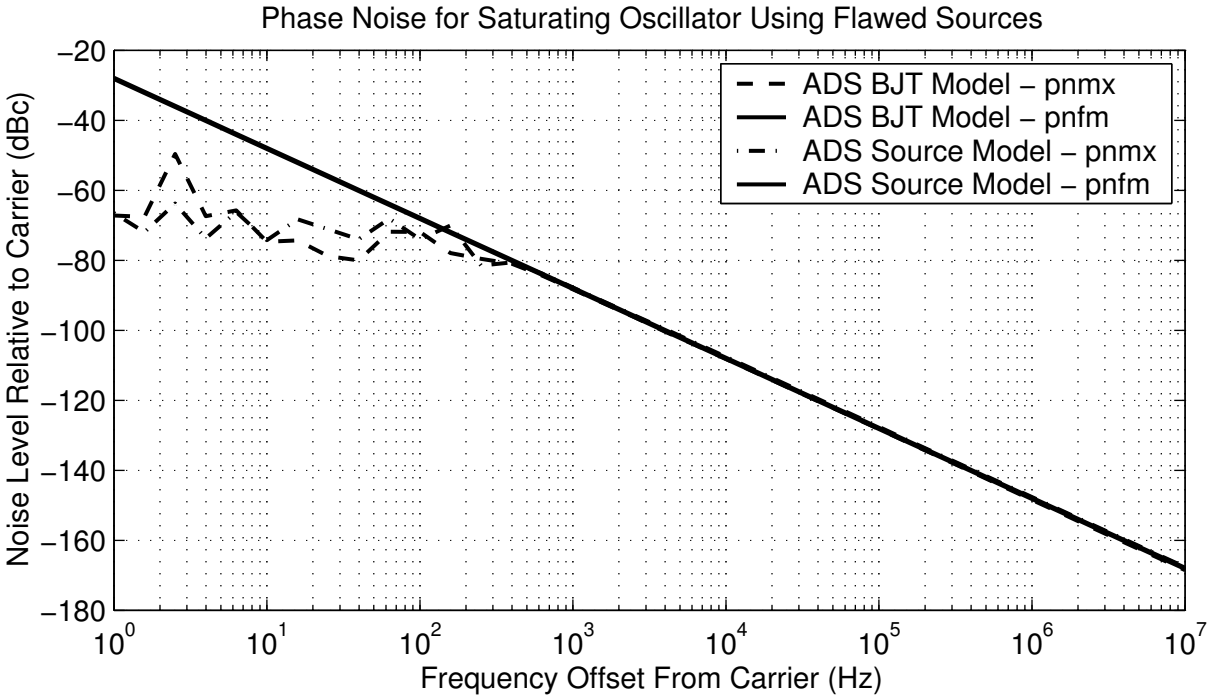

Figure 5.7: Phase noise of saturating oscillator using flawed noise sources

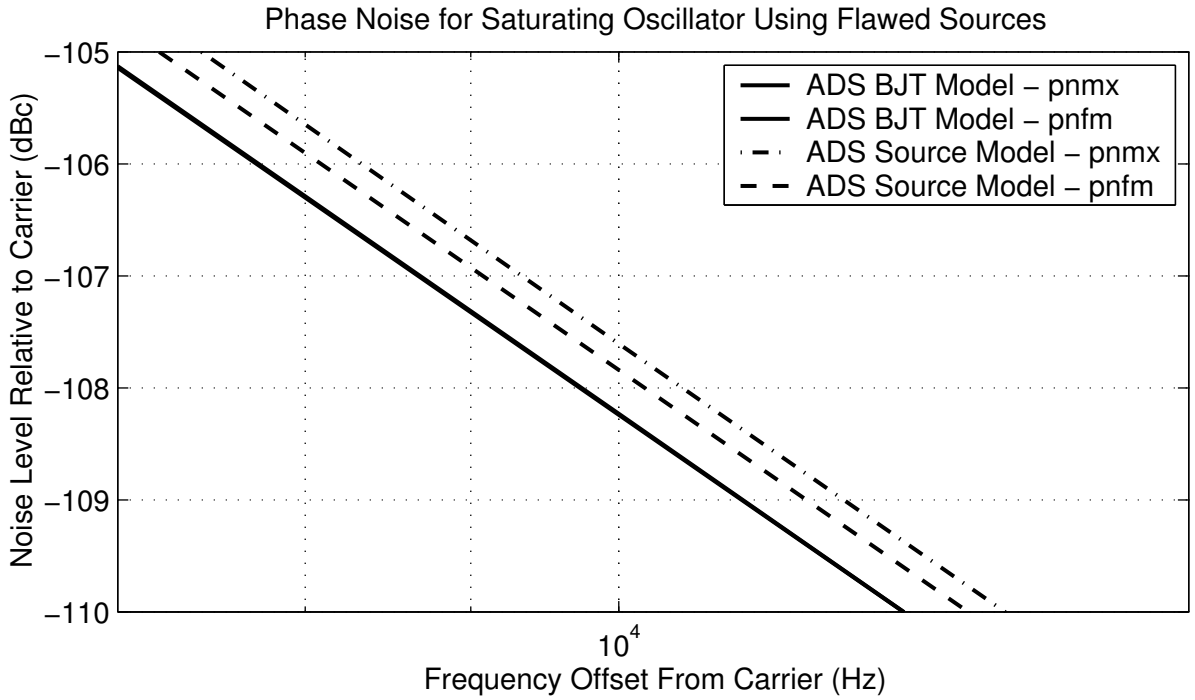

Figure 5.8: Phase noise of saturating oscillator using flawed noise sources (expanded)

saturating, the results still can be used to illustrate the effects of adding a load. When doing so, one should remember that the phase noise could be slightly worse than what the ADS simulation states for a saturating oscillator. A summary of the ADS simulations are shown in Table 5.3. The phase noise in this table is measured at the emitter terminal voltage.

As a result of these ADS simulations, we can make some conclusions about the effects of adding a load on the collector. Note that for the resistive load added to the non-saturating oscillator the transistor begins to saturate and the phase noise increases. Adding a tuned load allows the collector voltage to become sinusoidal. As long as the sinusoidal voltage on the collector is not too large, the transistor will not saturate and the phase noise performance will be the same as if there is no load on the collector.

Table 5.3: Phase noise of example oscillators with no load, a resistive load, and a tuned load

Oscillator	f_m	Phase Noise
Non-saturating oscillator with no load	10 kHz	-112.8 dBc
Resistive load added to non-saturating oscillator	10 kHz	-110.0 dBc
Tuned load added to non-saturating oscillator	10 kHz	-112.8 dBc
Saturating oscillator with no load	10 kHz	-108.2 dBc
Resistive load added to saturating oscillator	10 kHz	-102.7 dBc
Tuned load added to saturating oscillator	10 kHz	-102.8 dBc

Looking at the resistive load added to the saturating oscillator, note that the oscillator saturates harder and the phase noise increases significantly. Tuning the load on this oscillator does not improve the phase noise significantly because the voltage across the load is to big and the transistor still saturates hard. These results support the idea that for good phase noise performance the oscillator should be designed to prevent hard saturation.

Chapter 6

Conclusions and Recommendations

We have provided some theory of phase noise under non-saturating and saturating conditions. With this information, we can give insight into the low-noise design process. The drive level, Q of the feedback circuit, and bias current all affect the phase noise of an oscillator. From Equations 4.127 and 4.140 we can observe these effects. With saturation added to the problem we can see that the saturation lowers the Q of the tank circuit, lowers the drive level from what was designed for if it was designed for an oscillator that did not saturate, and increases the noise production due to the shot noise produced by turning on the base-collector junction for part of the cycle. Adding a load on the collector complicates the problem further by widening the current pulse. Although we did not go into the analysis with this load, it would seem that this widening of the pulse will bring the signal closer to a square wave reducing the second harmonic. This would indicate an increase in phase noise production from the formula having a dependence of $(I_0 - I_2/2)$. This increase in phase noise suggests that although designing an oscillator to saturate can provide a stable output level over a wide bandwidth, the added noise production may degrade the performance of the oscillator.

The results of this thesis provide some physical and mathematical support to the theory proposed by Hajimiri and Lee [9][10] which discusses the oscillator phase noise as a time-varying system through the use of an impulse sensitivity function. The results also show how we can use the Advanced Design System (ADS) [1] to simulate phase noise if we are careful. For the non-saturating case we have seen that the ADS does a satisfactory job. However, with saturation occurring we have to be careful to understand if the transistor model is accounting for the noise production correctly. To get around this problem we can add our own noise sources in the correct position. When adding our own noise sources we must make a small adjustment.

In this thesis, a major contribution is the decomposition of shot noise into in-phase and quadrature noise sources. In addition, these noise sources were applied in the analysis of

non-saturating and saturating oscillator phase noise by extending the three-teminal model of Davis [6].

Although we have developed a simple analysis method for oscillator phase noise, extending the analysis to account for parasitic effects could be a topic of future work. One extension could include the electron transit time in the shot noise calculation. Also, other sources of noise such as $1/f$ noise could be investigated and can be easily added to the analysis presented here with a slight modification of the noise sources. Actual measurement of the phase noise of some oscillators could provide a better understanding of the validity of this noise analysis and may be a good topic for future work.

Bibliography

[1] Agilent Technologies. *Advanced Design System Documentation*, 2003. http://eesof.tm.agilent.com/docs/adsdoc2003A/manuals.htm.

[2] Agilent Technologies. *BJT_Model (Bipolar Transistor Model)*, 2003. http://eesof.tm.agilent.com/docs/adsdoc2003A/ccnld/ccnld028.html.

[3] Agilent Technologies. *Phase Noise Overview*, 2003. http://eesof.tm.agilent.com/docs/adsdoc2003A/cktsimhb/ckhb044.html.

[4] M. J. Buckingham. *Noise in Electronic Devices and Systems*. Ellis Horwood Limited, 1983.

[5] Kenneth K. Clarke and Donald T. Hess. *Communication Circuits: Analysis and Design*. Addison-Wesley, 1971.

[6] William A. Davis. Radio and Microwave Engineering. Notes Created to Accompany EE 4605, Radio Engineering at Virginia Polytechnic Institute and State University, The Bradley Department of Electrical Engineering, 1992.

[7] H. Fukui. The Noise Performance of Microwave Transistors. *IEEE Transactions on Electron Devices*, ED-13(3):329–341, March 1966.

[8] Stanford Goldman. *Frequency Analysis, Modulation and Noise*. McGraw-Hill Book Company, Inc., 1948.

[9] Ali Hajimiri and Thomas H. Lee. A General Theory of Phase Noise in Electrical Oscillators. *IEEE Journal of Solid-State Circuits*, 33(2):179–194, February 1998.

[10] Ali Hajimiri and Thomas H. Lee. Oscillator Phase Noise: A Tutorial. *IEEE Journal of Solid-State Circuits*, 35(3):326–336, March 2000.

[11] R. J. Hawkins. Limitations of nielsen's and related noise equations applied to microwave bipolar transistors, and a new expression for the frequency and current dependent noise figure. *Solid-State Electronics*, 20(3):191–196, March 1977.

[12] J. B. Johnson. Thermal Agitation of Electricity in Conductors. *Physical Review*, 32:97–109, July 1928.

[13] Herbert L. Krauss, Charles W. Bostian, and Frederick H. Raab. *Solid State Radio Engineering*. John Wiley and Sons, 1980.

[14] Kaneyuki Kurokawa. Noise in Synchronized Oscillators. *IEEE Transactions on Microwave Theory and Techniques*, MTT-16(4):234–240, April 1968.

[15] W. Marshall Leach, Jr. *Noise Measurement*. CRC Press LLC, 2000. http://www.engnetbase.com.

[16] D. B. Leeson. A Simple Model of Feedback Oscillator Noise Spectrum. *Proceedings of the IEEE*, 54:329–330, February 1966.

[17] Alberto Leon-Garcia. *Probability and Random Processes for Electrical Engineering*. Addison-Wesley, second edition, 1994.

[18] Fred K. Manasse, John A. Ekiss, and Charles R. Gray. *Modern Transistor Electronics Analysis and Design*. Prentice-Hall, Inc., 1967.

[19] Edward G. Nielsen. Behavior of Noise Figure in Junction Transistors. *Proceedings of the IRE*, 45(7):957–963, July 1957.

[20] Guofu Niu, John D. Cressler, Shiming Zhang, William E. Ansley, Charles S. Webster, and David L. Harame. A Unified Approach to RF and Microwave Noise Parameter Modeling in Bipolar Transistors. *IEEE Transactions on Electron Devices*, 48(11):2568–2574, November 2001.

[21] H. Nyquist. Thermal Agitation of Electric Charge in Conductors. *Physical Review*, 32:110–113, July 1928.

[22] Alan V. Oppenheim, Alan S. Willsky, and S. Hamid Nawab. *Signals and Systems*. Prentice Hall, second edition, 1997.

[23] Paul Penfield, Jr. Circuit Theory of Periodically Driven Nonlinear Systems. *Proceedings of the IEEE*, 54(2):266–280, February 1966.

[24] Robert F. Pierret. *Semiconductor Device Fundamentals*. Addison-Wesley, 1996.

[25] R. A. Pucel and U. L. Rohde. An Exact Expression for the Noise Resistance Rn for the Hawkins Bipolar Noise Model. *IEEE Microwave and Guided Wave Letters*, 3(2):35–37, February 1993.

[26] W. P. Robins. *Phase Noise in Signal Sources*. Peter Peregrinus Ltd., 1982.

[27] F. N. H. Robinson. *Noise and Fluctuations in Electronic Devices and Circuits*. Clarendon Press, 1974.

[28] Ulrich L. Rohde. Theory of Intermodulation and Reciprocal Mixing: Practice, Definitions, and Measurements in Devices and Systems, Part 1. *QEX*, pages 3–15, Nov/Dec 2002.

[29] Ulrich L. Rohde, Ajay K. Poddar, and Georg Bock. *The Design of Modern Microwave Oscillators for Wireless Applications*. John Wiley and Sons, Inc., 2005.

[30] Richard D. Thornton, David DeWitt, Paul E. Gray, and E. R. Chenette. *Characteristics and Limitations of Transistors*. John Wiley and Sons, Inc., 1966.

[31] Aldert van der Ziel. Shot Noise in Junction Diodes and Transistors. *Proceedings of the IRE*, 43:1639–1646, November 1955.

[32] Aldert van der Ziel. *Noise: Sources, Characterization, Measurement*. Prentice-Hall, 1970.

[33] Gabriel Vasilescu. *Electronic Noise and Interfering Signals*. Springer, 2005.

Vita

Scott E. Brock was born in November of 1980 in Rushville, Indiana. He spent all of his early life in Rush County, Indiana working on the neighbors' farms. In high school he was interested in mechanical engineering. He became interested in amateur radio in 1998 and was licensed in June of 1998 as KB9SZW. This interest in amateur radio steered him toward attending Purdue University as an electrical engineering student. Scott received a Bachelor of Science in Electrical Engineering from Purdue University in May of 2003. Following his time at Purdue, he attended Virginia Polytechnic Institute and State University to pursue a Masters degree. His main interest in electrical engineering is radio frequency hardware design.